ISTANBUL TECHNICAL UNIVERSITY ★ GRADUATE SCHOOL OF SCIENCE ENGINEERING AND TECHNOLOGY

WAVE PROPAGATION IN AN ALLUVIAL VALLEY SUBJECTED TO A STRIKE-SLIP FAULT

Ph.D. THESIS

Hasan Faik KARA

Department of Civil Engineering

Structure Engineering Programme

FEBRUARY 2014

ISTANBUL TECHNICAL UNIVERSITY ★ GRADUATE SCHOOL OF SCIENCE ENGINEERING AND TECHNOLOGY

WAVE PROPAGATION IN AN ALLUVIAL VALLEY SUBJECTED TO A STRIKE-SLIP FAULT

Ph.D. THESIS

Hasan Faik KARA
(501082004)

Department of Civil Engineering

Structure Engineering Programme

Thesis Advisor: Prof. Dr. Hasan ENGİN

FEBRUARY 2014

İSTANBUL TEKNİK ÜNİVERSİTESİ ★ FEN BİLİMLERİ ENSTİTÜSÜ

DOĞRULTU ATIMLI FAY ETKİSİNDEKİ ALÜVYONAL VADİDE DALGA YAYILIMI

DOKTORA TEZİ

Hasan Faik KARA
(501082004)

İnşaat Mühendisliği Anabilim Dalı

Yapı Mühendisliği Programı

Tez Danışmanı: Prof. Dr. Hasan ENGİN

ŞUBAT 2014

Hasan Faik KARA, a Ph.D. student of ITU Graduate School of Science Engineering and Technology 501082004 successfully defended the thesis entitled **"WAVE PROPAGATION IN AN ALLUVIAL VALLEY SUBJECTED TO A STRIKE-SLIP FAULT"**, which he prepared after fulfilling the requirements specified in the associated legislations, before the jury whose signatures are below.

Thesis Advisor :	**Prof. Dr. Hasan ENGİN** Istanbul Technical University	.....
Jury Members :	**Prof. Dr. Abdul HAYIR** Istanbul Technical University	.....
	Prof. Dr. İrfan ÇOŞKUN Yildiz Technical University	.....
	Prof. Dr. Mehmet Hakkı OMURTAG Istanbul Technical University	.....
	Assoc. Prof. Dr. Mesut ŞİMŞEK Yildiz Technical University	.....

Date of Submission : **January 15th, 2014**
Date of Defense : **February 10th, 2014**

To my family

FOREWORD

During my Master and PhD studies, I have learned a lot of things about science and life from my advisor, Prof. Dr. Hasan ENGİN. He was always kind and understanding so I had always been feeling safe. I appreciate him.

I owe Prof. Dr. Mihailo D. TRIFUNAC a debt of gratitude. I've learned a lot from his wisdom. My PhD dissertation topic was conceptually his idea. Working with him was a privilege. During my stay in Los Angeles, he was very hospitable. We've spent lots of time together in addition to our scientific studies. The holiday vacation that we spent at his house in Big Bear was unforgettable. I also need to thank to Prof. Dr. TRIFUNAC's wife Prof. Dr. Maria TODOROVSKA and Prof. Dr. Vincent LEE for helping me in my research. They were very friendly and wise. I shouldn't forget to thank to my dear friends, Mehran, Judy, Ulaş, Adem, Olessya, Burcu and many others, in Los Angeles area. Living in Los Angeles was a wonderful experience because of their being. The financial support for my stay at USC that was provided by TUBITAK is gratefully acknowledged.

I would like to thank to Prof. Dr. Abdul HAYIR for helping me to find a visiting scholar position at USC. I'm grateful to him. I also need to thank to other members of the thesis Examination Committee, Prof. Dr. İrfan ÇOŞKUN, Prof. Dr. Mehmet Hakkı OMURTAG and Assoc. Prof. Dr. Mesut ŞİMŞEK for their valuable comments and corrections.

Assist. Prof. Dr. Aydın ÖZMUTLU taught me how to use the software to solve wave propagation problems and some techniques that help me for my research. I'm grateful to him. I want to thank to my roommate Dr. Murat YILMAZ for providing technical support and instructions whenever I need. I want to thank to Prof. Dr. Reha ARTAN, Prof. Dr. Necla KADIOĞLU, Assoc. Prof. Dr. Şenol ATAOĞLU, Dr. Bahar AYHAN TEZER and Dr. Akif KUTLU for teaching me LATEX and LATEX-Word interaction. By their help, writing my dissertation in correct format was easy. I wish to thank to Assoc. Prof. Dr. Abdullah GEDİKLİ, Erman Yiğit TUNCEL, Gökhan GÜÇLÜ, Arcan YANIK, Gülçin TEKİN, Merve ERMİŞ, Dr. Osman BULUT and other colleagues.

Finally, I express my appreciation to my mother, father and sister for their endless sacrifices. I'm grateful and honored for being a member of this family.

February 10th, 2014 Hasan Faik KARA

TABLE OF CONTENTS

Page

ABBREVIATIONS

SDA **:** Surface Displacement Amplitude

LIST OF FIGURES

Page

WAVE PROPAGATION IN AN ALLUVIAL VALLEY SUBJECTED TO A STRIKE-SLIP FAULT

SUMMARY

Wave propagation in a semi-circular alluvial valley embedded to a half-space has been studied. Alluvial valley and half-space are assumed to be homogeneous, isotropic and linear elastic. Either of the mediums includes a strike-slip fault. Fault trajectory is taken arc-shaped due to mathematical complexity of the problem. Movement of the fault is modeled by defining out-of-plane unit displacement difference between two sides of the arc. Therefore, the problem would be two dimensional and the fault generates only SH waves. Exact solutions in series form have been obtained by using analytical techniques for both static and steady state dynamic fault movement. Wave function expansion method is used for dynamic case. Displacement fields are expressed in terms of Fourier-Bessel series. Unknown complex constants of these series are calculated by applying boundary conditions. For the static case, time dependent parts don't exist so displacement fields are expressed in terms of power series. The following steps of the solution procedure remain same. Both Fourier-Bessel and power series are convergent which makes it possible to obtain numerical results by truncation. For variable positions and lengths of fault, valley radius and material coefficients, displacement and stress could be calculated any point for static case. In addition to static case, displacements and stress could be obtained as a function of time in dynamic case by adding a new variable, wave length. In results section, there are examples that show amplification effects on surface for different parameters. Parameters in length dimension are normalized with respect to valley radius. Several consequences are achieved from surface displacement amplitude profiles. Results show that displacement amplitudes converge to static displacements when wave lengths are relatively long. For shorter wave lengths, displacements differ significantly and changes more rapidly from point to point. Displacements in the surface increase when fault depth decreases for same fault length. Material inhomogeneities play a significant role on displacements. Higher displacements obtained when valley material has lower shear modulus compared to half-space material. When valley material has lower density compared to half-space material, surface displacements increase or decrease for different values of other parameters.

DOĞRULTU ATIMLI FAY ETKİSİNDEKİ ALÜVYONAL VADİDE DALGA YAYILIMI

ÖZET

Yer kabuğu içerisinde depolanmış enerjinin ani bir şekilde açığa çıkması, yer yüzünde bir titreşim hareketi meydana getirir. Bu olaya deprem denir. Depremlerin yer yüzüne olan etkisi büyüklüklük açısından değişiklik gösterir. Küçük depremlerin fark edilir bir etkisi olmazken şiddetli depremler yer üstü ve yer altı yapılarına verecekleri zarar ölçüsünde büyük çapta can ve mal kaybına neden olabilirler. Bu yüzden depremlerin olası etkileri çok önemli bir çalışma konusudur. Depremler, oluş nedenlerine göre üç sınıfa ayrılır, tektonik depremler, volkanik patlamalarla oluşan depremler ve göçük depremleri. En sık rastlanan ve en büyük tehlikeyi yaratan tür tektonik depremlerdir [1]. Tektonik depremler fay kırılmaları ile oluşur. Yer kabuğundaki hareketli tabakaların birleştikleri yüzeylere fay denir. Bu yüzeylerde tabakaların birbirlerine uyguladıkları kuvvet zamanla artar. Bu kuvvet sınır değerin üzerine çıktığında tabakalar ani olarak hareket eder ve büyük bir enerji açığa çıkar. Buna fay kırılması denir. Faylar üç farklı çeşittir, normal fay, ters fay ve doğrultu atımlı fay. Fayın doğrultusu boyunca yatay kaymalara yol açan faylanmalara doğrultu atımlı fay denir.

Bu çalışmanın nihai amacı doğrultu atımlı fay etkisindeki alüvyonal vadide dalga yayılımı probleminin kapalı çözümünü yapmaktır. Problem modeli olarak yarı sonsuz bir ortam ve içerisinde yarım silindirik geometriye sahip alüvyonal vadi kullanılmıştır. Yarı sonsuz ortamın ve vadinin homogen, izotropik ve doğrusal elastik olduğu varsayılmıştır. Ayrıca vadinin ve yarı sonsuz ortamın birlikte çalıştığı kabul edilmiştir. Doğrultu atımlı fay alüvyonal vadide ya da yarı sonsuz ortamda bulunmaktadır. Fay geometrisi, problemin matematiksel karmaşıklığı nedeni ile bir yay parçası olarak alınmıştır. Fay hareketi, fayın iki farklı tarafında düzlem dışı birim yer değiştirme farkı tanımlanarak modellenmiştir. Bu sayede problem iki boyutlu olacaktır ve fay sadece SH dalgaları üretecektir. Analitik yöntemler kullanılarak hem dinamik hem de statik fay hareketi için kesin çözümler sonsuz seri toplamı olarak elde edilmiştir.

Dinamik hal için dalga fonksiyonu açılım tekniği uygulanmıştır. Polar koordinatlarda yazılan dalga denklemi, kararlı hal çözümünün yapılması ile Helmholtz diferansiyel denklemine dönüşür. Helmholtz denklemine çarpanlara ayırma yöntemi uygulandığında çözüm fonksiyonu Fourier-Bessel serileri olarak elde edilir. Bu serilerdeki birinci nevi Hankel fonksiyonları giden dalgalara, ikinci nevi Hankel fonksiyonları gelen dalgalara karşı gelir. Fourier-Bessel serilerindeki bilinmeyen karmaşık katsayılar, sınır koşullarının uygulanması ile elde edilecektir. Fayın iki farklı tarafında birim yer değiştirme farkı tanımlayabilmek için, fayın bulunduğu ortam fay yörüngesi üzerinde iki farklı bölgeye ayrılmıştır. Bu şekildeki yer değiştirme farkı, Heaviside fonksiyonunu kullanılarak ifade edilmiştir. Bu fonksiyonun seri formu da açı değişkeni üzerinde sonlu kompleks Fourier dönüşümü yapılarak elde edilmiştir. Fay bulunduran ortamın fay üzerinde iki farklı bölgeye ayrılması ile birlikte toplamda üç farklı bölge

oluşur. Fay yörüngesi üzerindeki sınırda iki bölgede radyal gerilmeler eşittir. Yer değiştirmeler ise fay dışında eşit, fay içerisine ise bir birim farklıdır. Alüvyonal vadi ile yarı sonsuz ortamın birleştiği yüzeyde ise yer değiştirmeler ve radyal gerilmeler eşittir. Bu şekilde toplamda dört sınır koşulu vardır. Çözüm serilerinden her bölgede iki olmak üzere toplam altı bilinmeyen gelir. Ancak vadi merkezinde yer değiştirmenin sonlu olması ve Sommerfeld koşulu nedeni ile bilinmeyenlerden ikisi çözümden çıkarılır. Geri kalan dört bilinmeyen de dört sınır koşulu kullanılarak hesaplanır. Kapalı formda hesaplanan bilinmeyenler Fourier-Bessel serilerinde yerine yazıldığında, her bölge için yer değiştirme fonksiyonunun kesin çözümü elde edilir.

Statik hal için de çözüm adımları dinamik hal ile benzer şekildedir. Polar koordinatlarda yazılan dalga denkleminde zamana bağlı olan terimlerin atılması ile yönetici denklem, Laplace diferansiyel denklemine dönüşür. Laplace denklemine çarpanlara ayırma yöntemi uygulandığında çözüm fonksiyonu kuvvet serileri olarak elde edilir. Kuvvet serilerinde, argumanı sıfıra giderken değeri sonsuza giden ve argumanı sonsuza giderken değeri sonsuza giden fonksiyonlar içeren iki bağımsız seri çözümü vardır. Dinamik halde olduğu gibi fay içeren ortam fay yörüngesi üzerinde iki bölgeye ayrılır. Bu iki bölge arasında fay içerisinde birim yer değiştirme farkı, fay dışında eşit yer değiştirme tanımlanır. Dinamik hal için bulunan, fayın iki kenarındaki yer değiştirme farkını tanımlayan fonksiyon burada da aynen kullanılabilir. Fay yörüngesi üzerinde iki bölgedeki radyal gerilmeler eşittir. Alüvyonal vadi ve yarım uzay arasındaki gerilme ve süreklilik koşulları ile birlikte toplam dört adet sınır koşulu vardır. Her bölgede iki, toplamda altı çözüm serisi vardır. Ancak alüvyonal vadi merkezinde yer değiştirmenin sonlu olması ve yarıçap değişkeni sonsuza giderken yer değiştirmenin sıfıra gitmesi şartlarından çözüm serilerinden ikisi atılır. Kalan dört çözüm serisinin içindeki bilinmeyen katsayılar da dört sınır koşulundan elde edilir ve yer değiştirmelerin kesin çözümü her ortam için sonsuz kuvvet serisi toplamı formunda elde edilir.

Dinamik ve statik hal için elde edilen kesin çözümler sonsuz seri toplamı şeklindedir. Ancak sayısal sonuçlara ulaşmak için bu serilerin belirli bir sayıda kesilmesi gerekir. Hem Fourier-Bessel serileri hem de kuvvet serileri yakınsak serilerdir, dolayısıyla sonuçlar istenilen hassasiyette elde edilebilir. Genel olarak yüksek frekanslarda uygun mertebe bir yakınsaklık için daha fazla terim alınması gerekir. Çalışmada verilen sayısal çözümlerde serilerin alt ve üst sınırı yüz alınmıştır. Bu sayede oldukça yüksek hassasiyette sonuçlara ulaşılmıştır. Statik hal için doğrultu atımlı fayın konum ve genişlikleri, alüvyonal vadi yarıçapı ve malzeme katsayılarının çeşitli değerleri için istenilen bir noktada yer değiştirme hesaplanabilir. Buna ek olarak dinamik hal için istenilen her noktada yer değiştirmenin zamana bağlı fonksiyonu, dalga boyu değişkeninin eklenmesi ile elde edilebilir. İstenirse her hangi bir noktada gerilme bileşenleri de yer değiştirme fonksiyonlarının türevleri alınarak bulunabilir. Sayısal örneklerde alüvyonal vadi üzerinde ve çevresinde oluşan en büyük yer değiştirmelere ait grafikler verilmiştir. Problemin uzunluk boyutundaki değişkenleri, alüvyonal vadi yarıçapı ile normalize edilmiştir. Alüvyonal vadi ve yarım uzaya ait yoğunluk ve kayma modullerinin oranları kullanılmıştır. Ayrıca kolaylık olması açısından alüvyonal vadi çapının dalga boyuna oranı, η parametresi tariflenmiştir. Yüzey yer değiştirme genliği profillerinden çeşitli sonuçlar elde edilmiştir. η parametresinin küçük değerleri için dinamik ve statik çözümler üst üste düşmüştür. Küçük dalga boylarında yer değiştirmeler büyük farklılıklar göstermiş ve noktadan noktaya olan değişimleri de artmıştır. Fay uzunluğunun aynı olduğu durumda fayın derinliğinin

artmasıyla yüzey yer değiştirmeleri azalmıştır. Ortamdaki malzeme farklılıklarının yüzey yer değiştirmelerine olan etkisinin büyük olduğu görülmüştür. Yarım uzay malzemesinin kayma modülünün vadi malzemesinin kayma modülünden büyük olması durumunda yüzey yer değiştirmeleri büyümektedir. Yarım uzay malzemesinin birim hacim ağırlığının vadi malzemesinin birim hacim ağırlığından daha büyük olduğu durumlarda ise diğer değişkenlerin değelerine göre yer değiştirmeler artmakta ya da azalmaktadır.

1. INTRODUCTION

A sudden release of energy stored in the Earth's crust cause vibration in the surface. This is called Earthquake. Effect of earthquakes to Earth's surface could be minor or major. Small Earthquakes may not be felt whereas major earthquakes can cause catastrophic property and health losses according to their damage to surface and sub-surface structures. So, the possible effects of earthquakes are very important subjects for researchers. Earthquakes are classified into three groups by their mode of generation, which are tectonic earthquakes, volcanic earthquakes and collapse earthquakes. The most common and hazardous are tectonic earthquakes [1]. Tectonic earthquakes are caused by sudden break of faults. Faults are contact surfaces of tectonic plates in the Earth's crust. In these surfaces, tectonic plates apply forces to each other which increase by time. When this force exceed the limit, the plates move suddenly which releases high amount of energy. This is called fault break. There are three types of faults. Normal faults, reverse faults and strike-slip faults. Faulting that causes only horizontal displacements along the strike of the fault are called strike-slip faults. Alluvial deposits, often very irregular geometrically, may affect significantly the amplitudes of incident seismic waves. Since many human settlements are founded on alluvial valleys, it is important for the the design of earthquake resistant structures to study the mechanism of these amplification effects [2].

1.1 Purpose of Thesis

The ultimate purpose of this study is to obtain exact solutions of a semi-circular alluvial valley surrounded by a half-space subjected to a strike-slip fault.

1.2 Literature Review

Seismic response of linear elastic mediums are investigated by many researchers priorly.

The amplification and focusing properties of the semi-cylindrical alluvial valley subjected to incident SH-waves is investigated by Trifunac [2]. In this study, alluvial valley and half-space are assumed to be linear elastic, isotropic and homogeneous. Closed-form analytical solution of two dimensional wave-propagation problem is obtained in terms of Fourier-Bessel series. In the results, complicated wave interference phenomena characterized by nearly-standing wave patterns, rapid changes in the ground motion amplification along the free surface of the valley and significant dependence of motion on the incidence angle of SH waves are demonstrated.

In Another study of Trifunac [3], the two-dimensional scattering and diffraction of plane SH waves by a semi-cylindrical canyon is analyzed for a general angle of wave incidence. Results show that the surface amplification of displacement amplitudes around and in the canyon changes rapidly from one point to another. Two principle parameters that affect amplification patterns are the angle of incidence of plane SH waves and the ratio of radius of the canyon to one-half wave length of incident waves. More complex pattern of surface displacement amplitudes occur for shorter incident wave lengths compared to canyon radius.

The two-dimensional scattering and diffraction of plane SH-waves by a circular cavity in homogeneous elastic half space has been analyzed by Lee [4]. Using exact series solution of the problem for a general angle of wave incidence ground motion near cavity has been studied. Due to the nature of the problem, stress-free boundary condition at the surface of the cavity is defined in cylindrical coordinates whereas at the flat surface, it is defined in cartesian coordinates. In order to satisfy boundary conditions in closed form, imaging technique is used. In this technique, an imaginary cavity is added to the problem so that solution functions defined in polar coordinates directly satisfy stress free condition at flat surface.

Scattering of plane SH waves by a cylindrical alluvial valley of circular-arc cross-section is investigated by Yuan et al. [5]. A closed-form solution of two-dimensional scattering of plane SH waves by a cylindrical alluvial valley of circular-arc cross section in a half space is presented using the wave functions expansion. The solution is reduced to solving a set of infinite linear algebraic equations using the exterior region form of Graf's addition theorem. Numerical solutions are obtained by truncation of the infinite equations and their accuracies are demonstrated

by convergence of the numerical results to the exact boundary condition with the increasing of the truncation order. The present solution is compared with the existing one presented by Todorovska and Lee for the same problem and their differences are analyzed. Complicated effects of the depth-to-width ratio of the alluvial valley on surface ground motion are finally illustrated.

Antiplane response of a dike with flexible soil-structure interface to incident SH waves is investigated by Hayir et al [6]. This paper studies a simple model of a dike but considers both the soil-structure interaction and the flexibility of the foundation. The structure is represented by a wedge resting on a half-space and excited by incident plane SH-waves. The structural 'foundation' is a flexible surface that can deform during the passage of seismic waves. The wave function expansion method is used to solve for the motions in the half-pace and in the structure. The displacements and stresses in the structure are compared with those for a fixed-base model shaken by the free-field motion. The results show large displacements near the base of the structure due to the differential motion of the base caused by the wave passage.

An analytical solution for three-dimensional diffraction of plane p-waves by a hemispherical alluvial valley with saturated soil deposits is obtained by Chenggang et al [7]. Fourier-Bessel series expansion technique and Biot's dynamic theory for saturated porous media are used. The effects of the dimensionless frequency, the incidence angle of P-wave and the porosity of soil deposits on the surface displacement magnifications of the hemispherical alluvial valley are investigated. Numerical results show that the existence of a saturated hemispherical alluvial valley has much influence on the surface displacement magnifications.

Surface motion of multiple alluvial valleys for incident plane SH-waves was investigated by Chen et al [8] using a semi-analytical approach. In this paper, the degenerate kernels and Fourier series expansions are adopted in the null-field integral equation to solve the exterior Helmholtz problems with alluvial valleys. An adaptive observer system is addressed to fully employ the property of degenerate kernels for circular boundaries in the polar coordinate. Image concept and technique of decomposition are utilized for half-plane problems. Earthquake analysis for the site response of alluvial valley or canyon subject to the incident SH-wave is the main

concern. Numerical examples including single and successive alluvial valleys are given. Amplification of soft basin is also observed in this study.

Plane wave approximation on semi-circular alluvial valley was investigated by Kara et al [9]. It is shown that the plane-wave assumption for incident SH waves is a good approximation for cylindrical waves radiated from a finite source even when it is as close as twice the size of inhomogeneity. It is concluded that for out-of-plane SH waves the plane-wave approximation should be adequate for many earthquake engineering studies.

There also other studies [11-20] about wave propagation problems in linear elastic mediums.

1.3 Hypothesis

In the model, alluvial valley is represented by a half circular medium. Valley is surrounded by a semi-infinite medium which has different material properties. Alluvial valley and semi-infinite medium are assumed to be made of homogeneous, isotropic and linear elastic materials. Material properties and geometry does not change along out of plane direction so the problem would be two dimensional. Incident SH waves are produced by a strike-slip fault. Fault movement is modeled by defining unit out-of-plane displacement difference between each side of the fault. In addition to harmonic movement of fault, solutions of static movement of fault is also obtained by solving governing equations using analytical techniques.

2. FUNDAMENTAL EQUATIONS

2.1 Solution of Wave Equation

The equations for a homogeneous isotropic elastic solid may be summarized in Cartesian tensor notation as [10]

$$\tau_{ij,j} + \rho f_i = \rho \ddot{U} \tag{2.1}$$

$$\tau_{ij} = \lambda \varepsilon_{kk} \delta_{ij} + 2\mu \varepsilon_{ij} \tag{2.2}$$

$$\varepsilon_{ij} = \frac{1}{2}\left(U_{i,j} + U_{j,i}\right) \tag{2.3}$$

$$\omega_{ij} = \frac{1}{2}\left(U_{i,j} - U_{j,i}\right) \tag{2.4}$$

where τ_{ij} is the stress tensor, at point and U_i is the displacement vector of a material point. The stress tensor is symmetric, so that $\tau_{ij} = \tau_{ji}$. The mass density per unit mass of material is ρ and f_i is the body force per unit mass of material. The strain and rotation tensors are given by ε_{ij} and ω_{ij} respectively. The elastic constants for the material are λ and μ, the Lame constants. Governing equations in terms of displacements are obtained by substituting the expression for strain into stress-strain relation and that result into the stress equations of motion, giving Navier's equations for the media

$$(\lambda + \mu) U_{j,ji} + \mu U_{i,jj} + \rho f_i = \rho \ddot{U}_i \tag{2.5}$$

The vector equivalent of this expression is

$$(\lambda + \mu) \vec{\nabla} \times \vec{\nabla} \bullet \vec{U} + \mu \Delta \vec{U} + \rho \vec{f} = \rho \ddot{\vec{U}} \tag{2.6}$$

Displacements of a medium subjected to out-of-plane excitation are scalar which makes

$$\mu \Delta U + \rho f = \rho \ddot{U} \tag{2.7}$$

When the body force per unit mass of material is neglected and shear wave speed $c = \sqrt{\mu/\rho}$ introduced, governing wave equation is obtained

$$\Delta U = \frac{1}{c^2}\frac{\partial^2}{\partial t^2}U \tag{2.8}$$

In the wave equation, U is out-of-plane displacement, c is the wave speed, t is time and Δ is Laplace operator. In polar coordinate system, wave equation will be in this form:

$$\left(\frac{\partial^2}{\partial r^2}+\frac{1}{r}\frac{\partial}{\partial r}+\frac{1}{r^2}\frac{\partial^2}{\partial \theta^2}\right)U(r,\theta,t) = \frac{1}{c^2}\frac{\partial^2}{\partial t^2}U(r,\theta,t) \tag{2.9}$$

For steady state case, time dependence will be harmonic such that:

$$U(r,\theta,t) = u(r,\theta)e^{-i\omega t} \tag{2.10}$$

where ω is angular frequency and i is the imaginary unit. When Equation (2.10) is substituted into Equation (2.9) and wave number $k = \omega/c$ is introduced, Helmholtz wave equation is obtained:

$$\left(\frac{\partial^2}{\partial r^2}+\frac{1}{r}\frac{\partial}{\partial r}+\frac{1}{r^2}\frac{\partial^2}{\partial \theta^2}+k^2\right)u(r,\theta) = 0 \tag{2.11}$$

By using separation of variables method, displacement field can be expressed in terms of two functions:

$$u(r,\theta) = R(r)\Theta(\theta) \tag{2.12}$$

When Equation (2.12) is substituted into Equation (2.11), the following Equation is obtained:

$$\frac{r^2}{R(r)}\frac{\partial^2 R(r)}{\partial r^2}+\frac{r}{R(r)}\frac{\partial R(r)}{\partial r}+r^2k^2 = -\frac{1}{\Theta(\theta)}\frac{\partial^2\Theta(\theta)}{\partial\theta^2} \tag{2.13}$$

Since two sides of Equation (2.13) is a function of different variables, it holds only if both sides are equal to a constant. This constant is chosen to be n^2 for convenience. When the differential equation is solved for each variable separately, there follows:

$$\Theta(\theta) = \beta e^{in\theta}+\overline{\beta}e^{-in\theta} \tag{2.14}$$

$$R(r) = \sum_{n=-\infty}^{\infty} A_n C_n(kr) \tag{2.15}$$

Because of periodicity condition, n has to be an integer. In Equation (2.14) β is a complex constant and $\overline{\beta}$ is complex conjugate of β. In Equation (2.15), A_n 's are

complex constants and C_n 's are Bessel functions of order n. When separate solutions are combined:

$$u(r,\theta) = R(r)\Theta(\theta) = \sum_{n=-\infty}^{\infty} A_n C_n(kr)\left(\beta e^{in\theta} + \overline{\beta} e^{-in\theta}\right) \tag{2.16}$$

A simpler form of the solution can be obtained by removing duplications:

$$u(r,\theta) = \sum_{n=-\infty}^{\infty} A_n C_n(kr) e^{in\theta} \tag{2.17}$$

In these Fourier-Bessel series, outgoing waves will be represented by $H_n^{(1)}$ and incoming waves will be represented by $H_n^{(2)}$. $H_n^{(1)}$ and $H_n^{(2)}$ are Bessel functions of the third kind defined by:

$$H_n{}^{(1)}(x) = J_n(x) + iY_n(x) \tag{2.18}$$

$$H_n{}^{(2)}(x) = J_n(x) - iY_n(x) \tag{2.19}$$

2.2 Solution of Laplace Equation

In static solution of the problem there will not be time dependence ($\partial/\partial t = 0$). So, governing equation turns into Laplace equation.

$$\Delta U = 0 \tag{2.20}$$

In cylindrical coordinate system, Laplace equation will be in this form:

$$\left(\frac{\partial^2}{\partial r^2} + \frac{1}{r}\frac{\partial}{\partial r} + \frac{1}{r^2}\frac{\partial^2}{\partial \theta^2}\right) U(r,\theta,t) = 0 \tag{2.21}$$

By using separations of variables method, displacement field can be expressed in terms of two functions:

$$u(r,\theta) = R(r)\Theta(\theta) \tag{2.22}$$

When Equation (2.22) is substituted into equation (2.21), the following equation is obtained:

$$\frac{r^2}{R(r)}\frac{\partial^2 R(r)}{\partial r^2} + \frac{r}{R(r)}\frac{\partial R(r)}{\partial r} = -\frac{1}{\Theta(\theta)}\frac{\partial^2 \Theta(\theta)}{\partial \theta^2} \tag{2.23}$$

Since two sides of Equation (2.23) is a function of different variables, it holds only if both sides are equal to a constant. This constant is chosen to be n^2 for convenience. When the differential equation is solved for each variable separately, there follows:

$$\Theta(\theta) = \beta e^{in\theta} + \overline{\beta} e^{-in\theta} \tag{2.24}$$

$$R(r) = \sum_{n=-\infty}^{\infty} B_{1,n} r^n + B_{2,n} r^{-n} \tag{2.25}$$

Because of periodicity condition, n has to be an integer. In Equation (2.24) β is a complex constant and $\overline{\beta}$ is complex conjugate of β. In Equation (2.25), $B_{1,n}$ and $B_{2,n}$ are real constants. When separate solutions are combined:

$$u(r,\theta) = \sum_{n=-\infty}^{\infty} \left(B_{1,n} r^n + B_{2,n} r^{-n}\right) \beta e^{in\theta} + \left(B_{1,n} r^n + B_{2,n} r^{-n}\right) \bar{\beta} e^{-in\theta} \tag{2.26}$$

A simpler form of the solution can be obtained by removing duplications:

$$u(r,\theta) = \sum_{n=-\infty}^{\infty} \left(B_{1,n} r^n + B_{2,n} r^{-n}\right) e^{in\theta} \tag{2.27}$$

It is convenient to use absolute value of power r

$$u(r,\theta) = \sum_{n=-\infty}^{\infty} A_{1,n} r^{|n|} e^{in\theta} + \sum_{n=-\infty}^{\infty} A_{2,n} r^{-|n|} e^{in\theta} \tag{2.28}$$

such that

$$A_{1,n} = \begin{cases} B_{1,n} & n > 0 \\ B_{2,n} & n < 0 \end{cases} \tag{2.29}$$

$$A_{2,n} = \begin{cases} B_{2,n} & n > 0 \\ B_{1,n} & n < 0 \end{cases} \tag{2.30}$$

3. STEADY STATE WAVE PROPAGATION PROBLEM

3.1 Fault is Inside the Valley Case

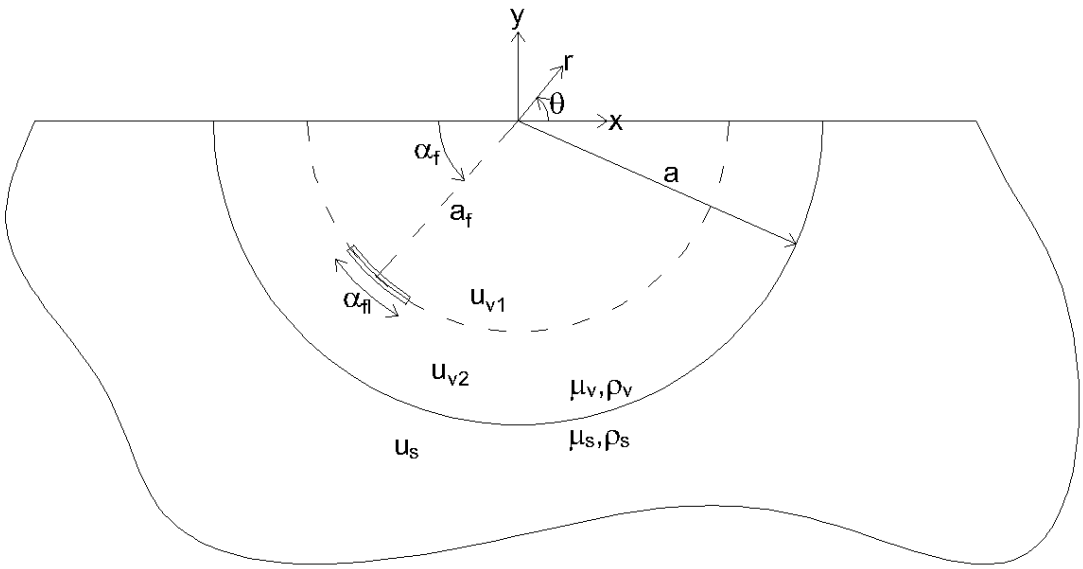

Figure 3.1 : Geometry of the dynamic problem when fault is inside the valley.

The model consist of a half-cylindrical alluvial valley with radius a surrounded by a half-space as shown in Figure (3.1) on page 9. Material properties are given by shear modulus (μ) and density (ρ). Material coefficients of valley and half-space are shown by indice v and s respectively. All materials are assumed to be isotropic, homogeneous and linear elastic. Strike-slip fault is located at $r = a_f$ and $\theta = \pi + \alpha_f$. Therefore, fault length would be $\alpha_{fl} a_f$. There is a unit and uniform displacement difference between two sides of fault. To simulate this motion, valley is divided into two sub-regions, $r < a_f$ and $r > a_f$.

3.1.1 Displacement fields

According to the solution (2.17) on page 7, general form of the displacement fields for each space would be the following form:

$$u_{v1}(r,\theta) = \sum_{n=-\infty}^{\infty} A_{v1h1,n} H_n^{(1)}(k_v r) e^{in\theta} + \sum_{n=-\infty}^{\infty} A_{v1h2,n} H_n^{(2)}(k_v r) e^{in\theta} \quad \textbf{(3.1)}$$

$$u_{v2}(r,\theta) = \sum_{n=-\infty}^{\infty} A_{v2h1,n} H_n^{(1)}(k_v r) e^{in\theta} + \sum_{n=-\infty}^{\infty} A_{v2h2,n} H_n^{(2)}(k_v r) e^{in\theta} \quad \textbf{(3.2)}$$

$$u_{s}(r,\theta) = \sum_{n=-\infty}^{\infty} A_{sh1,n} H_n^{(1)}(k_s r) e^{in\theta} + \sum_{n=-\infty}^{\infty} A_{sh2,n} H_n^{(2)}(k_s r) e^{in\theta} \quad \textbf{(3.3)}$$

Equation 3.1 can also be expressed in terms of J_n and Y_n as follows:

$$u_{v1}(r,\theta) = \sum_{n=-\infty}^{\infty} A_{v1j,n} J_n(k_v r) e^{in\theta} + \sum_{n=-\infty}^{\infty} A_{v1y,n} Y_n(k_v r) e^{in\theta} \quad \textbf{(3.4)}$$

3.1.2 Boundary conditions

Because displacement has to be finite at $r = 0$, $A_{v1y,n}$ would be zero. Due to Sommerfeld radiation condition, there would not be incoming waves from infinity which makes $A_{sh2,n} = 0$. Remaining potentials are:

$$u_{v1}(r,\theta) = \sum_{n=-\infty}^{\infty} A_{v1j,n} J_n(k_v r) e^{in\theta} \quad \textbf{(3.5)}$$

$$u_{v2}(r,\theta) = \sum_{n=-\infty}^{\infty} A_{v2h1,n} H_n^{(1)}(k_v r) e^{in\theta} + \sum_{n=-\infty}^{\infty} A_{v2h2,n} H_n^{(2)}(k_v r) e^{in\theta} \quad \textbf{(3.6)}$$

$$u_{s}(r,\theta) = \sum_{n=-\infty}^{\infty} A_{sh1,n} H_n^{(1)}(k_s r) e^{in\theta} \quad \textbf{(3.7)}$$

Due to stress-free boundary condition on flat surface, displacement fields have to satisfy following boundary condition.

$$\frac{\mu_v}{r}\frac{\partial}{\partial r} u_{v1}(r,\theta=0,\pi) = \frac{\mu_v}{r}\frac{\partial}{\partial r} u_{v2}(r,\theta=0,\pi) = \frac{\mu_s}{r}\frac{\partial}{\partial r} u_{s}(r,\theta=0,\pi) = 0 \quad \textbf{(3.8)}$$

Since out-of-plane waves reflect with same angle from flat surfaces, this condition would be automatically satisfied by imaging method. In this technique, an imaginary fault symmetric with respect to flat surface is placed. There is unit displacement difference between divided regions of valley on fault (at $r = a_f$ and θ is between $\pi + \alpha_f - \alpha_{fl}/2$ and $\pi + \alpha_f - \alpha_{fl}/2$) and zero elsewhere. When $\alpha_1 = \pi + \alpha_f - \alpha_{fl}/2$ and $\alpha_2 = \pi + \alpha_f - \alpha_{fl}/2$ are introduced as new variables for convenience, this condition could be expressed by a $f(\theta)$ function given below by the help of Heaviside step function:

$$f(\theta) = (H(\theta - \alpha_1) - H(\theta - \alpha_2)) + (H(\theta - (2\pi - \alpha_2)) - H(\theta - (2\pi - \alpha_1))) \quad \textbf{(3.9)}$$

Such that

$$H(\xi) = \begin{cases} 0 & \xi < 0 \\ 1 & \xi \geq 0 \end{cases} \tag{3.10}$$

Hence, displacement relation between divided regions of valley would be in the following form:

$$u_{v1}(r = a_f, \theta) - u_{v2}(r = a_f, \theta) = f(\theta) \tag{3.11}$$

Stress is continuous between divided regions such that

$$\mu_v \frac{\partial}{\partial r} u_{v1}(r = a_f, \theta) - \mu_v \frac{\partial}{\partial r} u_{v2}(r = a_f, \theta) = 0 \tag{3.12}$$

On the interface between valley and half-space, there are continuity of displacement and stress:

$$u_{v2}(r = a, \theta) - u_s(r = a, \theta) = 0 \tag{3.13}$$

$$\mu_v \frac{\partial}{\partial r} u_{v2}(r = a, \theta) - \mu_s \frac{\partial}{\partial r} u_s(r = a, \theta) = 0 \tag{3.14}$$

3.1.3 Linear systems of equations

Since displacement fields are in series form, it is convenient to express $f(\theta)$ in series form. Series form of $f(\theta)$ could be obtained by evaluating its finite Fourier transform and inverse.

$$\hat{f}(n) = \frac{1}{2\pi} \int_0^{2\pi} f(\theta) e^{-in\theta} d\theta \tag{3.15}$$

$$f(\theta) = \sum_{n=-\infty}^{\infty} \hat{f}(n) e^{in\theta} \tag{3.16}$$

For $\pi \leq \alpha_1 < \alpha_2 \leq 2\pi$ and $n \in \mathbb{Z}$, $\hat{f}(n)$ would be in this form:

$$\hat{f}(n) = \begin{cases} i\left(-e^{-i\alpha_1 n} + e^{i\alpha_1 n} + e^{-i\alpha_2 n} - e^{i\alpha_2 n}\right)/(2\pi n) & n \neq 0 \\ (\alpha_2 - \alpha_1)/\pi & n = 0 \end{cases} \tag{3.17}$$

When displacement fields (3.5)-(3.7) are substituted into boundary conditions (3.11)-(3.14), following equations are obtained.

$$\sum_{n=-\infty}^{\infty} \left(A_{v1j,n} J_n(k_v a_f) - A_{v2h1,n} H_n^{(1)}(k_v a_f) - A_{v2h2,n} H_n^{(2)}(k_v a_f) - \hat{f}(n) \right) e^{in\theta} = 0 \tag{3.18}$$

$$\sum_{n=-\infty}^{\infty}\Bigg(A_{v1j,n}\frac{k_v\mu_v}{2}(J_{n-1}(k_va_f)-J_{n+1}(k_va_f))- A_{v2h1,n}\frac{k_v\mu_v}{2}(H^{(1)}_{n-1}(k_va_f)-H^{(1)}_{n+1}(k_va_f))- A_{v2h2,n}\frac{k_v\mu_v}{2}(H^{(2)}_{n-1}(k_va_f)-H^{(2)}_{n+1}(k_va_f))\Bigg)e^{in\theta}=0 \tag{3.19}$$

$$\sum_{n=-\infty}^{\infty}\Big(A_{v2h1,n}H^{(1)}_n(k_va)+A_{v2h2,n}H^{(2)}_n(k_va)- A_{sh1,n}(H^{(1)}_n(k_sa))\Big)e^{in\theta}=0 \tag{3.20}$$

$$\sum_{n=-\infty}^{\infty}\Bigg(A_{v2h1,n}\frac{k_v\mu_v}{2}(H^{(1)}_{n-1}(k_va)-H^{(1)}_{n+1}(k_va))+ A_{v2h2,n}\frac{k_v\mu_v}{2}(H^{(2)}_{n-1}(k_va)-H^{(2)}_{n+1}(k_va))- A_{sh1,n}\frac{k_s\mu_s}{2}(H^{(1)}_{n-1}(k_sa)-H^{(1)}_{n+1}(k_sa))\Bigg)e^{in\theta}=0 \tag{3.21}$$

Since four equations above have to hold for all θ, coefficients of $e^{in\theta}$ have to be equal to zero for all integer values of n such that:

$$A_{v1j,n}J_n(k_va_f)-A_{v2h1,n}H^{(1)}_n(k_va_f)- A_{v2h2,n}H^{(2)}_n(k_va_f)-\hat{f}(n)=0 \tag{3.22}$$

$$A_{v1j,n}\frac{k_v\mu_v}{2}(J_{n-1}(k_va_f)-J_{n+1}(k_va_f))- A_{v2h1,n}\frac{k_v\mu_v}{2}(H^{(1)}_{n-1}(k_va_f)-H^{(1)}_{n+1}(k_va_f))- A_{v2h2,n}\frac{k_v\mu_v}{2}(H^{(2)}_{n-1}(k_va_f)-H^{(2)}_{n+1}(k_va_f))=0 \tag{3.23}$$

$$A_{v2h1,n}H^{(1)}_n(k_va)+A_{v2h2,n}H^{(2)}_n(k_va)- A_{sh1,n}(H^{(1)}_n(k_sa))=0 \tag{3.24}$$

$$A_{v2h1,n}\frac{k_v\mu_v}{2}(H^{(1)}_{n-1}(k_va)-H^{(1)}_{n+1}(k_va))+ A_{v2h2,n}\frac{k_v\mu_v}{2}(H^{(2)}_{n-1}(k_va)-H^{(2)}_{n+1}(k_va))- A_{sh1,n}\frac{k_s\mu_s}{2}(H^{(1)}_{n-1}(k_sa)-H^{(1)}_{n+1}(k_sa))=0 \tag{3.25}$$

When these four equations are solved simultaneously, unknowns could be calculated as follows:

$$
\begin{aligned}
A_{v1\,j,n} = -(\hat{f}(n)(((H_{n-1}^{(1)}(k_v a_f) - H_{n+1}^{(1)}(k_v a_f))H_n^{(2)}(k_v a_f) + \\
H_n^{(1)}(k_v a_f)(H_{n+1}^{(2)}(k_v a_f) - H_{n-1}^{(2)}(k_v a_f))) \\
(k_s \mu_s H_{n-1}^{(1)}(k_s a)H_n^{(2)}(k_v a) - k_s \mu_s H_{n+1}^{(1)}(k_s a)H_n^{(2)}(k_v a) + \\
k_v \mu_v H_n^{(1)}(k_s a)(H_{n+1}^{(2)}(k_v a) - H_{n-1}^{(2)}(k_v a))) + \\
(H_{n-1}^{(2)}(k_v a_f) - H_{n+1}^{(2)}(k_v a_f))(H_n^{(1)}(k_v a_f)(k_s \mu_s (H_{n-1}^{(1)}(k_s a) - H_{n+1}^{(1)}(k_s a)) \\
H_n^{(2)}(k_v a) - k_v \mu_v H_n^{(1)}(k_s a)(H_{n-1}^{(2)}(k_v a) - H_{n+1}^{(2)}(k_v a))) - \\
H_n^{(2)}(k_v a_f)(k_s \mu_s (H_{n-1}^{(1)}(k_s a) - H_{n+1}^{(1)}(k_s a))H_n^{(1)}(k_v a) - \\
k_v \mu_v H_n^{(1)}(k_s a)(H_{n-1}^{(1)}(k_v a) - H_{n+1}^{(1)}(k_v a)))))) / \\
(J_n(k_v a_f)((H_{n+1}^{(1)}(k_v a_f) - H_{n-1}^{(1)}(k_v a_f))H_n^{(2)}(k_v a_f) + \\
H_n^{(1)}(k_v a_f)(H_{n-1}^{(2)}(k_v a_f) - H_{n+1}^{(2)}(k_v a_f))) \\
(k_s \mu_s H_{n-1}^{(1)}(k_s a)H_n^{(2)}(k_v a) - k_s \mu_s H_{n+1}^{(1)}(k_s a)H_n^{(2)}(k_v a) + \\
k_v \mu_v H_n^{(1)}(k_s a)(H_{n+1}^{(2)}(k_v a) - H_{n-1}^{(2)}(k_v a))) - \\
(J_n(k_v a_f)(H_{n-1}^{(2)}(k_v a_f) - H_{n+1}^{(2)}(k_v a_f)) - \\
(J_{n-1}(k_v a_f) - J_{n+1}(k_v a_f))H_n^{(2)}(k_v a_f)) \\
(H_n^{(1)}(k_v a_f)(k_s \mu_s (H_{n-1}^{(1)}(k_s a) - H_{n+1}^{(1)}(k_s a))H_n^{(2)}(k_v a) - \\
k_v \mu_v H_n^{(1)}(k_s a)(H_{n-1}^{(2)}(k_v a) - H_{n+1}^{(2)}(k_v a))) - \\
H_n^{(2)}(k_v a_f)(k_s \mu_s (H_{n-1}^{(1)}(k_s a) - H_{n+1}^{(1)}(k_s a))H_n^{(1)}(k_v a) - \\
k_v \mu_v H_n^{(1)}(k_s a)(H_{n-1}^{(1)}(k_v a) - H_{n+1}^{(1)}(k_v a)))))
\end{aligned}
\tag{3.26}
$$

$$
\begin{aligned}
A_{v2h1,n} = (\hat{f}(n)(H^{(2)}_{n+1}(k_v a_f) - H^{(2)}_{n-1}(k_v a_f)))/ \\
((H^{(1)}_{n+1}(k_v a_f) - H^{(1)}_{n-1}(k_v a_f))H^{(2)}_n(k_v a_f) + \\
H^{(1)}_n(k_v a_f)(H^{(2)}_{n-1}(k_v a_f) - H^{(2)}_{n+1}(k_v a_f))) + \\
(\hat{f}(n)(J_n(k_v a_f)(H^{(2)}_{n-1}(k_v a_f) - H^{(2)}_{n+1}(k_v a_f)) - (J_{n-1}(k_v a_f) - J_{n+1}(k_v a_f)) \\
H^{(2)}_n(k_v a_f))(((H^{(1)}_{n-1}(k_v a_f) - H^{(1)}_{n+1}(k_v a_f))H^{(2)}_n(k_v a_f) + \\
H^{(1)}_n(k_v a_f)(H^{(2)}_{n+1}(k_v a_f) - H^{(2)}_{n-1}(k_v a_f))) \\
(H^{(1)}_{n-1}(k_s a)H^{(2)}_n(k_v a)k_s\mu_s - H^{(1)}_{n+1}(k_s a)H^{(2)}_n(k_v a)k_s\mu_s + \\
H^{(1)}_n(k_s a)(H^{(2)}_{n+1}(k_v a) - H^{(2)}_{n-1}(k_v a))k_v\mu_v) + \\
(H^{(2)}_{n-1}(k_v a_f) - H^{(2)}_{n+1}(k_v a_f)) \\
(H^{(1)}_n(k_v a_f)((H^{(1)}_{n-1}(k_s a) - H^{(1)}_{n+1}(k_s a))H^{(2)}_n(k_v a)k_s\mu_s - \\
H^{(1)}_n(k_s a)(H^{(2)}_{n-1}(k_v a) - H^{(2)}_{n+1}(k_v a))k_v\mu_v) - \\
H^{(2)}_n(k_v a_f)(H^{(1)}_n(k_v a)(H^{(1)}_{n-1}(k_s a) - H^{(1)}_{n+1}(k_s a))k_s\mu_s - \\
H^{(1)}_n(k_s a)(H^{(1)}_{n-1}(k_v a) - H^{(1)}_{n+1}(k_v a))k_v\mu_v)))))/ \qquad \textbf{(3.27)} \\
(((H^{(1)}_{n-1}(k_v a_f) - H^{(1)}_{n+1}(k_v a_f))H^{(2)}_n(k_v a_f) + H^{(1)}_n(k_v a_f) \\
(H^{(2)}_{n+1}(k_v a_f) - H^{(2)}_{n-1}(k_v a_f))) \\
(J_n(k_v a_f)((H^{(1)}_{n+1}(k_v a_f) - H^{(1)}_{n-1}(k_v a_f))H^{(2)}_n(k_v a_f) + \\
H^{(1)}_n(k_v a_f)(H^{(2)}_{n-1}(k_v a_f) - H^{(2)}_{n+1}(k_v a_f))) \\
(H^{(1)}_{n-1}(k_s a)H^{(2)}_n(k_v a)k_s\mu_s - H^{(1)}_{n+1}(k_s a)H^{(2)}_n(k_v a)k_s\mu_s + \\
H^{(1)}_n(k_s a)(H^{(2)}_{n+1}(k_v a) - H^{(2)}_{n-1}(k_v a))k_v\mu_v) - \\
(J_n(k_v a_f)(H^{(2)}_{n-1}(k_v a_f) - H^{(2)}_{n+1}(k_v a_f)) - \\
(J_{n-1}(k_v a_f) - J_{n+1}(k_v a_f))H^{(2)}_n(k_v a_f)) \\
(H^{(1)}_n(k_v a_f)((H^{(1)}_{n-1}(k_s a) - H^{(1)}_{n+1}(k_s a))H^{(2)}_n(k_v a)k_s\mu_s - \\
H^{(1)}_n(k_s a)(H^{(2)}_{n-1}(k_v a) - H^{(2)}_{n+1}(k_v a))k_v\mu_v) - \\
H^{(2)}_n(k_v a_f)(H^{(1)}_n(k_v a)(H^{(1)}_{n-1}(k_s a) - H^{(1)}_{n+1}(k_s a))k_s\mu_s - \\
H^{(1)}_n(k_s a)(H^{(1)}_{n-1}(k_v a) - H^{(1)}_{n+1}(k_v a))k_v\mu_v))))
\end{aligned}
$$

$$
\begin{aligned}
A_{v2h2,n} = (\hat{f}(n)(-H_{n-1}^{(1)}(k_v a_f) + H_{n+1}^{(1)}(k_v a_f) + \\
((-J_n(k_v a_f)H_{n-1}^{(1)}(k_v a_f) + (J_{n-1}(k_v a_f) - J_{n+1}(k_v a_f))H_n^{(1)}(k_v a_f) + \\
J_n(k_v a_f)H_{n+1}^{(1)}(k_v a_f))(((H_{n-1}^{(1)}(k_v a_f) - H_{n+1}^{(1)}(k_v a_f))H_n^{(2)}(k_v a_f) + \\
H_n^{(1)}(k_v a_f)(H_{n+1}^{(2)}(k_v a_f) - H_{n-1}^{(2)}(k_v a_f))) \\
(H_{n-1}^{(1)}(k_s a)H_n^{(2)}(k_v a)k_s\mu_s - H_{n+1}^{(1)}(k_s a)H_n^{(2)}(k_v a)k_s\mu_s + H_n^{(1)}(k_s a) \\
(H_{n+1}^{(2)}(k_v a) - H_{n-1}^{(2)}(k_v a))k_v\mu_v) + (H_{n-1}^{(2)}(k_v a_f) - H_{n+1}^{(2)}(k_v a_f)) \\
(H_n^{(1)}(k_v a_f)((H_{n-1}^{(1)}(k_s a) - H_{n+1}^{(1)}(k_s a))H_n^{(2)}(k_v a)k_s\mu_s - \\
H_n^{(1)}(k_s a)(H_{n-1}^{(2)}(k_v a) - H_{n+1}^{(2)}(k_v a))k_v\mu_v) - \\
H_n^{(2)}(k_v a_f)(H_n^{(1)}(k_v a)(H_{n-1}^{(1)}(k_s a) - H_{n+1}^{(1)}(k_s a))k_s\mu_s - \\
H_n^{(1)}(k_s a)(H_{n-1}^{(1)}(k_v a) - H_{n+1}^{(1)}(k_v a))k_v\mu_v)))) / \\
(J_n(k_v a_f)((H_{n+1}^{(1)}(k_v a_f) - H_{n-1}^{(1)}(k_v a_f))H_n^{(2)}(k_v a_f) + \\
H_n^{(1)}(k_v a_f)(H_{n-1}^{(2)}(k_v a_f) - H_{n+1}^{(2)}(k_v a_f))) \\
(H_{n-1}^{(1)}(k_s a)H_n^{(2)}(k_v a)k_s\mu_s - H_{n+1}^{(1)}(k_s a)H_n^{(2)}(k_v a)k_s\mu_s + \\
H_n^{(1)}(k_s a)(H_{n+1}^{(2)}(k_v a) - H_{n-1}^{(2)}(k_v a))k_v\mu_v) - \\
(J_n(k_v a_f)(H_{n-1}^{(2)}(k_v a_f) - H_{n+1}^{(2)}(k_v a_f)) - \\
(J_{n-1}(k_v a_f) - J_{n+1}(k_v a_f))H_n^{(2)}(k_v a_f)) \\
(H_n^{(1)}(k_v a_f)((H_{n-1}^{(1)}(k_s a) - H_{n+1}^{(1)}(k_s a))H_n^{(2)}(k_v a)k_s\mu_s - \\
H_n^{(1)}(k_s a)(H_{n-1}^{(2)}(k_v a) - H_{n+1}^{(2)}(k_v a))k_v\mu_v) - \\
H_n^{(2)}(k_v a_f)(H_n^{(1)}(k_v a)(H_{n-1}^{(1)}(k_s a) - H_{n+1}^{(1)}(k_s a))k_s\mu_s - \\
H_n^{(1)}(k_s a)(H_{n-1}^{(1)}(k_v a) - H_{n+1}^{(1)}(k_v a))k_v\mu_v))))) / \\
((H_{n-1}^{(1)}(k_v a_f) - H_{n+1}^{(1)}(k_v a_f))H_n^{(2)}(k_v a_f) + \\
H_n^{(1)}(k_v a_f)(H_{n+1}^{(2)}(k_v a_f) - H_{n-1}^{(2)}(k_v a_f)))
\end{aligned}
\tag{3.28}
$$

$$
\begin{aligned}
A_{sh1,n} = (\hat{f}(n)(J_{n-1}(k_v a_f) - \\
J_{n+1}(k_v a_f))((H^{(1)}_{n+1}(k_v a) - H^{(1)}_{n-1}(k_v a))H^{(2)}_n(k_v a) + \\
H^{(1)}_n(k_v a)(H^{(2)}_{n-1}(k_v a) - H^{(2)}_{n+1}(k_v a)))k_v\mu_v)/ \\
(J_n(k_v a_f)H^{(1)}_{n-1}(k_v a_f)H^{(1)}_{n+1}(k_s a)H^{(2)}_n(k_v a)k_s\mu_s - \\
J_{n-1}(k_v a_f)H^{(1)}_n(k_v a_f)H^{(1)}_{n+1}(k_s a)H^{(2)}_n(k_v a)k_s\mu_s + \\
J_{n+1}(k_v a_f)H^{(1)}_n(k_v a_f)H^{(1)}_{n+1}(k_s a)H^{(2)}_n(k_v a)k_s\mu_s - \\
J_n(k_v a_f)H^{(1)}_{n+1}(k_s a)H^{(1)}_{n+1}(k_v a_f)H^{(2)}_n(k_v a)k_s\mu_s + H^{(1)}_n(k_v a) \\
H^{(1)}_{n+1}(k_s a)(-J_n(k_v a_f)H^{(2)}_{n-1}(k_v a_f) + (J_{n-1}(k_v a_f) - J_{n+1}(k_v a_f)) \\
H^{(2)}_n(k_v a_f) + J_n(k_v a_f)H^{(2)}_{n+1}(k_v a_f))k_s\mu_s + \\
H^{(1)}_{n-1}(k_s a)((-J_n(k_v a_f)H^{(1)}_{n-1}(k_v a_f) + (J_{n-1}(k_v a_f) - J_{n+1}(k_v a_f)) \\
H^{(1)}_n(k_v a_f) + J_n(k_v a_f)H^{(1)}_{n+1}(k_v a_f))H^{(2)}_n(k_v a) + \\
H^{(1)}_n(k_v a)(J_n(k_v a_f)H^{(2)}_{n-1}(k_v a_f) + (J_{n+1}(k_v a_f) - J_{n-1}(k_v a_f)) \\
H^{(2)}_n(k_v a_f) - J_n(k_v a_f)H^{(2)}_{n+1}(k_v a_f)))k_s\mu_s + \\
J_n(k_v a_f)H^{(1)}_{n-1}(k_v a_f)H^{(1)}_n(k_s a)H^{(2)}_{n-1}(k_v a)k_v\mu_v - \\
J_{n-1}(k_v a_f)H^{(1)}_n(k_s a)H^{(1)}_n(k_v a_f)H^{(2)}_{n-1}(k_v a)k_v\mu_v + \\
J_{n+1}(k_v a_f)H^{(1)}_n(k_s a)H^{(1)}_n(k_v a_f)H^{(2)}_{n-1}(k_v a)k_v\mu_v - \\
J_n(k_v a_f)H^{(1)}_n(k_s a)H^{(1)}_{n+1}(k_v a_f)H^{(2)}_{n-1}(k_v a)k_v\mu_v - \\
J_n(k_v a_f)H^{(1)}_{n-1}(k_v a)H^{(1)}_n(k_s a)H^{(2)}_{n-1}(k_v a_f)k_v\mu_v + \\
J_n(k_v a_f)H^{(1)}_n(k_s a)H^{(1)}_{n+1}(k_v a)H^{(2)}_{n-1}(k_v a_f)k_v\mu_v + \\
J_{n-1}(k_v a_f)H^{(1)}_{n-1}(k_v a)H^{(1)}_n(k_s a)H^{(2)}_n(k_v a_f)k_v\mu_v - \\
J_{n+1}(k_v a_f)H^{(1)}_{n-1}(k_v a)H^{(1)}_n(k_s a)H^{(2)}_n(k_v a_f)k_v\mu_v - \\
J_{n-1}(k_v a_f)H^{(1)}_n(k_s a)H^{(1)}_{n+1}(k_v a)H^{(2)}_n(k_v a_f)k_v\mu_v + \\
J_{n+1}(k_v a_f)H^{(1)}_n(k_s a)H^{(1)}_{n+1}(k_v a)H^{(2)}_n(k_v a_f)k_v\mu_v - \\
J_n(k_v a_f)H^{(1)}_{n-1}(k_v a_f)H^{(1)}_n(k_s a)H^{(2)}_{n+1}(k_v a)k_v\mu_v + \\
J_{n-1}(k_v a_f)H^{(1)}_n(k_s a)H^{(1)}_n(k_v a_f)H^{(2)}_{n+1}(k_v a)k_v\mu_v - \\
J_{n+1}(k_v a_f)H^{(1)}_n(k_s a)H^{(1)}_n(k_v a_f)H^{(2)}_{n+1}(k_v a)k_v\mu_v + \\
J_n(k_v a_f)H^{(1)}_n(k_s a)H^{(1)}_{n+1}(k_v a_f)H^{(2)}_{n+1}(k_v a)k_v\mu_v + \\
J_n(k_v a_f)H^{(1)}_{n-1}(k_v a)H^{(1)}_n(k_s a)H^{(2)}_{n+1}(k_v a_f)k_v\mu_v - \\
J_n(k_v a_f)H^{(1)}_n(k_s a)H^{(1)}_{n+1}(k_v a)H^{(2)}_{n+1}(k_v a_f)k_v\mu_v)
\end{aligned}
\tag{3.29}
$$

3.2 Fault is Inside the Half-Space Case

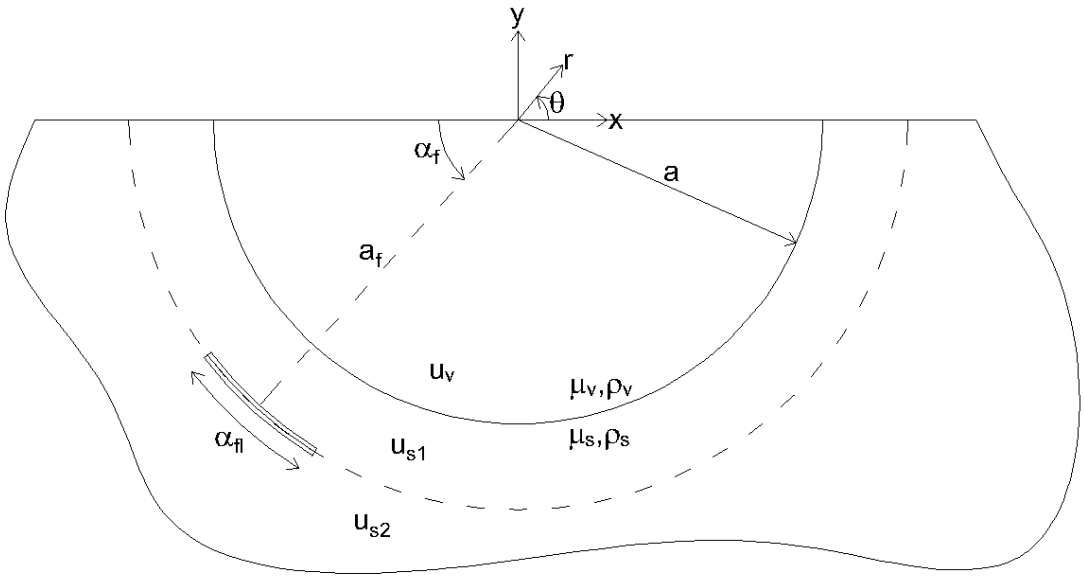

Figure 3.2 : Geometry of the dynamic problem when fault is inside the half space.

In this case, the fault inside the half-space. Solution technique is the same as the previous case, but displacement fields and boundary conditions are different.

3.2.1 Displacement fields

When solution (2.17) on page 7 is used and the terms in solutions which does not satisfy finite displacement in the center and Sommerfeld condtion are omitted, remaining displacement fields would be as follows:

$$u_v(r,\theta) = \sum_{n=-\infty}^{\infty} A_{vj,n} J_n(k_v r) e^{in\theta} \tag{3.30}$$

$$u_{s1}(r,\theta) = \sum_{n=-\infty}^{\infty} A_{s1h1,n} H_n^{(1)}(k_s r) e^{in\theta} + \sum_{n=-\infty}^{\infty} A_{s1h2,n} H_n^{(2)}(k_s r) e^{in\theta} \tag{3.31}$$

$$u_{s2}(r,\theta) = \sum_{n=-\infty}^{\infty} A_{s2h1,n} H_n^{(1)}(k_s r) e^{in\theta} \tag{3.32}$$

3.2.2 Boundary conditions

Boundary conditions between divided regions would be in the following form:

$$u_v(r=a,\theta) - u_{s1}(r=a,\theta) = 0 \tag{3.33}$$

$$\mu_v \frac{\partial}{\partial r} u_v(r=a,\theta) - \mu_s \frac{\partial}{\partial r} u_{s1}(r=a,\theta) = 0 \tag{3.34}$$

$$u_{s1}(r=a_f,\theta) - u_{s2}(r=a_f,\theta) = f(\theta) \tag{3.35}$$

$$\mu_s \frac{\partial}{\partial r} u_{s1}(r=a_f,\theta) - \mu_s \frac{\partial}{\partial r} u_{s2}(r=a_f,\theta) = 0 \tag{3.36}$$

$f(\theta)$ in (3.35) is defined in (3.16) on page 11 which assures the zero stress conditions on flat surfaces.

3.2.3 Linear systems of equations

When displacement fields (3.30)-(3.32) are substituted into boundary conditions (3.33)-(3.36), following equations are obtained.

$$\sum_{n=-\infty}^{\infty} \Big(A_{vj,n} J_n(k_v a) - A_{s1h1,n} H_n^{(1)}(k_s a) - A_{s1h2,n} H_n^{(2)}(k_s a) \Big) e^{in\theta} = 0 \tag{3.37}$$

$$\sum_{n=-\infty}^{\infty} \Big(A_{vj,n} \frac{k_v \mu_v}{2} (J_{n-1}(k_v a) - J_{n+1}(k_v a)) - A_{s1h1,n} \frac{k_s \mu_s}{2} (H_{n-1}^{(1)}(k_s a) - H_{n+1}^{(1)}(k_s a)) - A_{s1h2,n} \frac{k_s \mu_s}{2} (H_{n-1}^{(2)}(k_s a) - H_{n+1}^{(2)}(k_s a)) \Big) e^{in\theta} = 0 \tag{3.38}$$

$$\sum_{n=-\infty}^{\infty} \Big(A_{s1h1,n} H_n^{(1)}(k_s a_f) + A_{s1h2,n} H_n^{(2)}(k_s a_f) - A_{s2h1,n} (H_n^{(1)}(k_s a_f)) - \hat{f}(n) \Big) e^{in\theta} = 0 \tag{3.39}$$

$$\sum_{n=-\infty}^{\infty} \Big(A_{s1h1,n} \frac{k_s \mu_s}{2} (H_{n-1}^{(1)}(k_s a_f) - H_{n+1}^{(1)}(k_s a_f)) + A_{s1h2,n} \frac{k_s \mu_s}{2} (H_{n-1}^{(2)}(k_s a_f) - H_{n+1}^{(2)}(k_s a_f)) - A_{s2h1,n} \frac{k_s \mu_s}{2} (H_{n-1}^{(1)}(k_s a_f) - H_{n+1}^{(1)}(k_s a_f)) \Big) e^{in\theta} = 0 \tag{3.40}$$

Since four equations above have to hold for all θ, coefficients of $e^{in\theta}$ have to be equal to zero for all integer values of n such that:

$$A_{vj,n}J_n(k_va) - A_{s1h1,n}H_n^{(1)}(k_sa) - A_{s1h2,n}H_n^{(2)}(k_sa) = 0 \tag{3.41}$$

$$A_{vj,n}\frac{k_v\mu_v}{2}(J_{n-1}(k_va) - J_{n+1}(k_va)) - A_{s1h1,n}\frac{k_s\mu_s}{2}(H_{n-1}^{(1)}(k_sa) - H_{n+1}^{(1)}(k_sa)) - A_{s1h2,n}\frac{k_s\mu_s}{2}(H_{n-1}^{(2)}(k_sa) - H_{n+1}^{(2)}(k_sa)) = 0 \tag{3.42}$$

$$A_{s1h1,n}H_n^{(1)}(k_sa_f) + A_{s1h2,n}H_n^{(2)}(k_sa_f) - A_{s2h1,n}(H_n^{(1)}(k_sa_f)) - \hat{f}(n) = 0 \tag{3.43}$$

$$A_{s1h1,n}\frac{k_s\mu_s}{2}(H_{n-1}^{(1)}(k_sa_f) - H_{n+1}^{(1)}(k_sa_f)) + A_{s1h2,n}\frac{k_s\mu_s}{2}(H_{n-1}^{(2)}(k_sa_f) - H_{n+1}^{(2)}(k_sa_f)) - A_{s2h1,n}\frac{k_s\mu_s}{2}(H_{n-1}^{(1)}(k_sa_f) - H_{n+1}^{(1)}(k_sa_f)) = 0 \tag{3.44}$$

When these four equations are solved simultaneously, unknowns could be calculated as follows:

$$\begin{aligned} A_{vj,n} = {} & (\hat{f}(n)k_s\mu_s(H_{n-1}^{(1)}(k_sa_f) - H_{n+1}^{(1)}(k_sa_f)) \\ & ((H_{n+1}^{(1)}(k_sa) - H_{n-1}^{(1)}(k_sa))H_n^{(2)}(k_sa) + \\ & H_n^{(1)}(k_sa)(H_{n-1}^{(2)}(k_sa) - H_{n+1}^{(2)}(k_sa)))) / \\ & (((H_{n+1}^{(1)}(k_sa_f) - H_{n-1}^{(1)}(k_sa_f))H_n^{(2)}(k_sa_f) + \\ & H_n^{(1)}(k_sa_f)(H_{n-1}^{(2)}(k_sa_f) - H_{n+1}^{(2)}(k_sa_f))) \\ & (k_s\mu_sH_{n-1}^{(1)}(k_sa)J_n(k_va) - k_s\mu_sH_{n+1}^{(1)}(k_sa)J_n(k_va) + \\ & k_v\mu_vH_n^{(1)}(k_sa)(J_{n+1}(k_va) - J_{n-1}(k_va)))) \end{aligned} \tag{3.45}$$

$$
\begin{aligned}
A_{s1h1,n} = (\hat{f}(n)(H_{n-1}^{(1)}(k_s a_f) - H_{n+1}^{(1)}(k_s a_f))\\
(k_s \mu_s H_{n-1}^{(2)}(k_s a) J_n(k_v a) - k_s \mu_s H_{n+1}^{(2)}(k_s a) J_n(k_v a) +\\
k_v \mu_v H_n^{(2)}(k_s a)(J_{n+1}(k_v a) - J_{n-1}(k_v a))))/\\
(((H_{n+1}^{(1)}(k_s a_f) - H_{n-1}^{(1)}(k_s a_f)) H_n^{(2)}(k_s a_f) +\\
H_n^{(1)}(k_s a_f)(H_{n-1}^{(2)}(k_s a_f) - H_{n+1}^{(2)}(k_s a_f)))\\
(k_s \mu_s H_{n-1}^{(1)}(k_s a) J_n(k_v a) - k_s \mu_s H_{n+1}^{(1)}(k_s a) J_n(k_v a) +\\
k_v \mu_v H_n^{(1)}(k_s a)(J_{n+1}(k_v a) - J_{n-1}(k_v a))))
\end{aligned}
\tag{3.46}
$$

$$
\begin{aligned}
A_{s1h2,n} = (\hat{f}(n)(H_{n-1}^{(1)}(k_s a_f) - H_{n+1}^{(1)}(k_s a_f)))/\\
((H_{n-1}^{(1)}(k_s a_f) - H_{n+1}^{(1)}(k_s a_f)) H_n^{(2)}(k_s a_f) +\\
H_n^{(1)}(k_s a_f)(H_{n+1}^{(2)}(k_s a_f) - H_{n-1}^{(2)}(k_s a_f)))
\end{aligned}
\tag{3.47}
$$

$$
\begin{aligned}
A_{s2h1,n} = (\hat{f}(n)(-(H_{n-1}^{(2)}(k_s a_f) - H_{n+1}^{(2)}(k_s a_f))\\
(k_s \mu_s H_{n-1}^{(1)}(k_s a) J_n(k_v a) - k_s \mu_s H_{n+1}^{(1)}(k_s a) J_n(k_v a) +\\
k_v \mu_v H_n^{(1)}(k_s a)(J_{n+1}(k_v a) - J_{n-1}(k_v a))) + H_{n+1}^{(1)}(k_s a_f)\\
(k_s \mu_s H_{n-1}^{(2)}(k_s a)(-J_n(k_v a)) + k_s \mu_s H_{n+1}^{(2)}(k_s a) J_n(k_v a) +\\
k_v \mu_v H_n^{(2)}(k_s a)(J_{n-1}(k_v a) - J_{n+1}(k_v a))) + H_{n-1}^{(1)}(k_s a_f)\\
(k_s \mu_s H_{n-1}^{(2)}(k_s a) J_n(k_v a) - k_s \mu_s H_{n+1}^{(2)}(k_s a) J_n(k_v a) +\\
k_v \mu_v H_n^{(2)}(k_s a)(J_{n+1}(k_v a) - J_{n-1}(k_v a)))))/\\
(((H_{n+1}^{(1)}(k_s a_f) - H_{n-1}^{(1)}(k_s a_f)) H_n^{(2)}(k_s a_f) +\\
H_n^{(1)}(k_s a_f)(H_{n-1}^{(2)}(k_s a_f) - H_{n+1}^{(2)}(k_s a_f)))\\
(k_s \mu_s H_{n-1}^{(1)}(k_s a) J_n(k_v a) - k_s \mu_s H_{n+1}^{(1)}(k_s a) J_n(k_v a) +\\
k_v \mu_v H_n^{(1)}(k_s a)(J_{n+1}(k_v a) - J_{n-1}(k_v a))))
\end{aligned}
\tag{3.48}
$$

4. STATIC DISLOCATIONS

In this chapter, static dislocations caused by a unit fault movement would be presented. Because there is no time dependence, the governing equation is Laplace equation and its solution is given in Chapter 2. Similar as the previous chapter, there are two cases: fault is inside the valley or inside the half-space. In the following sections, solutions are given for both cases.

4.1 Fault is Inside the Valley Case

Geometry of the problem is same as Figure (3.1). Variables are also the same except density, which is no more a variable in static problems presented in this chapter.

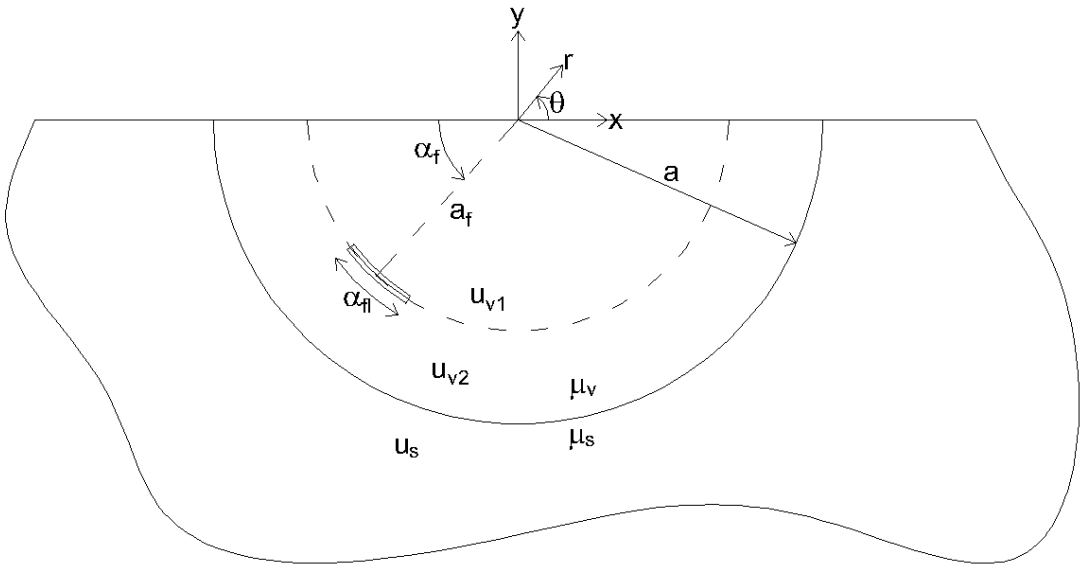

Figure 4.1 : Geometry of the static problem when fault is inside the valley.

4.1.1 Displacement fields

By using general solution obtained Chapter 2 Equation (2.28), displacement fields for all regions and sub-regions would be in the following form:

$$u_{v1}(r,\theta) = \sum_{n=-\infty}^{\infty} A_{1v1,n} r^{|n|} e^{in\theta} + \sum_{n=-\infty}^{\infty} A_{2v1,n} r^{-|n|} e^{in\theta} \qquad \textbf{(4.1)}$$

$$u_{v2}(r,\theta) = \sum_{n=-\infty}^{\infty} A_{1v2,n} r^{|n|} e^{in\theta} + \sum_{n=-\infty}^{\infty} A_{2v2,n} r^{-|n|} e^{in\theta} \tag{4.2}$$

$$u_s(r,\theta) = \sum_{n=-\infty}^{\infty} A_{1s,n} r^{|n|} e^{in\theta} + \sum_{n=-\infty}^{\infty} A_{2s,n} r^{-|n|} e^{in\theta} \tag{4.3}$$

4.1.2 Boundary conditions

Displacement has to be finite everywhere. $A_{2v1,n}$ would be zero in order to obtain finite displacement at $r = 0$. Similarly $A_{1s,n}$ would be zero to avoid infinite displacement for $r = \infty$. When these terms are omitted, displacement fields would be as follows:

$$u_{v1}(r,\theta) = \sum_{n=-\infty}^{\infty} A_{1v1,n} r^{|n|} e^{in\theta} \tag{4.4}$$

$$u_{v2}(r,\theta) = \sum_{n=-\infty}^{\infty} A_{1v2,n} r^{|n|} e^{in\theta} + \sum_{n=-\infty}^{\infty} A_{2v2,n} r^{-|n|} e^{in\theta} \tag{4.5}$$

$$u_s(r,\theta) = \sum_{n=-\infty}^{\infty} A_{2s,n} r^{-|n|} e^{in\theta} \tag{4.6}$$

Similar as dynamic case, flat surfaces have to satisfy stress-free boundary condition as shown below:

$$\frac{\mu_v}{r}\frac{\partial}{\partial r} u_{v1}(r,\theta=0,\pi) = \frac{\mu_v}{r}\frac{\partial}{\partial r} u_{v2}(r,\theta=0,\pi) = \frac{\mu_s}{r}\frac{\partial}{\partial r} u_s(r,\theta=0,\pi) = 0 \tag{4.7}$$

Since the imaging method used in dynamic case is also used here, this condition is satisfied automatically by the help of $f(\theta)$ in Equation (3.16). Displacement relation between divided regions of valley would be in the following form:

$$u_{v1}(r = a_f,\theta) - u_{v2}(r = a_f,\theta) = f(\theta) \tag{4.8}$$

Stress is continuous between divided regions such that

$$\mu_v \frac{\partial}{\partial r} u_{v1}(r = a_f,\theta) - \mu_v \frac{\partial}{\partial r} u_{v2}(r = a_f,\theta) = 0 \tag{4.9}$$

On the interface between valley and half-space, there is continuity of displacement and stress:

$$u_{v2}(r = a,\theta) - u_s(r = a,\theta) = 0 \tag{4.10}$$

$$\mu_v \frac{\partial}{\partial r} u_{v2}(r = a,\theta) - \mu_s \frac{\partial}{\partial r} u_s(r = a,\theta) = 0 \tag{4.11}$$

4.1.3 Linear systems of equations

When displacement fields (4.4)-(4.6) are substituted into boundary conditions (4.8)-(4.11), following equations are obtained.

$$\sum_{n=-\infty}^{\infty}\left(A_{1v1,n}a_f^{|n|}-A_{1v2,n}a_f^{|n|}-A_{2v2,n}a_f^{-|n|}-\hat{f}(n)\right)e^{in\theta}=0 \tag{4.12}$$

$$\sum_{n=-\infty}^{\infty}\left(A_{1v1,n}(|n|\mu_v a_f^{|n|-1})-A_{1v2,n}(|n|\mu_v a_f^{|n|-1})-A_{2v2,n}(-|n|\mu_v a_f^{-|n|-1})\right)e^{in\theta}=0 \tag{4.13}$$

$$\sum_{n=-\infty}^{\infty}\left(A_{1v2,n}a^{|n|}+A_{2v2,n}a^{-|n|}-A_{2s,n}a^{-|n|}\right)e^{in\theta}=0 \tag{4.14}$$

$$\sum_{n=-\infty}^{\infty}\left(A_{1v2,n}(|n|\mu_v a^{|n|-1})+A_{2v2,n}(-|n|\mu_v a^{-|n|-1})-A_{2s,n}(-|n|\mu_s a^{-|n|-1})\right)e^{in\theta}=0 \tag{4.15}$$

Since four equations above have to hold for all θ, coefficients of $e^{in\theta}$ have to be equal to zero for all integer values of n such that:

$$A_{1v1,n}a_f^{|n|}-A_{1v2,n}a_f^{|n|}-A_{2v2,n}a_f^{-|n|}-\hat{f}(n)=0 \tag{4.16}$$

$$A_{1v1,n}(|n|\mu_v a_f^{|n|-1})-A_{1v2,n}(|n|\mu_v a_f^{|n|-1})-A_{2v2,n}(-|n|\mu_v a_f^{-|n|-1})=0 \tag{4.17}$$

$$A_{1v2,n}a^{|n|}+A_{2v2,n}a^{-|n|}-A_{2s,n}a^{-|n|}=0 \tag{4.18}$$

$$A_{1v2,n}(|n|\mu_v a^{|n|-1})+A_{2v2,n}(-|n|\mu_v a^{-|n|-1})-A_{2s,n}(-|n|\mu_s a^{-|n|-1})=0 \tag{4.19}$$

When these four equations are solved simultaneously, unknowns could be calculated as follows:

$$A_{1v1,n}=\frac{\hat{f}(n)a^{-2|n|}a_f^{-|n|}\left(\mu_s\left(a^{2|n|}+a_f^{2|n|}\right)+\mu_v\left(a^{2|n|}-a_f^{2|n|}\right)\right)}{2\left(\mu_s+\mu_v\right)} \tag{4.20}$$

$$A_{1v2,n} = \frac{\hat{f}(n) a^{-2|n|} (\mu_s - \mu_v) a_f^{|n|}}{2(\mu_s + \mu_v)} \tag{4.21}$$

$$A_{2v2,n} = -\frac{1}{2} \hat{f}(n) a_f^{|n|} \tag{4.22}$$

$$A_{2s,n} = -\frac{\hat{f}(n) \mu_v a_f^{|n|}}{\mu_s + \mu_v} \tag{4.23}$$

4.2 Fault is Inside the Half-Space Case

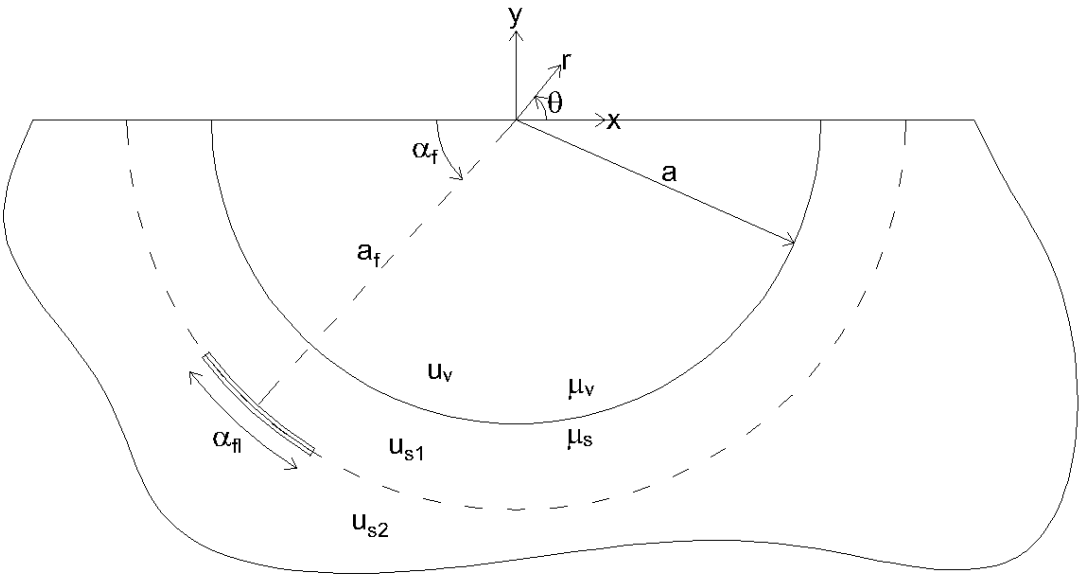

Figure 4.2 : Geometry of the static problem when fault is inside the half space.

In this case, the fault is inside the half-space. Solution technique is the same as the previous case, but displacement fields and boundary conditions are different.

4.2.1 Displacement fields

When solution (2.28) on page 8 is used and the terms in solutions which does not satisfy finite displacement in the center and at infinity are omitted, remaining displacement fields for each space/subspace would be as follows:

$$u_v(r,\theta) = \sum_{n=-\infty}^{\infty} A_{1v,n} r^{|n|} e^{in\theta} \tag{4.24}$$

$$u_{s1}(r,\theta) = \sum_{n=-\infty}^{\infty} A_{1s1,n} r^{|n|} e^{in\theta} + \sum_{n=-\infty}^{\infty} A_{2s1,n} r^{-|n|} e^{in\theta} \tag{4.25}$$

$$u_{s2}(r,\theta) = \sum_{n=-\infty}^{\infty} A_{2s2,n} r^{-|n|} e^{in\theta} \tag{4.26}$$

4.2.2 Boundary conditions

Boundary conditions between divided regions would be in the following form:

$$u_v(r=a,\theta) - u_{s1}(r=a,\theta) = 0 \tag{4.27}$$

$$\mu_v \frac{\partial}{\partial r} u_v(r=a,\theta) - \mu_s \frac{\partial}{\partial r} u_{s1}(r=a,\theta) = 0 \tag{4.28}$$

$$u_{s1}(r=a_f,\theta) - u_{s2}(r=a_f,\theta) = f(\theta) \tag{4.29}$$

$$\mu_s \frac{\partial}{\partial r} u_{s1}(r=a_f,\theta) - \mu_s \frac{\partial}{\partial r} u_{s2}(r=a_f,\theta) = 0 \tag{4.30}$$

$f(\theta)$ in (4.29) is defined in (3.16) on page 11 which assures the zero stress conditions on flat surfaces.

4.2.3 Linear systems of equations

When displacement fields (4.24)-(4.26) are substituted into boundary conditions (4.27)-(4.30), following equations are obtained.

$$\sum_{n=-\infty}^{\infty} \left(A_{1v,n} a^{|n|} - A_{1s1,n} a^{|n|} - A_{2s1,n} a^{-|n|} \right) e^{in\theta} = 0 \tag{4.31}$$

$$\sum_{n=-\infty}^{\infty} \left(A_{1v,n}(|n|\mu_v a^{|n|-1}) - A_{1s1,n}(|n|\mu_s a^{|n|-1}) - A_{2s1,n}(-|n|\mu_s a^{-|n|-1}) \right) e^{in\theta} = 0 \tag{4.32}$$

$$\sum_{n=-\infty}^{\infty} \left(A_{1s1,n} a_f^{|n|} + A_{2s1,n} a_f^{-|n|} - A_{2s2,n} a_f^{-|n|} - \hat{f}(n) \right) e^{in\theta} = 0 \tag{4.33}$$

$$\sum_{n=-\infty}^{\infty} \left(A_{1s1,n}(|n|\mu_s a_f^{|n|-1}) + A_{2s1,n}(-|n|\mu_s a_f^{-|n|-1}) - A_{2s2,n}(-|n|\mu_s a_f^{-|n|-1}) \right) e^{in\theta} = 0 \tag{4.34}$$

Since four equations above have to hold for all θ, coefficients of $e^{in\theta}$ have to be equal to zero for all integer values of n such that:

$$A_{1v,n}a^{|n|} - A_{1s1,n}a^{|n|} - A_{2s1,n}a^{-|n|} = 0 \tag{4.35}$$

$$A_{1v,n}(|n|\mu_v a^{|n|-1}) - A_{1s1,n}(|n|\mu_s a^{|n|-1}) - A_{2s1,n}(-|n|\mu_s a^{-|n|-1}) = 0 \tag{4.36}$$

$$A_{1s1,n}a_f^{|n|} + A_{2s1,n}a_f^{-|n|} - A_{2s2,n}a_f^{-|n|} - \hat{f}(n) = 0 \tag{4.37}$$

$$A_{1s1,n}(|n|\mu_s a_f^{|n|-1}) + A_{2s1,n}(-|n|\mu_s a_f^{-|n|-1}) - A_{2s2,n}(-|n|\mu_s a_f^{-|n|-1}) = 0 \tag{4.38}$$

When these four equations are solved simultaneously, unknowns could be calculated as follows:

$$A_{1v,n} = \frac{\hat{f}(n)\mu_s a_f^{-|n|}}{\mu_s + \mu_v} \tag{4.39}$$

$$A_{1s1,n} = \frac{1}{2}\hat{f}(n)a_f^{-|n|} \tag{4.40}$$

$$A_{2s1,n} = \frac{\hat{f}(n)a^{2|n|}\left(\mu_s - \mu_v\right)a_f^{-|n|}}{2\left(\mu_s + \mu_v\right)} \tag{4.41}$$

$$A_{2s2,n} = \frac{1}{2}\hat{f}(n)a_f^{-|n|}\left(\frac{a^{2|n|}\left(\mu_s - \mu_v\right)}{\mu_s + \mu_v} - a_f^{2|n|}\right) \tag{4.42}$$

5. RESULTS

Displacement fields for steady state dynamic case and static case are obtained in closed form in Chapter 3 and 4 respectively. Solution functions are expressed in terms of infinite series. In order to achieve numerical results, these series have to be truncated. In other words, lower and upper limit of the series has to be $-N$ and $+N$ where N is a finite number. All to the good, both Fourier-Bessel series and power series are convergent so results could be obtained at desired accuracy. Convergence highly depends on variables of the problem, especially wave length. For the range of the variables of following examples, desired convergence is satisfied for N between 16 to 50. However, N is taken 100 for all calculations. Truncated Fourier-Bessel series are in complex space. Displacement as a function of time could be obtained by multiplying these series by $e^{-i\omega t}$ and calculating either real or imaginary part. Modulus of the series gives displacement amplitudes. There are some numerical results that demonstrate surface displacement amplitudes for variable parameters. Parameters in length dimension are normalized with respect to valley radius a. A new dimensionless parameter η is introduced such that:

$$\eta = \frac{2a}{\lambda_s} \tag{5.1}$$

where λ_s denotes wave length in half-space.

5.1 Comparison Between Static and Dynamic Cases

Following plots show the comparison between static and dynamic cases. Results show that the difference between dynamic and static case increases when η increases. In Figures (A.1) to (A.4), when $a_f = 0.25a$, dynamic displacements amplitudes for $\eta = 0.1$ are very close to those of static case. When $\eta = 0.2$, displacements are slightly different. For $\eta = 0.6$, displacement profile is totally different except for Figure (A.1), in which incident wave is approaching vertically to the valley. In Figures (A.5) to (A.8), when $a_f = 0.75a$, the difference between static case and dynamic case for $\eta =$

0.1 increases. In Figures (A.9) to (A.16), when faults is outside the valley, further differences are obtained even when $\eta = 0.1$.

5.2 Effect of Fault Distance

In Figures (A.17) to (A.24), surface displacement amplitudes are plotted for fixed fault length, $0.25a$. Results show that surface displacements increase when the distance between fault center and valley center decrease. Between Figures (A.17) to (A.20), fault distances are relatively close, from $1.25a$ to $3a$. Displacements profiles are similar and amplitudes are close. In Figures (A.21) to (A.24), fault distance change from $2a$ to $16a$, difference is more significant.

5.3 Effect of Material Coefficient Differentness

In Figures (A.25) to (A.72), surface displacement amplitudes are plotted for different values of material coefficient ratios. In Figures (A.25) to (A.48), SDA's are plotted when same shear modulus but different densities. Continuous line shows SDA when densities of valley and half-space are the same. In this case the effect of alluvial valley disappears and the problem geometry converts to half-space. Other plots displays SDA's when alluvial valley material has less density. Results show that SDA increases or decreases for different values of other parameters when the ratio of half-space density to alluvial density increase. In Figures (A.49) to (A.72), densities are taken same to see the effect of shear modulus. Continuous lines show the half-space case. SDA's significantly increase as the ratio of half-space shear modulus to alluvial valley shear modulus increases.

6. CONCLUSIONS

In this study, out-of-plane response of a semi-alluvial valley surrounded by a half-space is investigated. Alluvial valley and half-space are assumed to be homogeneous, isotropic and linear elastic. The mediums are subjected to a strike-slip fault which is either inside or outside the valley. Fault motion is modeled by defining unit displacement difference between two sides. Fault trajectory is taken arc-shaped. Exact displacements are obtained for both steady state dynamic and static fault motion as a function of parameters of the problem. So, these displacements contain all information about amplification and deamplification effects on alluvial valley surface with respect to strike-slip fault position and size and material properties of alluvial valley and half-space. These results are very valuable because many human settlements are founded on alluvial valleys and they must be designed considering these amplification effects.

There are many studies that investigate out-of-plane response of alluvial valleys in literature. In most of these studies, analytical solution techniques are used but exact solutions aren't provided. In this study, exact solutions are also provided. In similar former studies, the disturbances are plane SH waves. But in this study, the disturbance is SH waves originated from strike-slip fault motion. This model is conceptually new and much more realistic. And also, since the disturbance arise from fault motion, solutions of static equivalent of the problem can be obtained whereas when the disturbance is plane SH waves, that is not possible.

In this study, geometry of the problem is relatively simple, fault is taken arc-shaped and there aren't any kind of nonlinearity. These assumptions and simplifications allows obtaining closed form analytic solutions. But the solution techniques used in this study could be applied to some more complicated geometries provided that the geometry should be expressed by using polar coordinates. For more general geometries, numerical solution methods such as Finite Differences, Finite Element and Boundary element should be used.

For further studies, problem geometry could be modified. If single coordinate axis isn't sufficient, then addition theorems could be used. In that case, analytic solutions could be obtained but exact solutions may not. Also, in plane motions could be considered. In that case, satisfying stress free boundary conditions on flat surfaces would be very challenging.

REFERENCES

[1] **Bolt, B.A.** (1999). *Earthquakes*, W. H. Freeman and Company.

[2] **Trifunac, M.** (1971). Surface motion of a semi-cylindrical alluvial valley for incident plane SH waves, *Bulletin of the Seismological Society of America*, *61*(6), 1755–1770.

[3] **Trifunac, M.** (1973). Scattering of plane sh waves by a semi-cylindrical canyon, *Earthquake Engineering & Structural Dynamics*, *1*(3), 267–281.

[4] **Lee, V.** (1977). On deformations near circular underground cavity subjected to incident plane SH waves, *Proceedings of the Application of Computer Methods in Engineering Conference*, volume 2, pp.951–962.

[5] **Yuan, X. and Liao, Z.P.** (1995). Scattering of plane SH waves by a cylindrical alluvial valley of circular-arc cross-section, *Earthquake engineering & structural dynamics*, *24*(10), 1303–1313.

[6] **Hayir, A.**, **Todorovska, M.I. and Trifunac, M.D.** (2001). Antiplane response of a dike with flexible soil-structure interface to incident SH waves, *Soil Dynamics and Earthquake Engineering*, *21*(7), 603–613.

[7] **Chenggang, Z.**, **Jun, D. and Fuping, G.** (2006). An analytical solution for three-dimensional diffraction of plane P-waves by a hemispherical alluvial valley with saturated soil deposits, *Acta Mechanica Solida Sinica*, *19*(2), 141–151.

[8] **Chen, J.T.**, **Chen, P.Y. and Chen, C.T.** (2008). Surface motion of multiple alluvial valleys for incident plane SH-waves by using a semi-analytical approach, *Soil Dynamics and Earthquake Engineering*, *28*(1), 58–72.

[9] **Kara, H.F. and Trifunac, M.D.** (2013). A note on plane-wave approximation, *Soil Dynamics and Earthquake Engineering*, *51*, 9–13.

[10] **Graff, K.F.** (1975). *Wave motion in elastic solids*, Courier Dover Publications.

[11] **Gamer, U.** (1977). Dynamic stress concentration in an elastic half space with a semi-circular cavity excited by SH waves, *International Journal of Solids and Structures*, *13*(7), 675–681.

[12] **Lee, V. and Karl, J.** (1992). Diffraction of SV waves by underground, circular, cylindrical cavities, *Soil Dynamics and Earthquake Engineering*, *11*(8), 445–456.

[13] **De Barros, F. and Luco, J.** (1995). Dynamic response of a two-dimensional semi-circular foundation embedded in a layered viscoelastic half-space, *Soil Dynamics and Earthquake Engineering*, *14*(1), 45–57.

[14] **Lee, V. and Sherif, R.** (1996). Diffraction around circular canyon in elastic wedge space by plane SH-waves, *Journal of engineering mechanics*, *122*(6), 539–544.

[15] **Hayir, A. and Bakirtas, I.** (2004). A note on a plate having a circular cavity excited by plane harmonic SH waves, *Journal of Sound and Vibration*, *271*(1), 241–255.

[16] **Hasheminejad, S.M. and Avazmohammadi, R.** (2007). Harmonic wave diffraction by two circular cavities in a poroelastic formation, *Soil Dynamics and Earthquake Engineering*, *27*(1), 29–41.

[17] **Zhou, X.L.**, **Wang, J.H.**, **Xu, B. and Jiang, L.F.** (2009). Dynamic response of a circular pipeline in a poroelastic medium, *Mechanics Research Communications*, *36*(8), 898–905.

[18] **Lin, C.H.**, **Lee, V.W.**, **Todorovska, M.I. and Trifunac, M.D.** (2010). Zero-stress, cylindrical wave functions around a circular underground tunnel in a flat, elastic half-space: Incident P-waves, *Soil Dynamics and Earthquake Engineering*, *30*(10), 879–894.

[19] **Coşkun, İ.**, **Engin, H. and Özmutlu, A.** (2011). Dynamic stress and displacement in an elastic half-space with a cylindrical cavity, *Shock and Vibration*, *18*(6), 827–838.

[20] **Liang, J.**, **Fu, J.**, **Todorovska, M.I. and Trifunac, M.D.** (2013). Effects of the site dynamic characteristics on soil–structure interaction (I): Incident SH-Waves, *Soil Dynamics and Earthquake Engineering*, *44*, 27–37.

APPENDICES

APPENDIX A.1 : Comparisons between Static and Dynamic Cases
APPENDIX A.2 : Effect of Fault Distance
APPENDIX A.3 : Effect of Material Coefficient Differentness

APPENDIX A.1

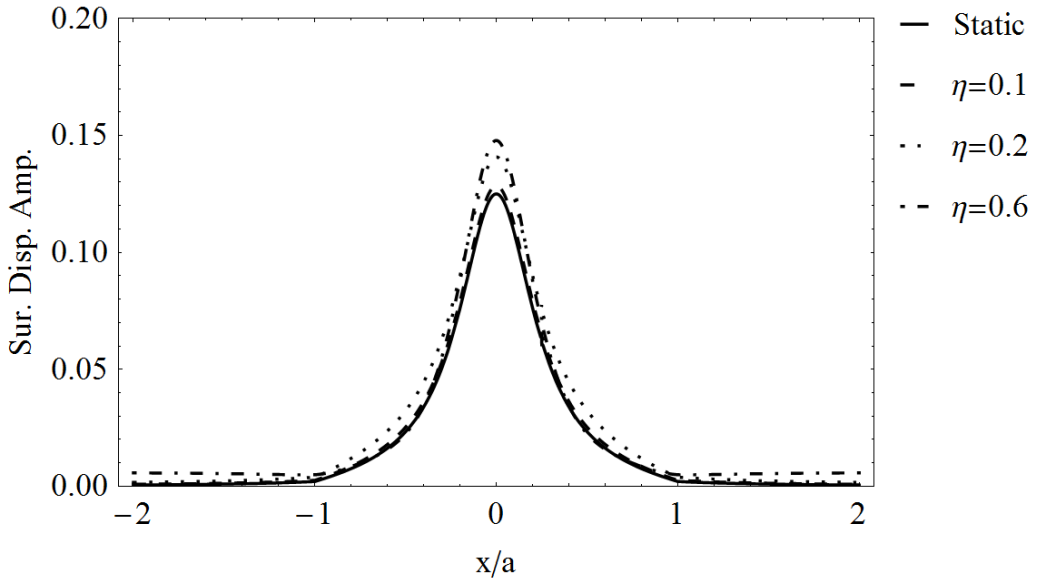

Figure A.1 : SDA Comparison for $N = 100$, $a_f/a = 0.25$, $\alpha_f = \pi/2$, $\alpha_{fl} = \pi/8$, $\mu_s/\mu_v = 6$, $\rho_s/\rho_v = 1.5$.

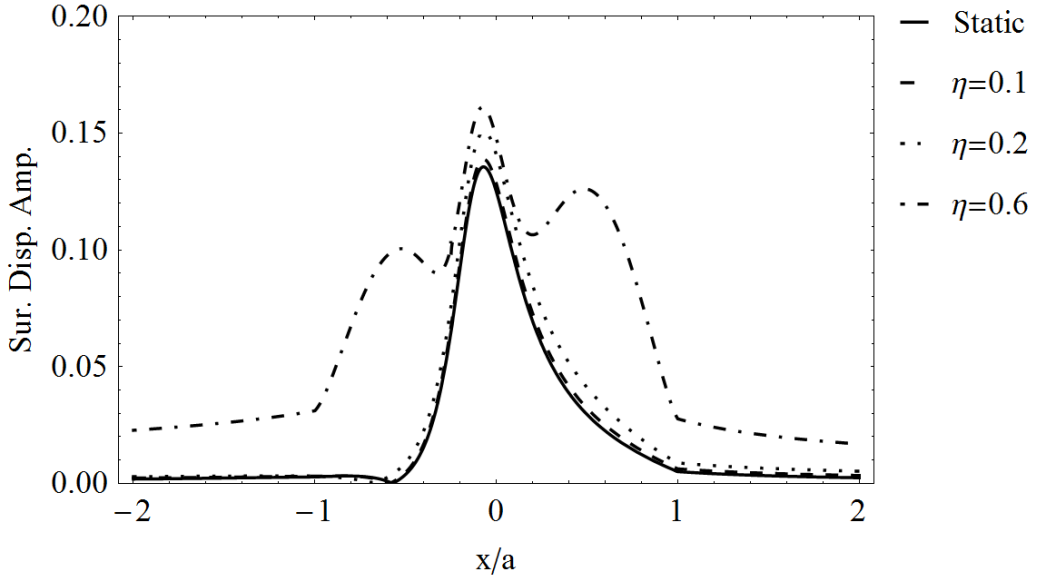

Figure A.2 : SDA Comparison for $N = 100$, $a_f/a = 0.25$, $\alpha_f = \pi/3$, $\alpha_{fl} = \pi/8$, $\mu_s/\mu_v = 6$, $\rho_s/\rho_v = 1.5$.

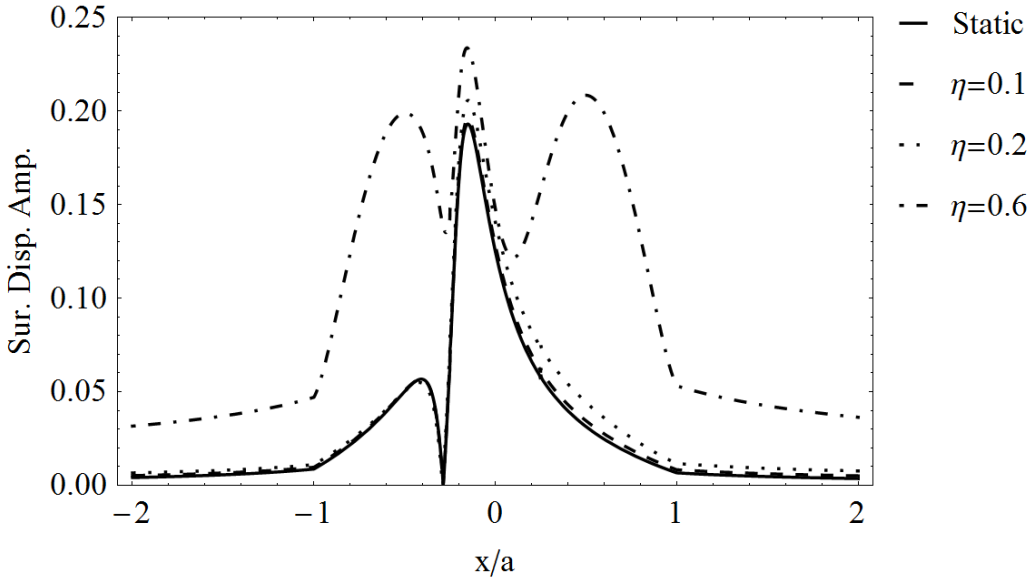

Figure A.3 : SDA Comparison for $N = 100$, $a_f/a = 0.25$, $\alpha_f = \pi/6$, $\alpha_{fl} = \pi/8$, $\mu_s/\mu_v = 6$, $\rho_s/\rho_v = 1.5$.

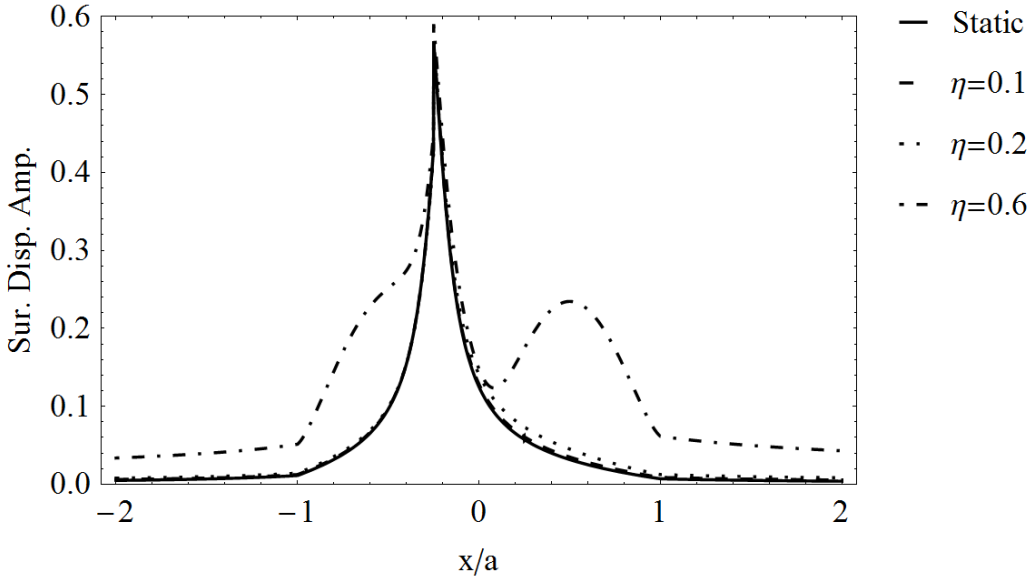

Figure A.4 : SDA Comparison for $N = 100$, $a_f/a = 0.25$, $\alpha_f = \pi/16$, $\alpha_{fl} = \pi/8$, $\mu_s/\mu_v = 6$, $\rho_s/\rho_v = 1.5$.

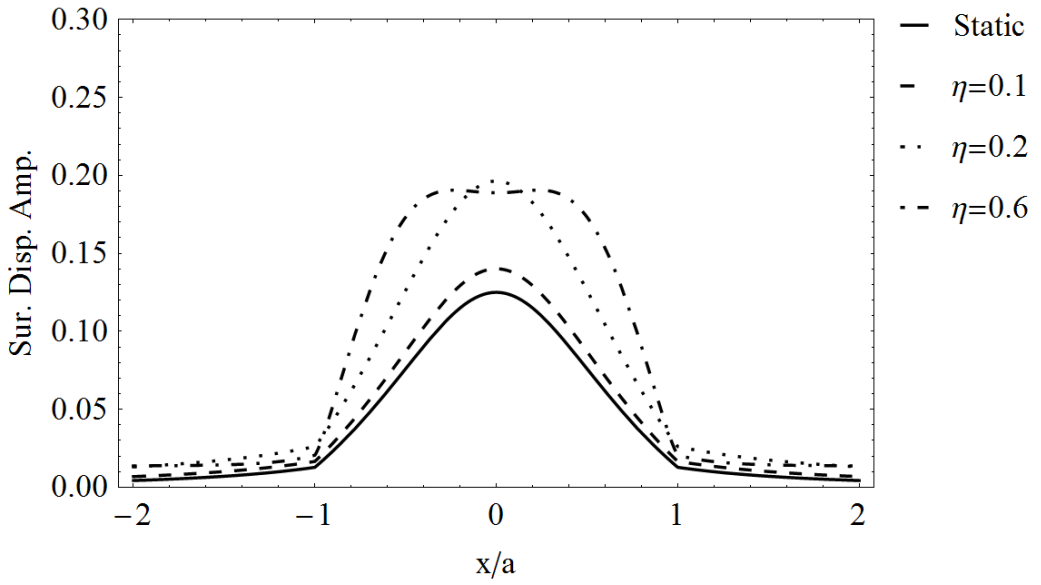

Figure A.5 : SDA Comparison for $N = 100$, $a_f/a = 0.75$, $\alpha_f = \pi/2$, $\alpha_{fl} = \pi/8$, $\mu_s/\mu_v = 6$, $\rho_s/\rho_v = 1.5$.

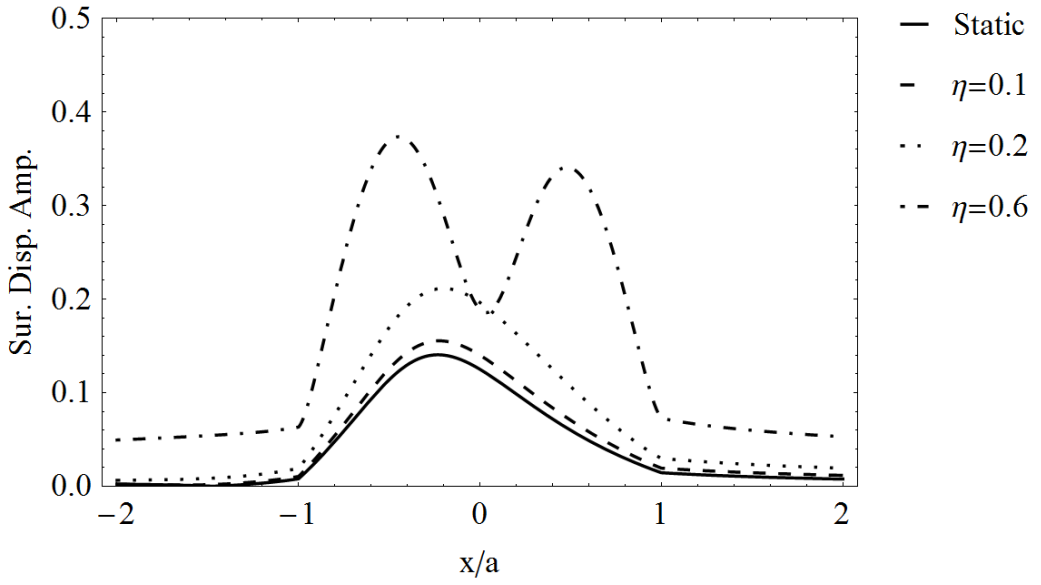

Figure A.6 : SDA Comparison for $N = 100$, $a_f/a = 0.75$, $\alpha_f = \pi/3$, $\alpha_{fl} = \pi/8$, $\mu_s/\mu_v = 6$, $\rho_s/\rho_v = 1.5$.

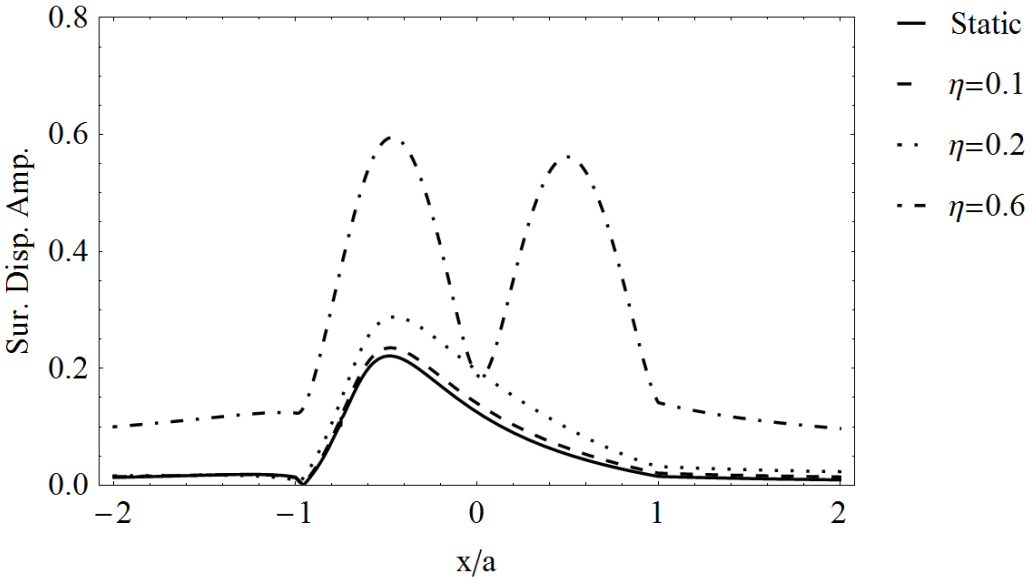

Figure A.7 : SDA Comparison for $N = 100$, $a_f/a = 0.75$, $\alpha_f = \pi/6$, $\alpha_{fl} = \pi/8$, $\mu_s/\mu_v = 6$, $\rho_s/\rho_v = 1.5$.

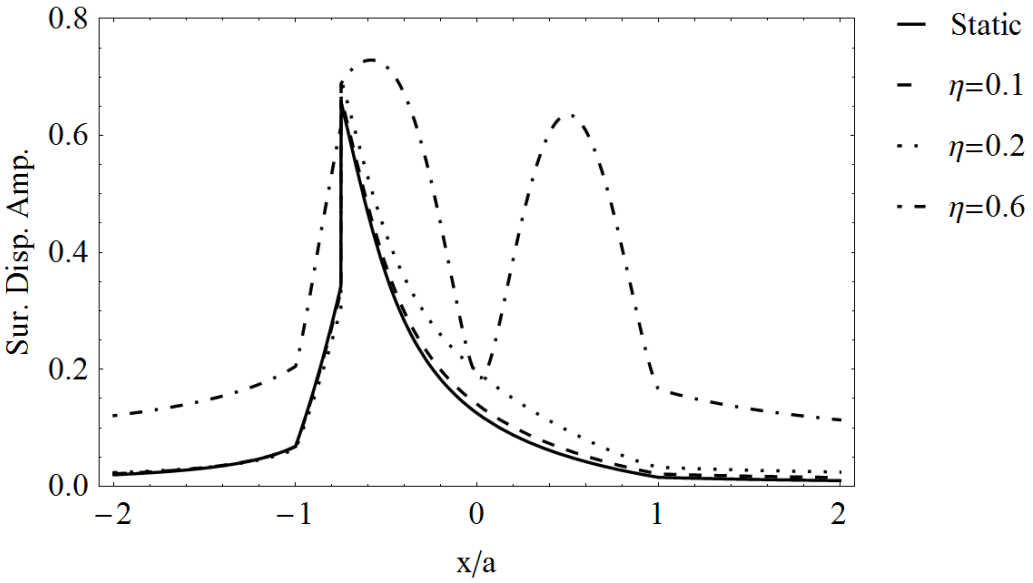

Figure A.8 : SDA Comparison for $N = 100$, $a_f/a = 0.75$, $\alpha_f = \pi/16$, $\alpha_{fl} = \pi/8$, $\mu_s/\mu_v = 6$, $\rho_s/\rho_v = 1.5$.

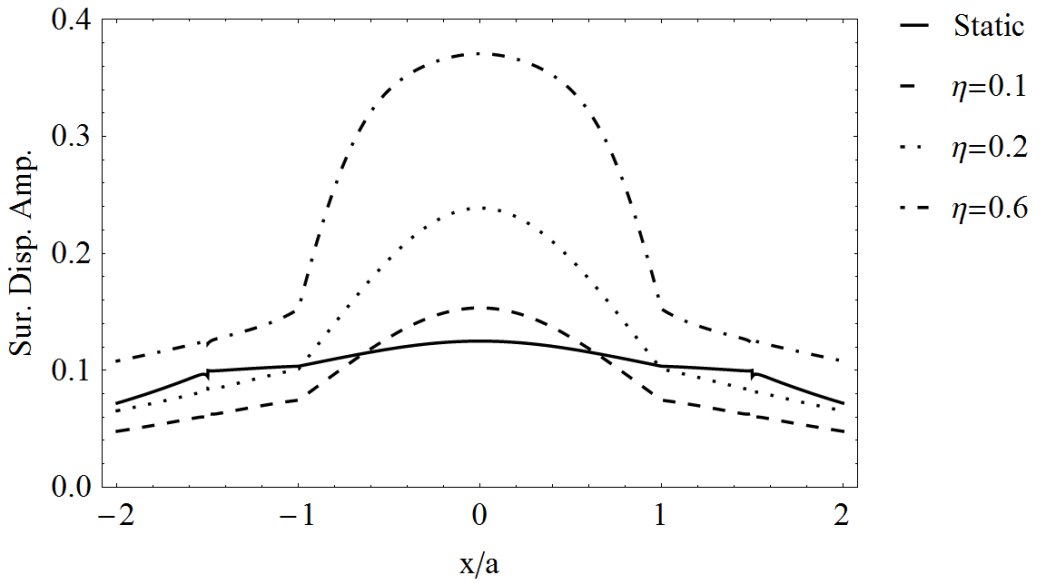

Figure A.9 : SDA Comparison for $N = 100$, $a_f/a = 1.5$, $\alpha_f = \pi/2$, $\alpha_{fl} = \pi/8$, $\mu_s/\mu_v = 6$, $\rho_s/\rho_v = 1.5$.

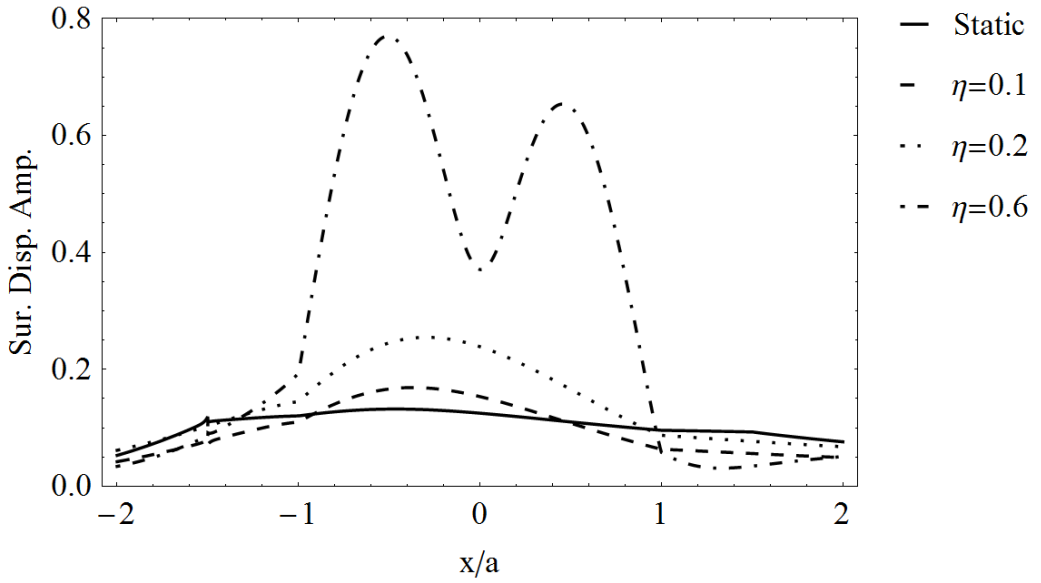

Figure A.10 : SDA Comparison for $N = 100$, $a_f/a = 1.5$, $\alpha_f = \pi/3$, $\alpha_{fl} = \pi/8$, $\mu_s/\mu_v = 6$, $\rho_s/\rho_v = 1.5$.

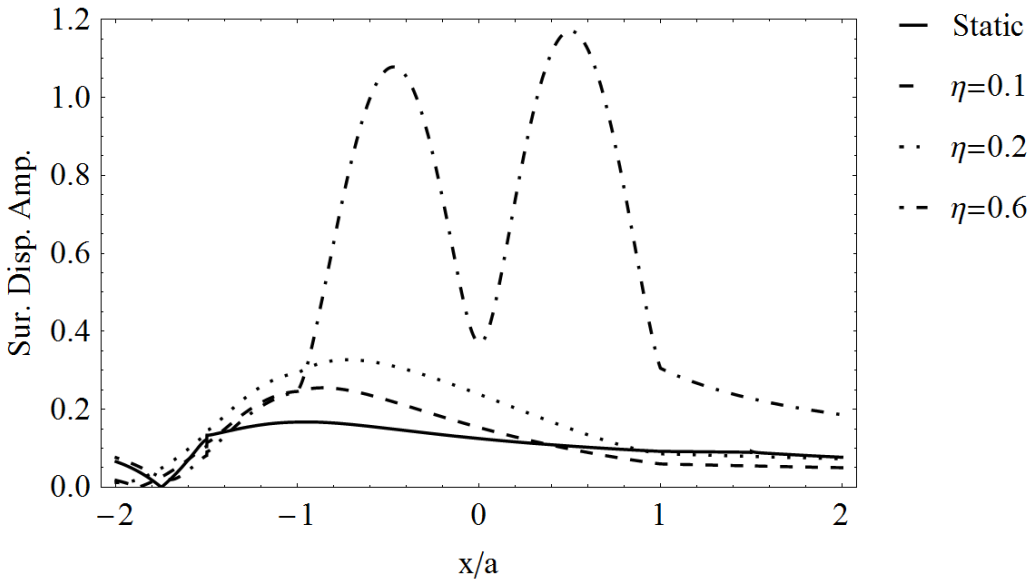

Figure A.11 : SDA Comparison for $N = 100$, $a_f/a = 1.5$, $\alpha_f = \pi/6$, $\alpha_{fl} = \pi/8$, $\mu_s/\mu_v = 6$, $\rho_s/\rho_v = 1.5$.

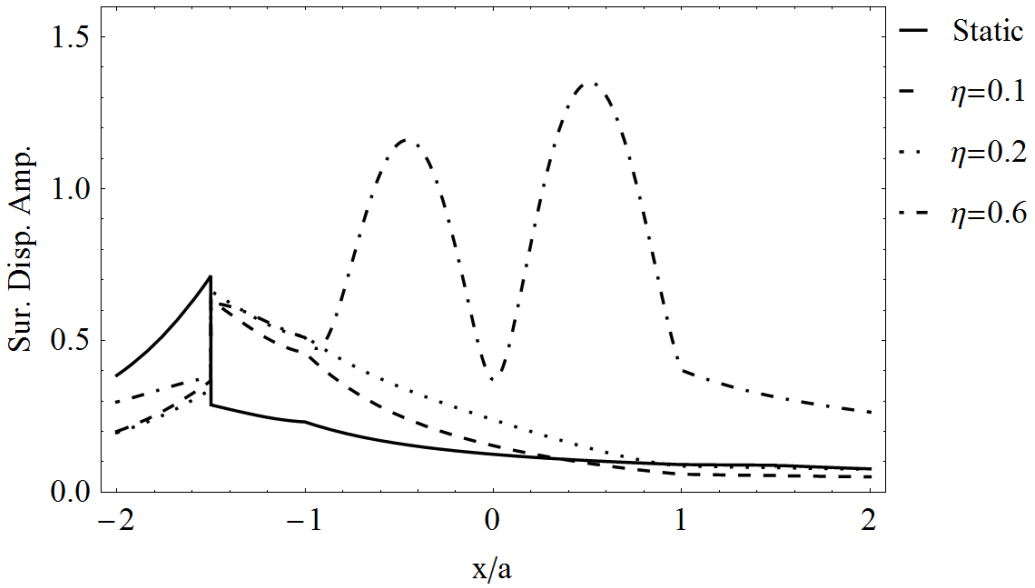

Figure A.12 : SDA Comparison for $N = 100$, $a_f/a = 1.5$, $\alpha_f = \pi/16$, $\alpha_{fl} = \pi/8$, $\mu_s/\mu_v = 6$, $\rho_s/\rho_v = 1.5$.

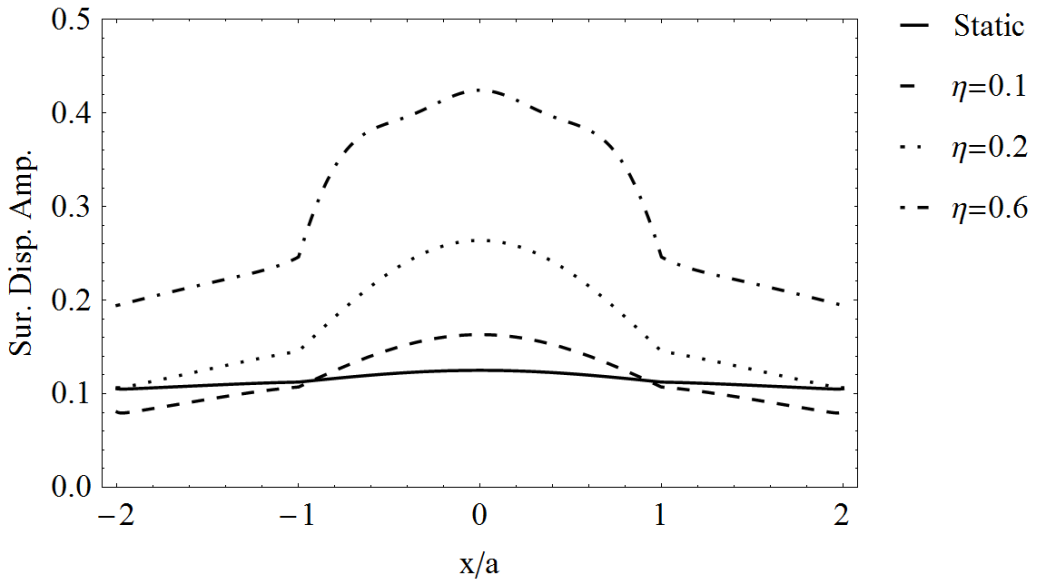

Figure A.13 : SDA Comparison for $N = 100$, $a_f/a = 2$, $\alpha_f = \pi/2$, $\alpha_{fl} = \pi/8$, $\mu_s/\mu_v = 6$, $\rho_s/\rho_v = 1.5$.

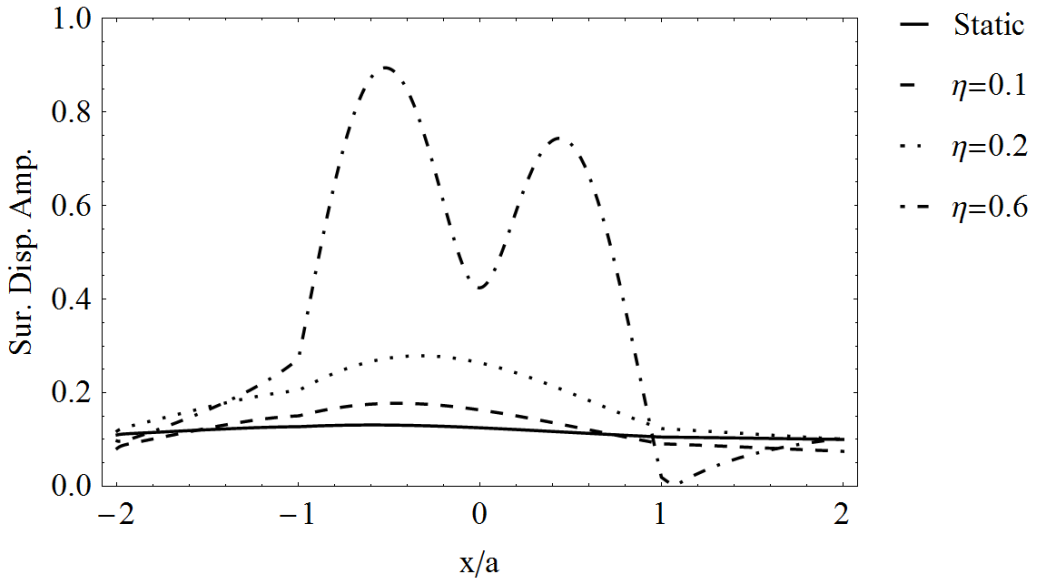

Figure A.14 : SDA Comparison for $N = 100$, $a_f/a = 2$, $\alpha_f = \pi/3$, $\alpha_{fl} = \pi/8$, $\mu_s/\mu_v = 6$, $\rho_s/\rho_v = 1.5$.

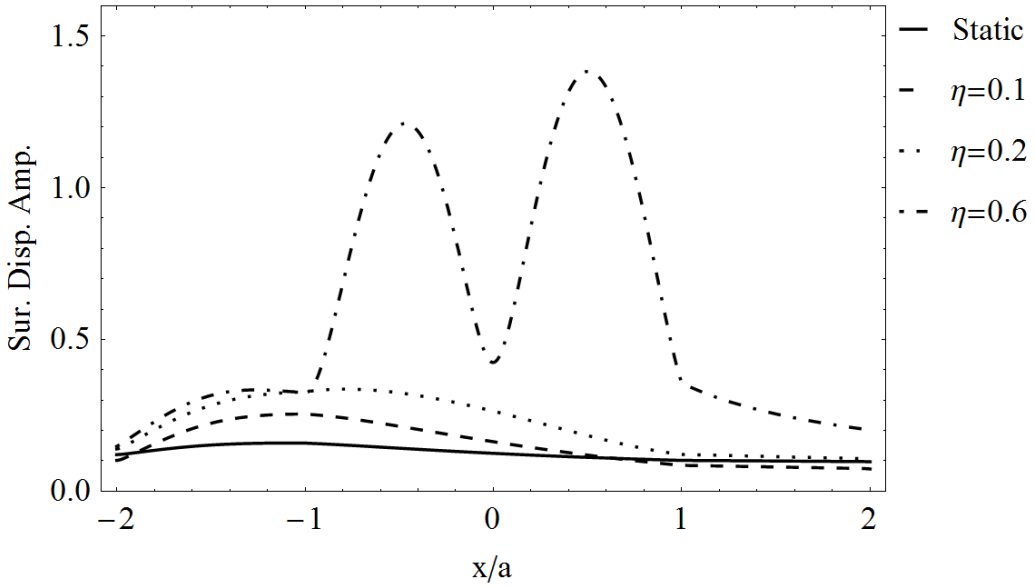

Figure A.15 : SDA Comparison for $N = 100$, $a_f/a = 2$, $\alpha_f = \pi/6$, $\alpha_{fl} = \pi/8$, $\mu_s/\mu_v = 6$, $\rho_s/\rho_v = 1.5$.

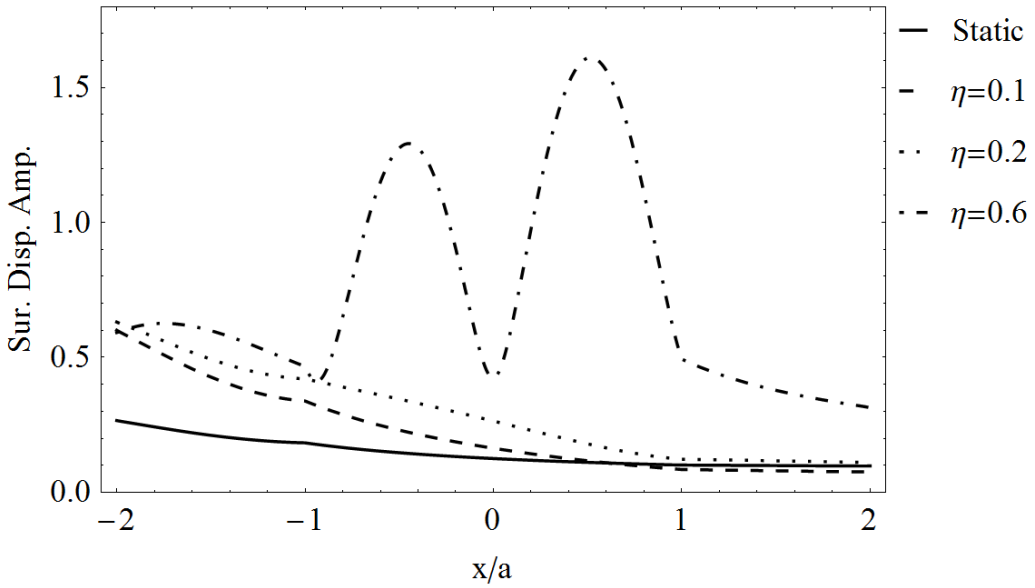

Figure A.16 : SDA Comparison for $N = 100$, $a_f/a = 2$, $\alpha_f = \pi/16$, $\alpha_{fl} = \pi/8$, $\mu_s/\mu_v = 6$, $\rho_s/\rho_v = 1.5$.

APPENDIX A.2

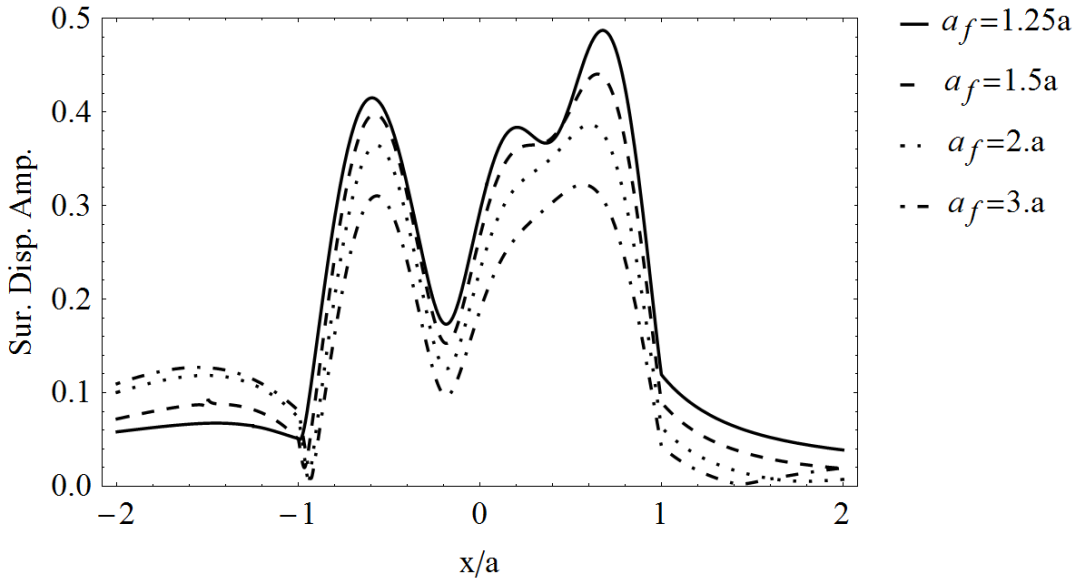

Figure A.17 : Effect of Fault Distance for $N = 100$, $\eta = 1$, $\alpha_f = \pi/3$, $\alpha_{fl} a_f/a = 0.25$, $\mu_s/\mu_v = 6$, $\rho_s/\rho_v = 1.5$.

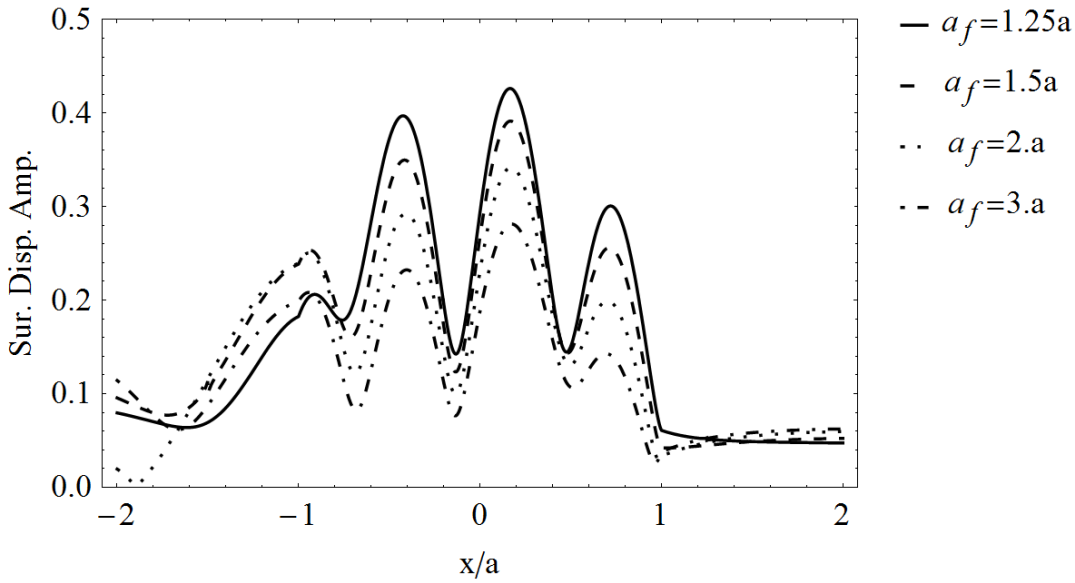

Figure A.18 : Effect of Fault Distance for $N = 100$, $\eta = 1$, $\alpha_f = \pi/6$, $\alpha_{fl} a_f/a = 0.25$, $\mu_s/\mu_v = 6$, $\rho_s/\rho_v = 1.5$.

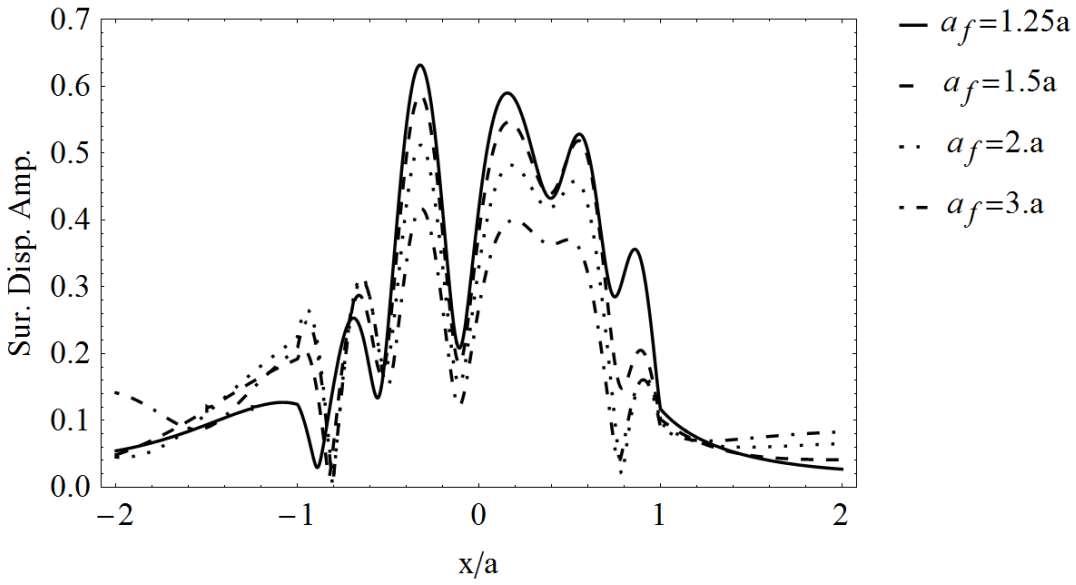

Figure A.19 : Effect of Fault Distance for $N = 100$, $\eta = 2$, $\alpha_f = \pi/3$, $\alpha_{fl} a_f/a = 0.25$, $\mu_s/\mu_v = 6$, $\rho_s/\rho_v = 1.5$.

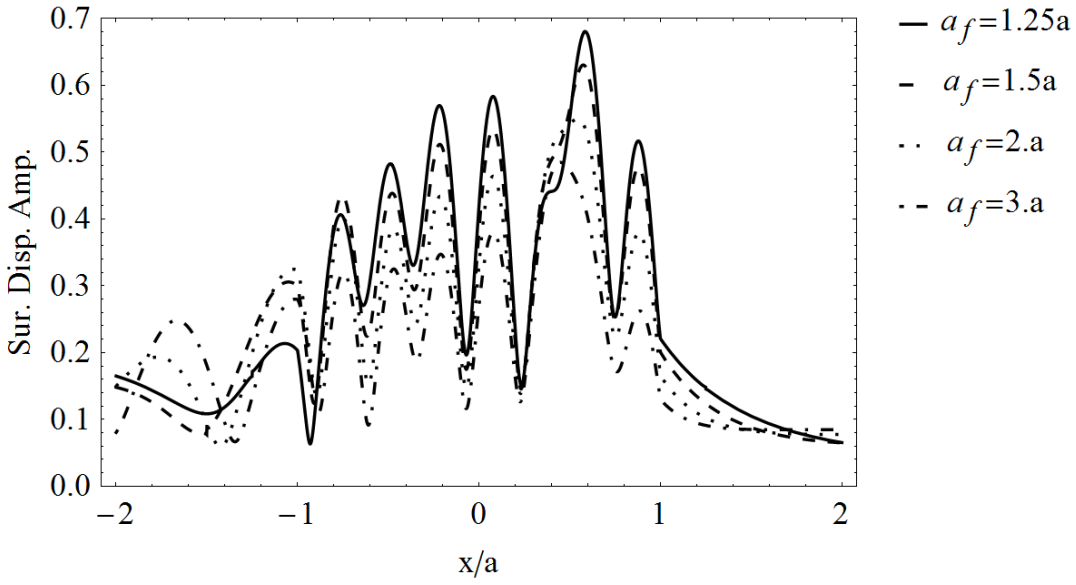

Figure A.20 : Effect of Fault Distance for $N = 100$, $\eta = 2$, $\alpha_f = \pi/6$, $\alpha_{fl} a_f/a = 0.25$, $\mu_s/\mu_v = 6$, $\rho_s/\rho_v = 1.5$.

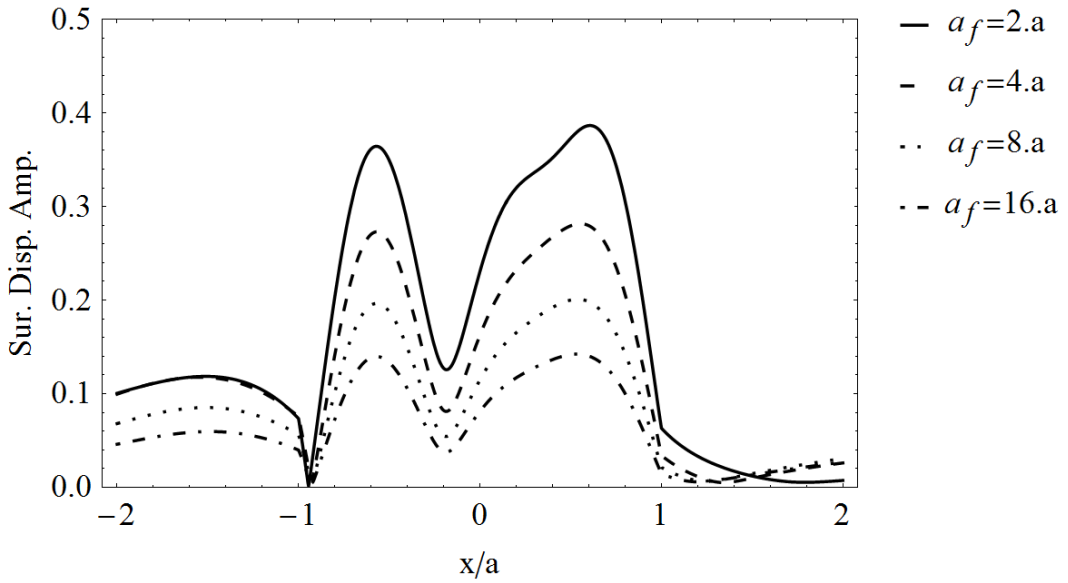

Figure A.21 : Effect of Fault Distance for $N = 100$, $\eta = 1$, $\alpha_f = \pi/3$, $\alpha_{fl} a_f/a = 0.25$, $\mu_s/\mu_v = 6$, $\rho_s/\rho_v = 1.5$.

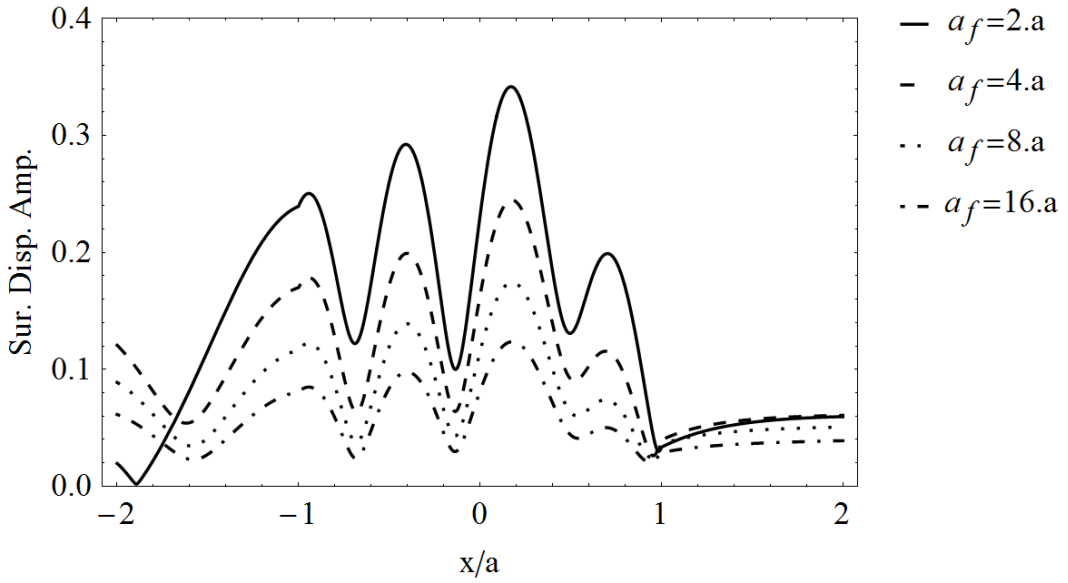

Figure A.22 : Effect of Fault Distance for $N = 100$, $\eta = 1$, $\alpha_f = \pi/6$, $\alpha_{fl} a_f/a = 0.25$, $\mu_s/\mu_v = 6$, $\rho_s/\rho_v = 1.5$.

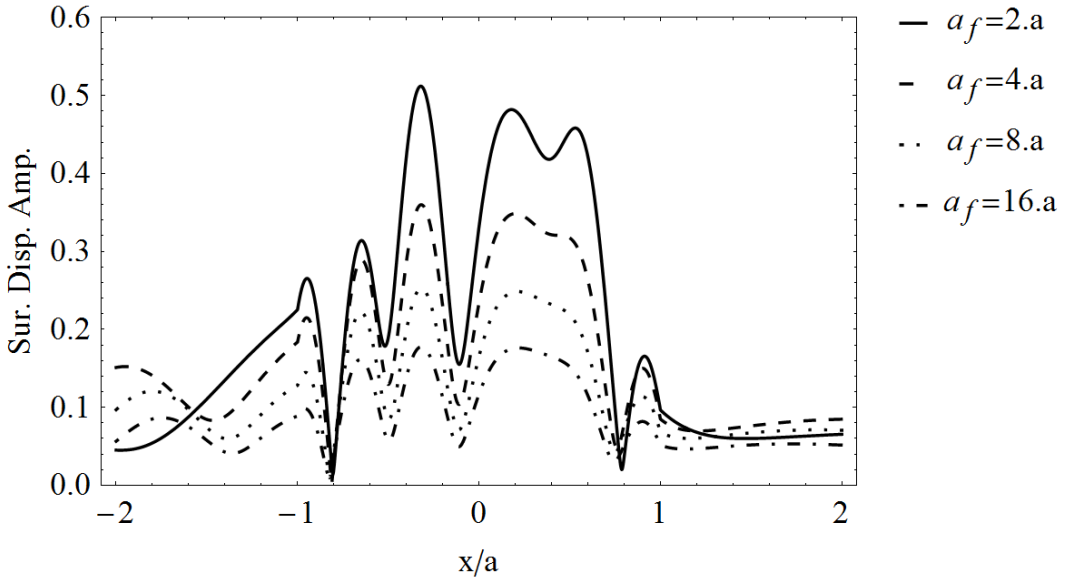

Figure A.23 : Effect of Fault Distance for $N = 100$, $\eta = 2$, $\alpha_f = \pi/3$, $\alpha_{fl} a_f/a = 0.25$, $\mu_s/\mu_v = 6$, $\rho_s/\rho_v = 1.5$.

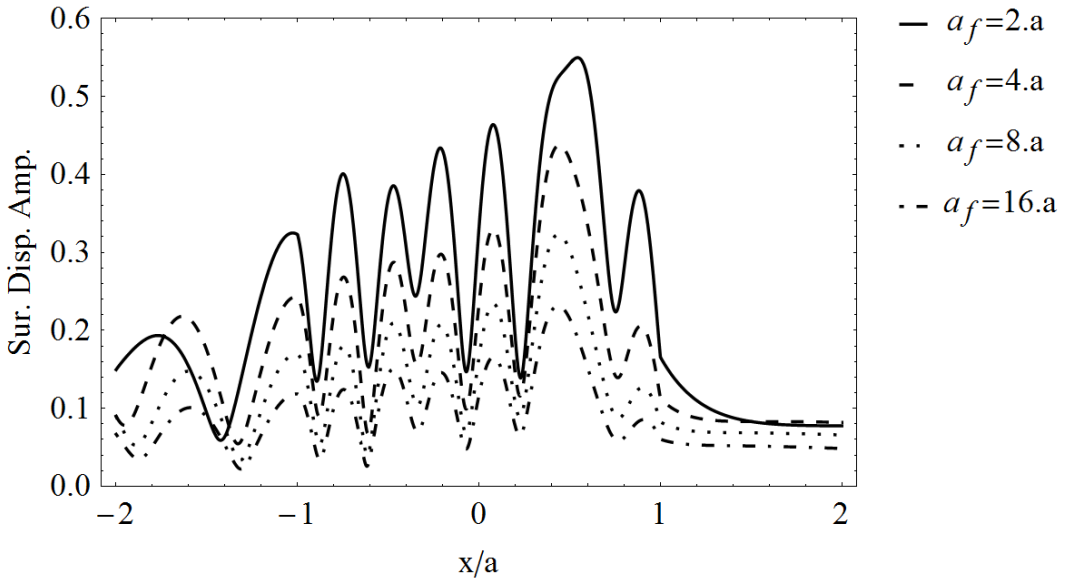

Figure A.24 : Effect of Fault Distance for $N = 100$, $\eta = 2$, $\alpha_f = \pi/6$, $\alpha_{fl} a_f/a = 0.25$, $\mu_s/\mu_v = 6$, $\rho_s/\rho_v = 1.5$.

APPENDIX A.3

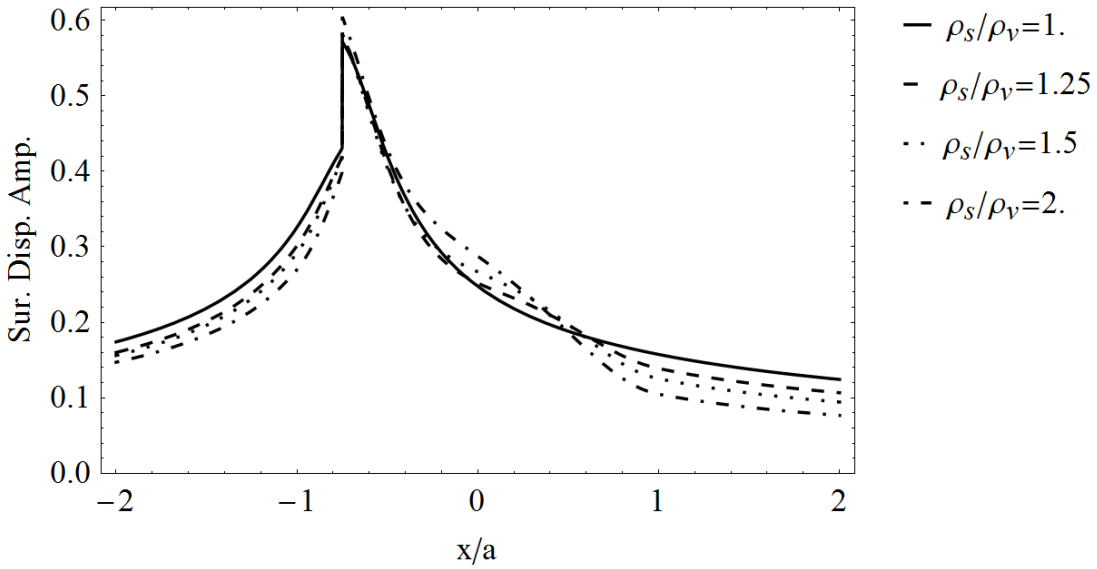

Figure A.25 : Effect of Density Differentness for $N = 100$, $\eta = 1$, $a_f/a = 0.75$, $\alpha_f = \pi/16$, $\alpha_{fl} = \pi/8$, $\mu_s/\mu_v = 1$.

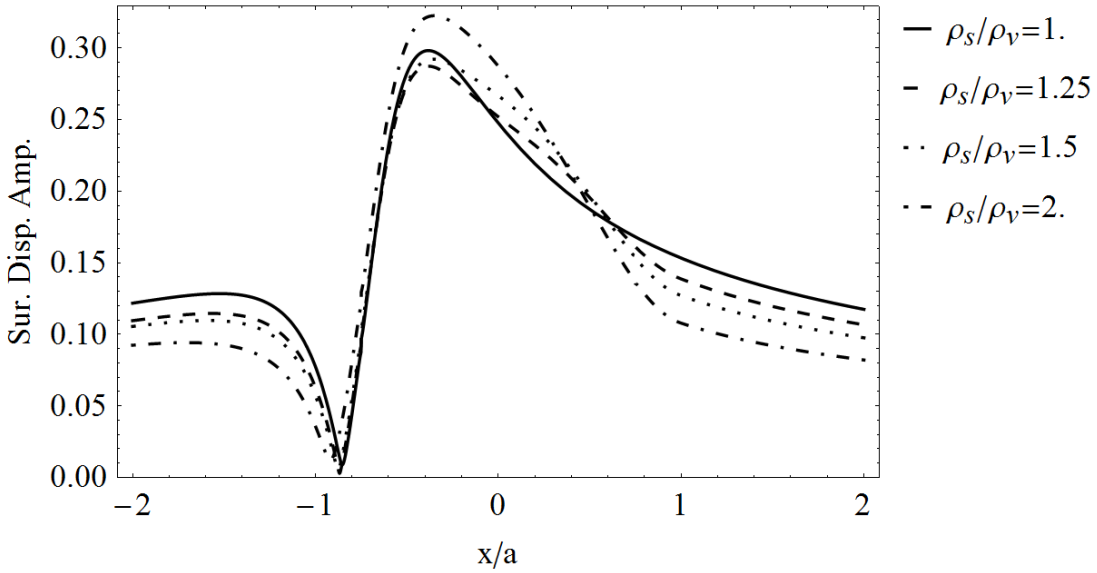

Figure A.26 : Effect of Density Differentness for $N = 100$, $\eta = 1$, $a_f/a = 0.75$, $\alpha_f = \pi/6$, $\alpha_{fl} = \pi/8$, $\mu_s/\mu_v = 1$.

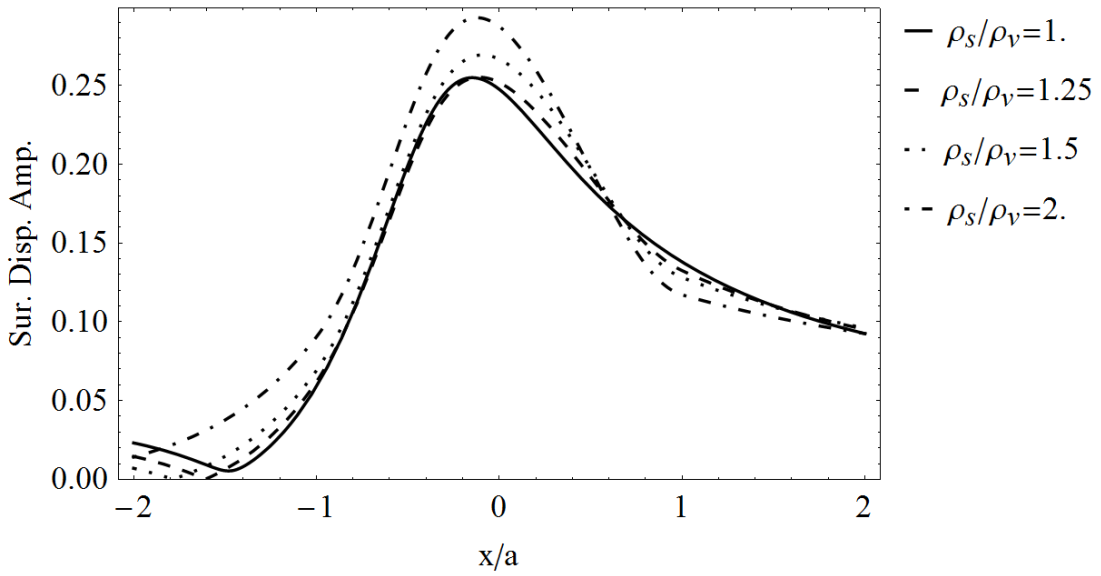

Figure A.27 : Effect of Density Differentness for $N = 100$, $\eta = 1$, $a_f/a = 0.75$, $\alpha_f = \pi/3$, $\alpha_{fl} = \pi/8$, $\mu_s/\mu_v = 1$.

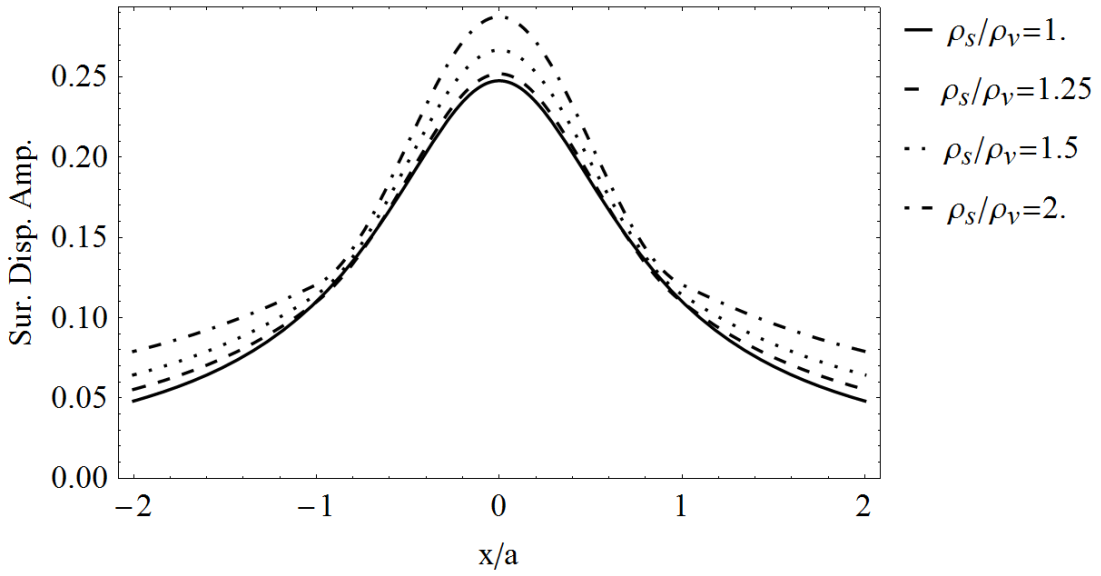

Figure A.28 : Effect of Density Differentness for $N = 100$, $\eta = 1$, $a_f/a = 0.75$, $\alpha_f = \pi/2$, $\alpha_{fl} = \pi/8$, $\mu_s/\mu_v = 1$.

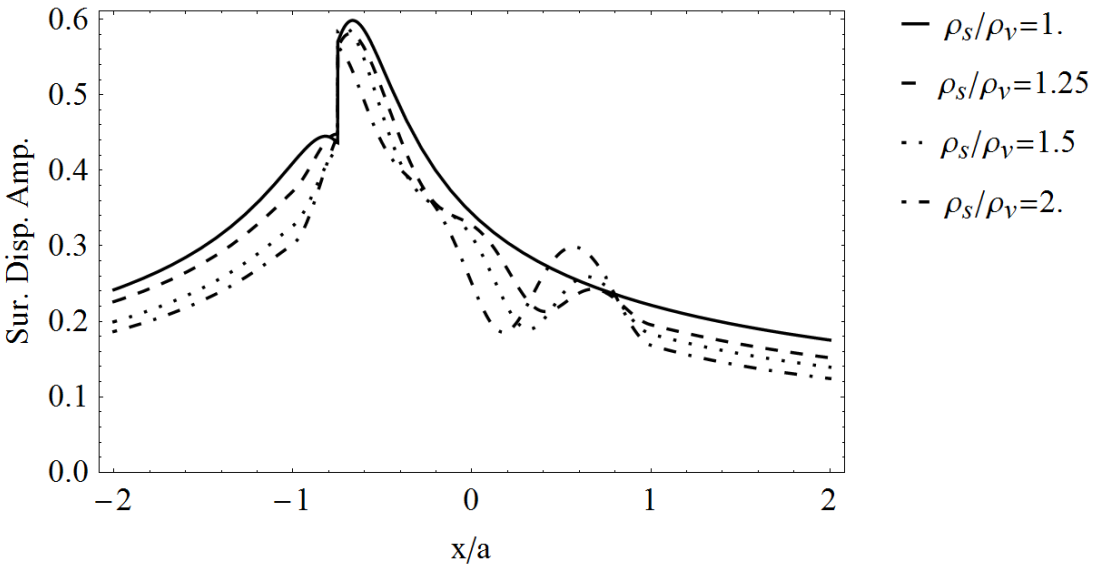

Figure A.29 : Effect of Density Differentness for $N = 100$, $\eta = 2$, $a_f/a = 0.75$, $\alpha_f = \pi/16$, $\alpha_{fl} = \pi/8$, $\mu_s/\mu_v = 1$.

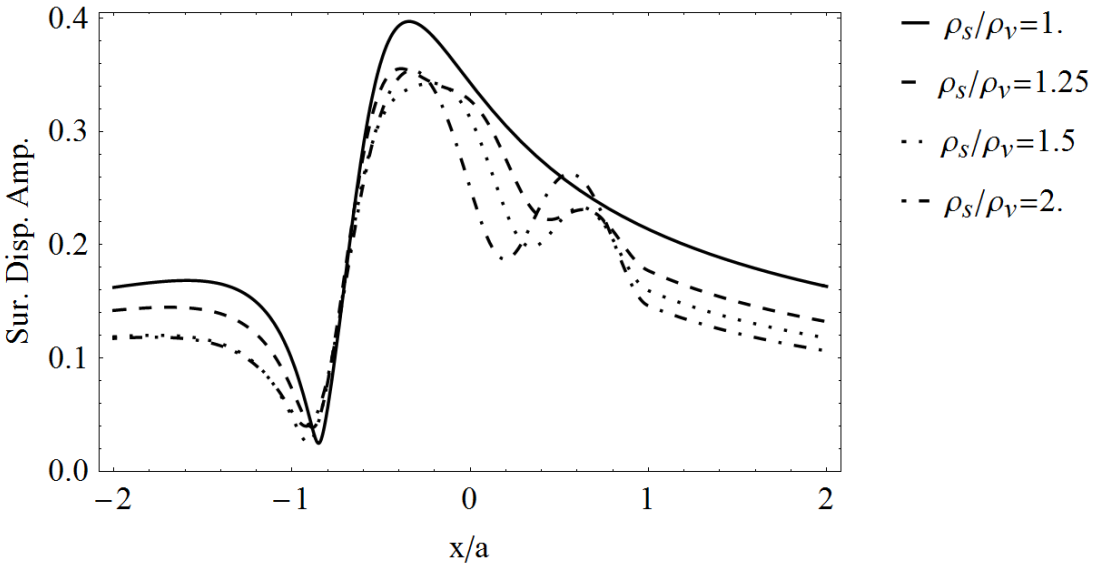

Figure A.30 : Effect of Density Differentness for $N = 100$, $\eta = 2$, $a_f/a = 0.75$, $\alpha_f = \pi/6$, $\alpha_{fl} = \pi/8$, $\mu_s/\mu_v = 1$.

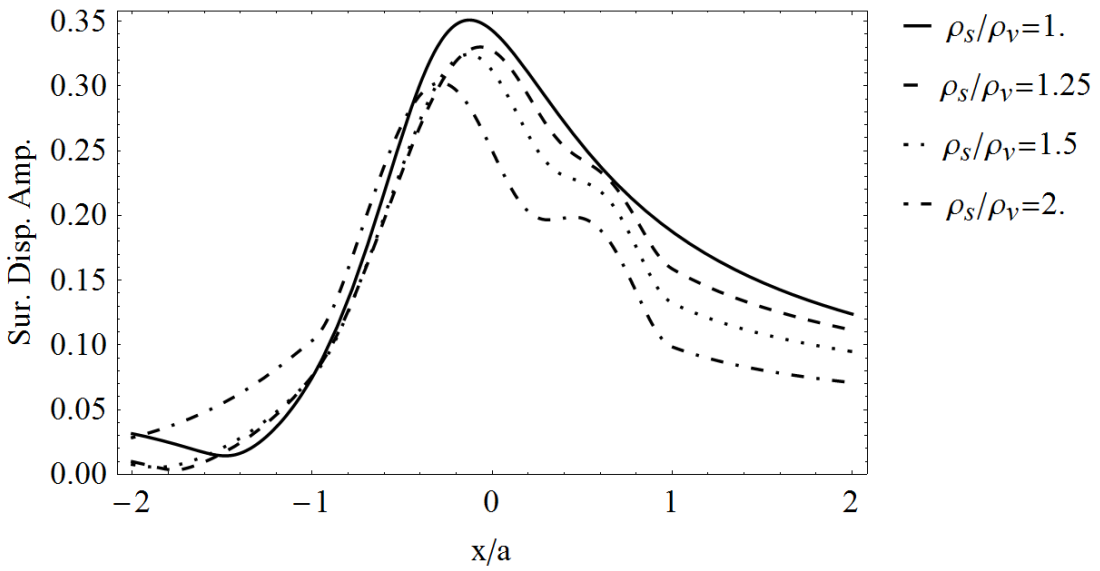

Figure A.31 : Effect of Density Differentness for $N = 100$, $\eta = 2$, $a_f/a = 0.75$, $\alpha_f = \pi/3$, $\alpha_{fl} = \pi/8$, $\mu_s/\mu_v = 1$.

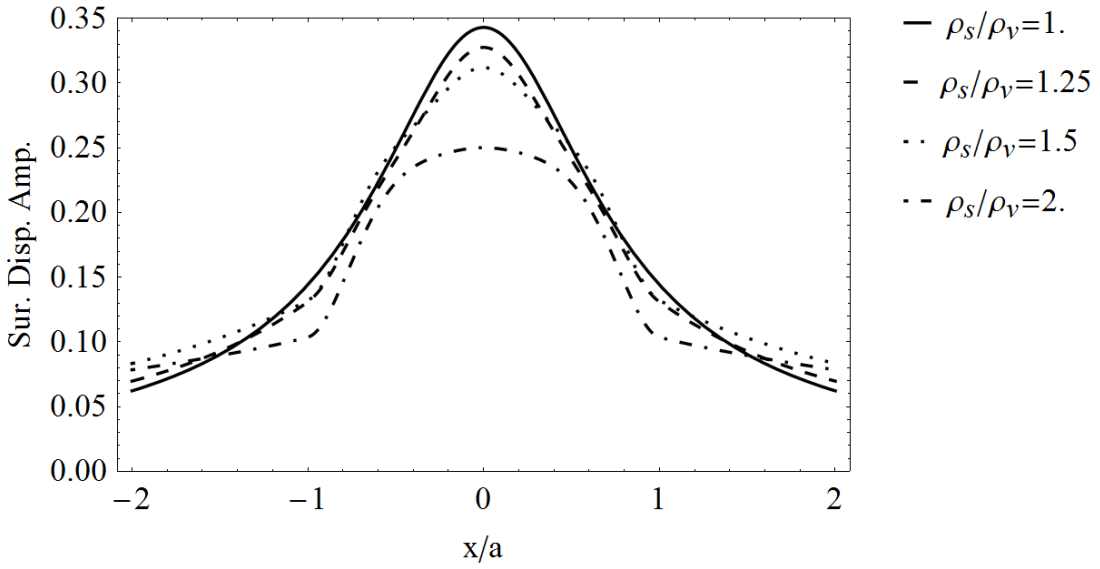

Figure A.32 : Effect of Density Differentness for $N = 100$, $\eta = 2$, $a_f/a = 0.75$, $\alpha_f = \pi/2$, $\alpha_{fl} = \pi/8$, $\mu_s/\mu_v = 1$.

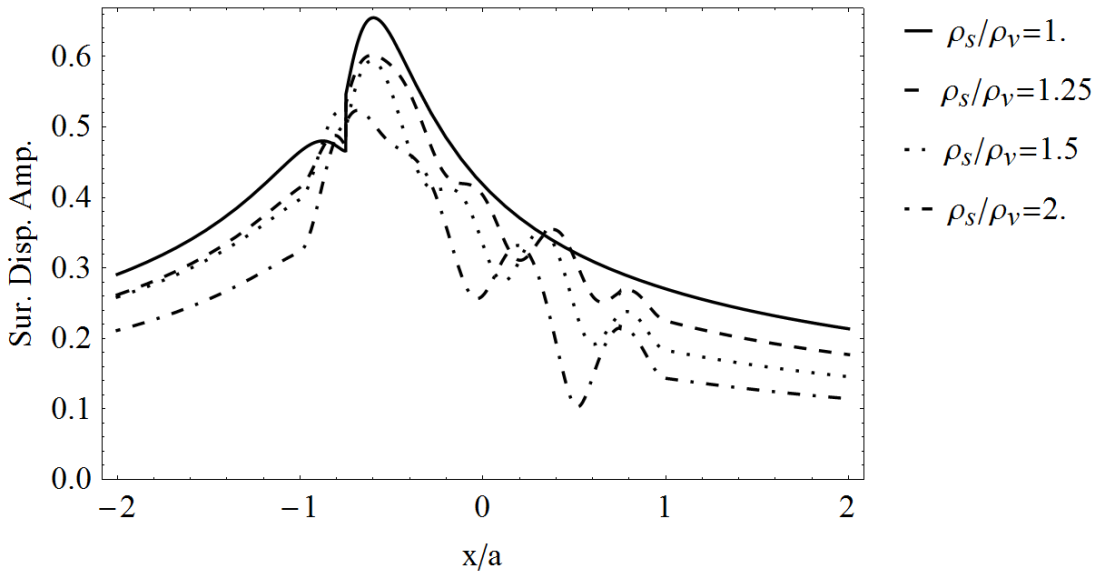

Figure A.33 : Effect of Density Differentness for $N = 100$, $\eta = 3$, $a_f/a = 0.75$, $\alpha_f = \pi/16$, $\alpha_{fl} = \pi/8$, $\mu_s/\mu_v = 1$.

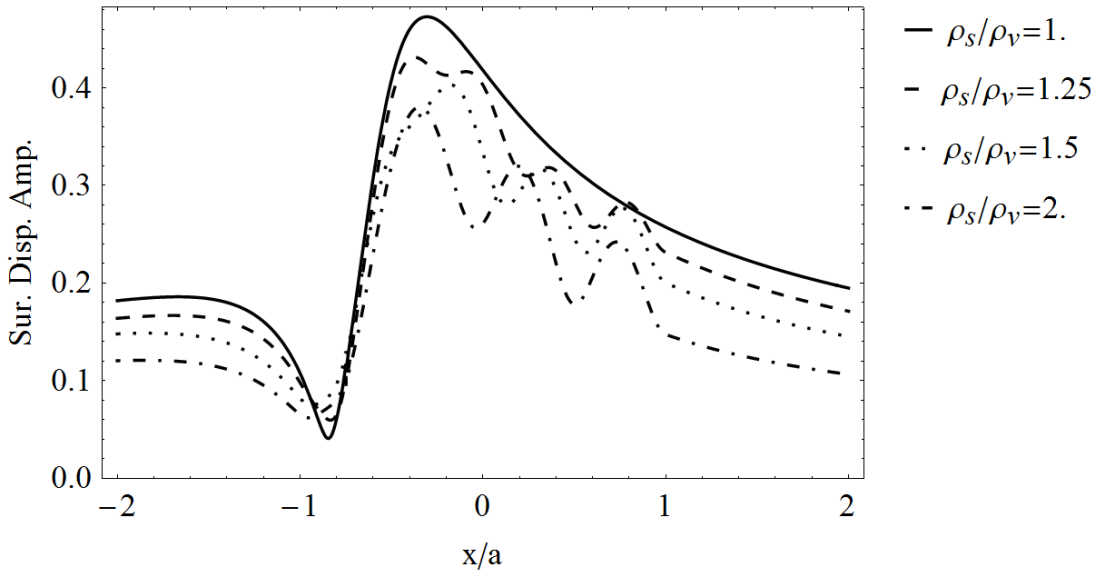

Figure A.34 : Effect of Density Differentness for $N = 100$, $\eta = 3$, $a_f/a = 0.75$, $\alpha_f = \pi/6$, $\alpha_{fl} = \pi/8$, $\mu_s/\mu_v = 1$.

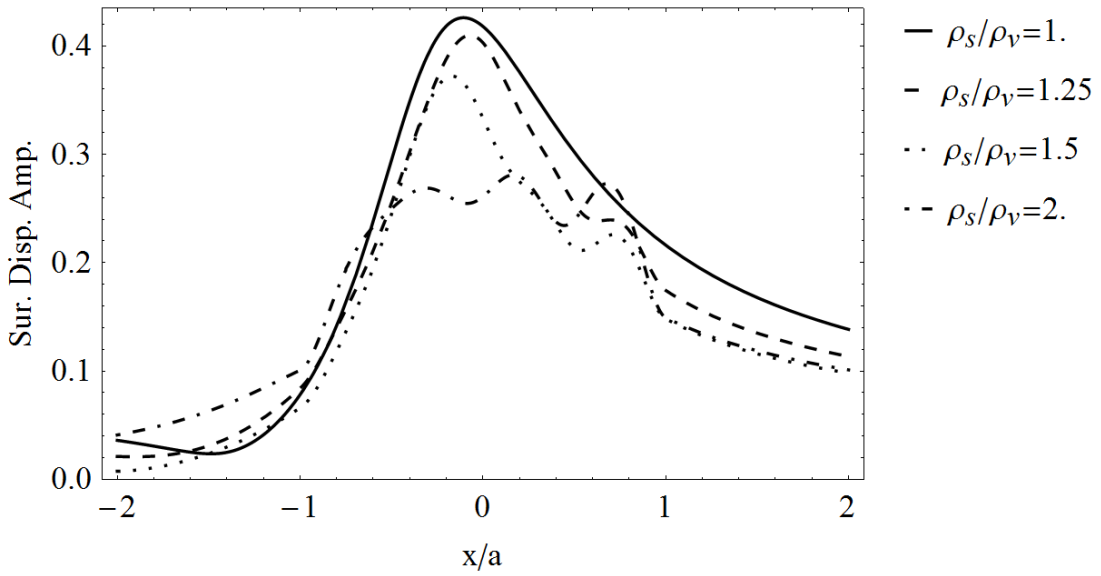

Figure A.35 : Effect of Density Differentness for $N = 100$, $\eta = 3$, $a_f/a = 0.75$, $\alpha_f = \pi/3$, $\alpha_{fl} = \pi/8$, $\mu_s/\mu_v = 1$.

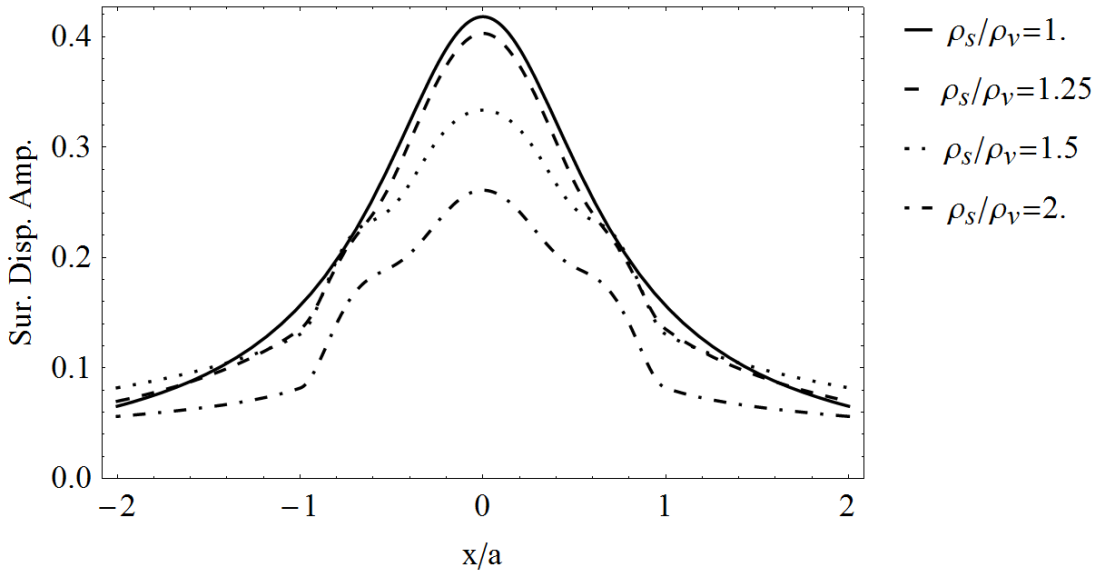

Figure A.36 : Effect of Density Differentness for $N = 100$, $\eta = 3$, $a_f/a = 0.75$, $\alpha_f = \pi/2$, $\alpha_{fl} = \pi/8$, $\mu_s/\mu_v = 1$.

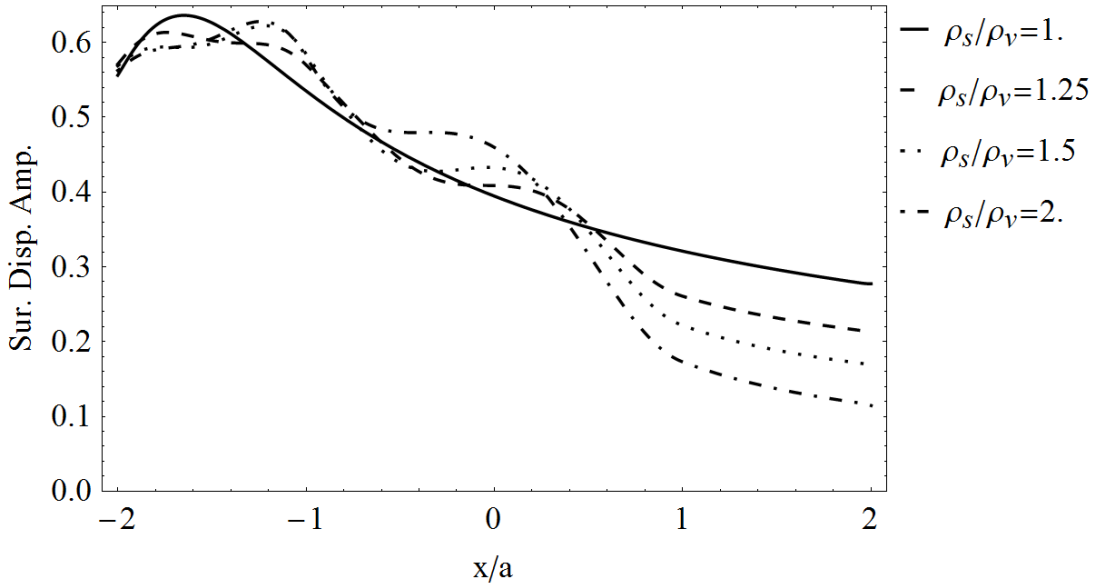

Figure A.37 : Effect of Density Differentness for $N = 100$, $\eta = 1$, $a_f/a = 2$, $\alpha_f = \pi/16$, $\alpha_{fl} = \pi/8$, $\mu_s/\mu_v = 1$.

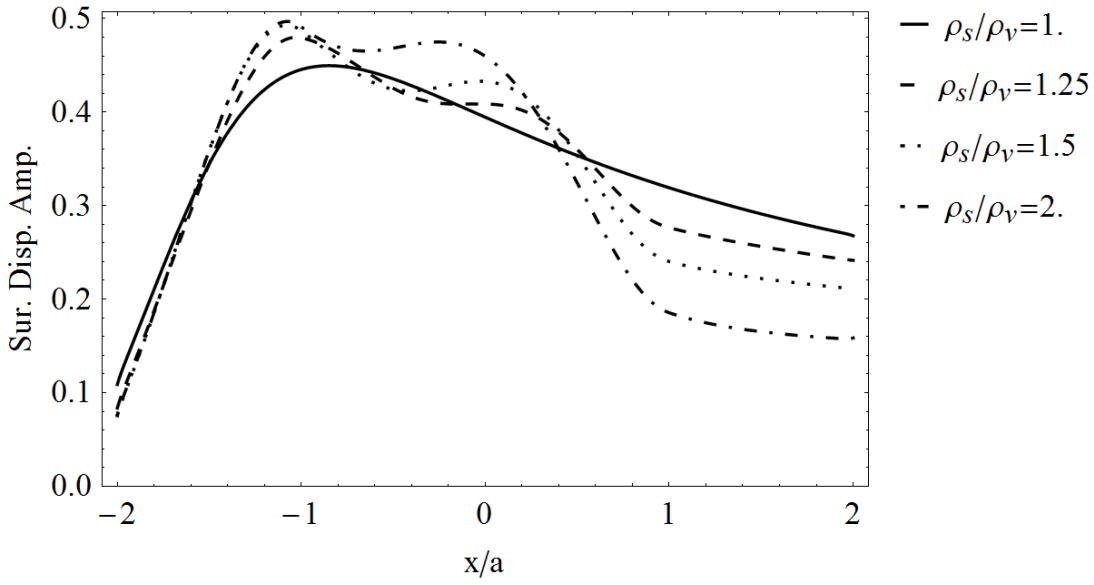

Figure A.38 : Effect of Density Differentness for $N = 100$, $\eta = 1$, $a_f/a = 2$, $\alpha_f = \pi/6$, $\alpha_{fl} = \pi/8$, $\mu_s/\mu_v = 1$.

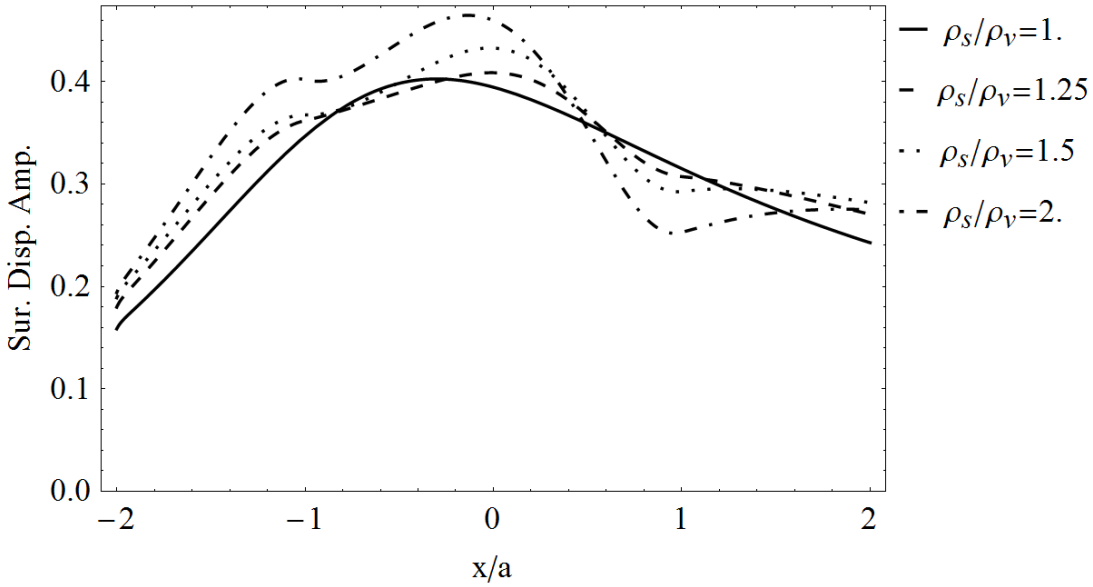

Figure A.39 : Effect of Density Differentness for $N = 100$, $\eta = 1$, $a_f/a = 2$, $\alpha_f = \pi/3$, $\alpha_{fl} = \pi/8$, $\mu_s/\mu_v = 1$.

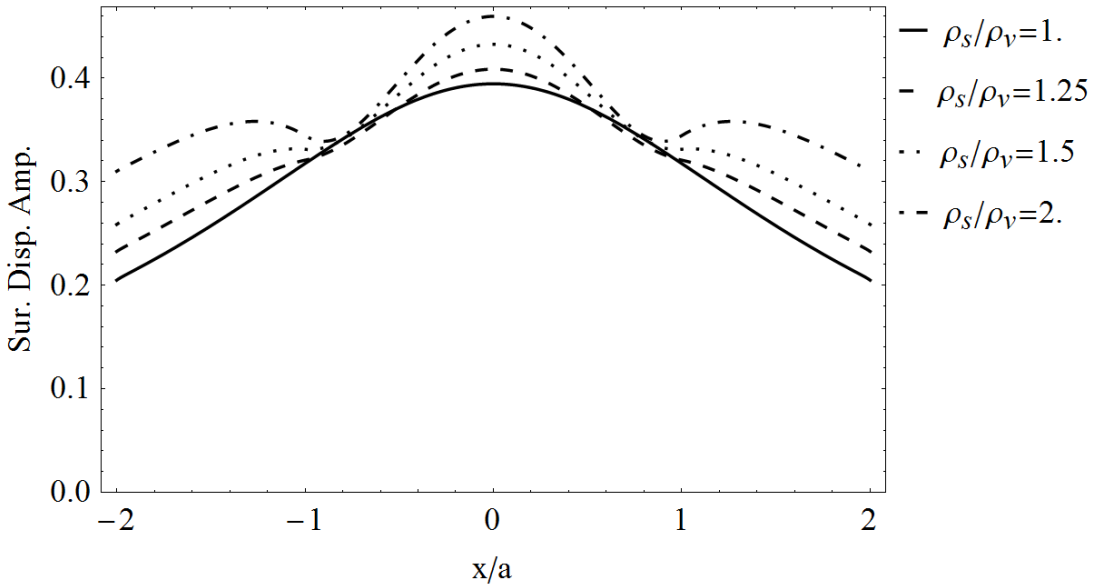

Figure A.40 : Effect of Density Differentness for $N = 100$, $\eta = 1$, $a_f/a = 2$, $\alpha_f = \pi/2$, $\alpha_{fl} = \pi/8$, $\mu_s/\mu_v = 1$.

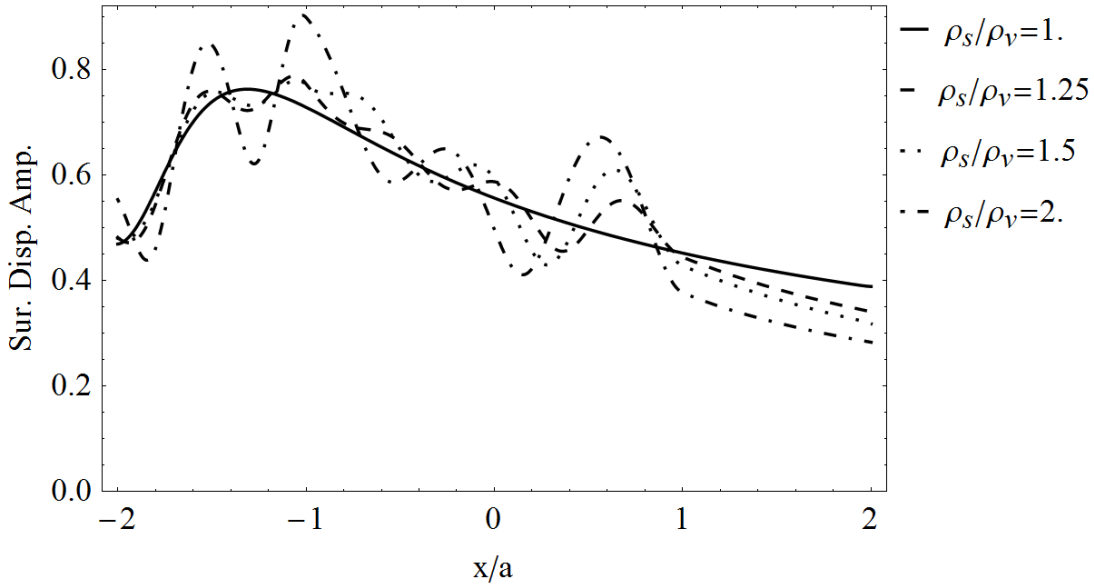

Figure A.41 : Effect of Density Differentness for $N = 100$, $\eta = 2$, $a_f/a = 2$, $\alpha_f = \pi/16$, $\alpha_{fl} = \pi/8$, $\mu_s/\mu_v = 1$.

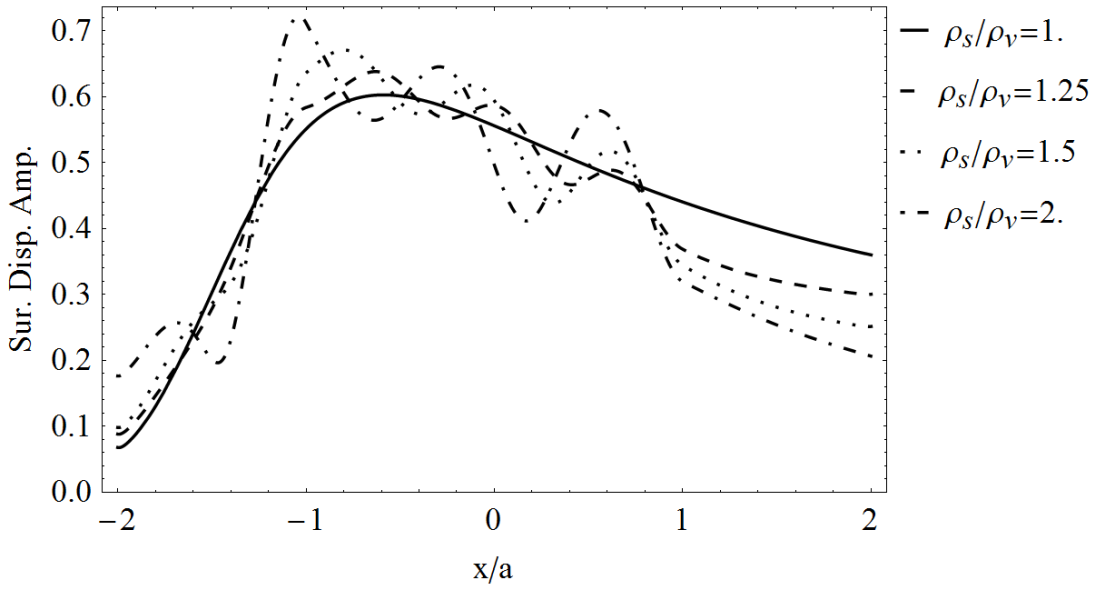

Figure A.42 : Effect of Density Differentness for $N = 100$, $\eta = 2$, $a_f/a = 2$, $\alpha_f = \pi/6$, $\alpha_{fl} = \pi/8$, $\mu_s/\mu_v = 1$.

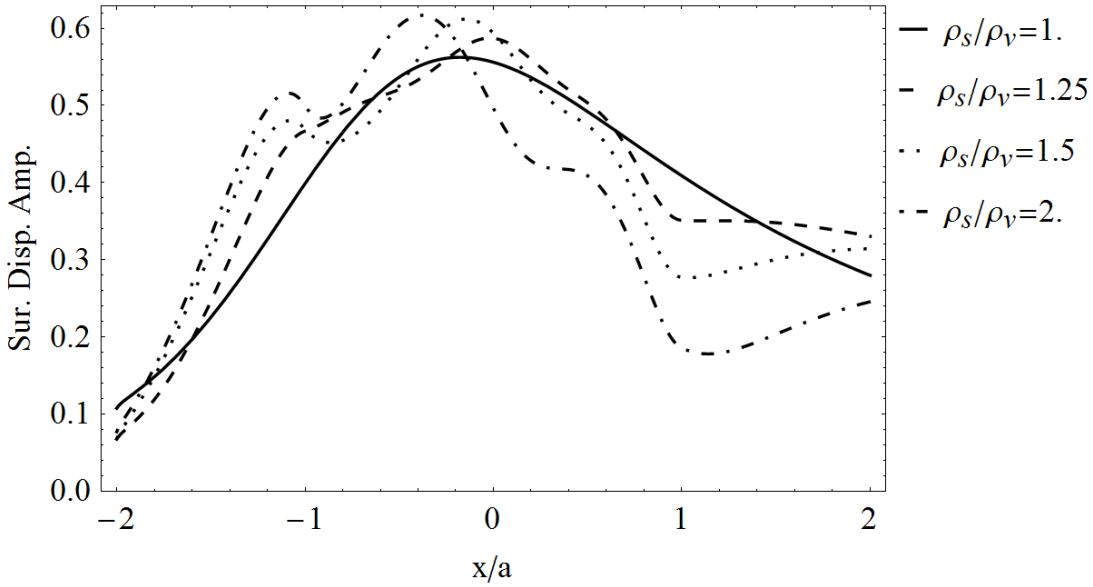

Figure A.43 : Effect of Density Differentness for $N = 100$, $\eta = 2$, $a_f/a = 2$, $\alpha_f = \pi/3$, $\alpha_{fl} = \pi/8$, $\mu_s/\mu_v = 1$.

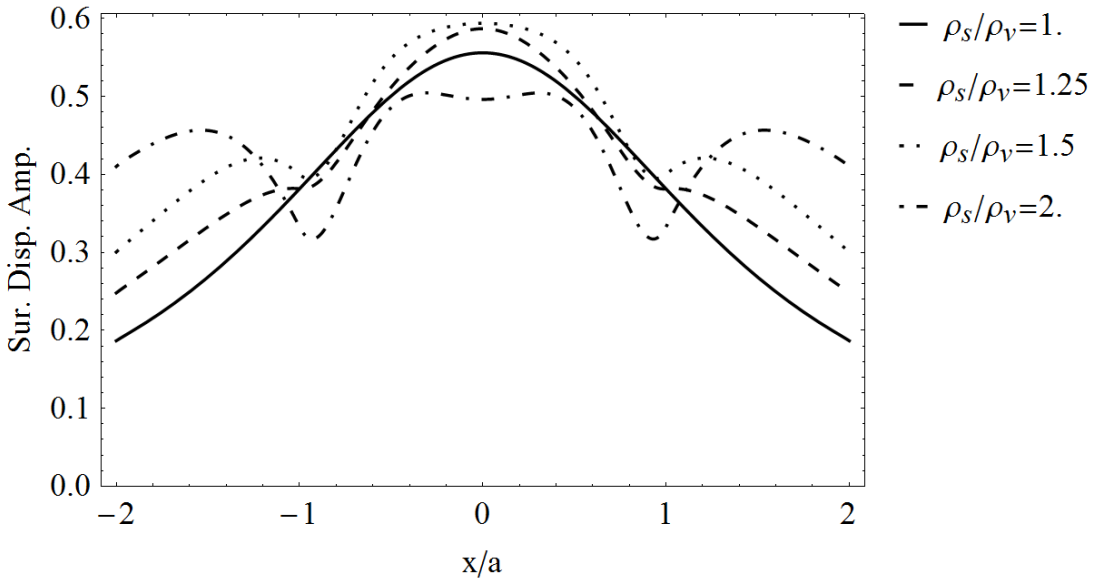

Figure A.44 : Effect of Density Differentness for $N = 100$, $\eta = 2$, $a_f/a = 2$, $\alpha_f = \pi/2$, $\alpha_{fl} = \pi/8$, $\mu_s/\mu_v = 1$.

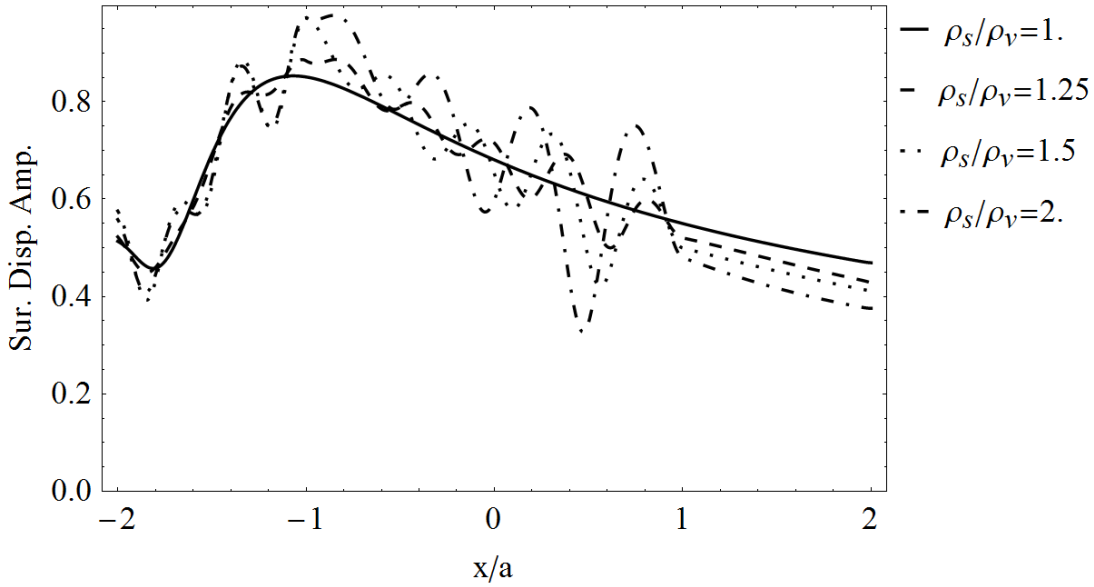

Figure A.45 : Effect of Density Differentness for $N = 100$, $\eta = 3$, $a_f/a = 2$, $\alpha_f = \pi/16$, $\alpha_{fl} = \pi/8$, $\mu_s/\mu_v = 1$.

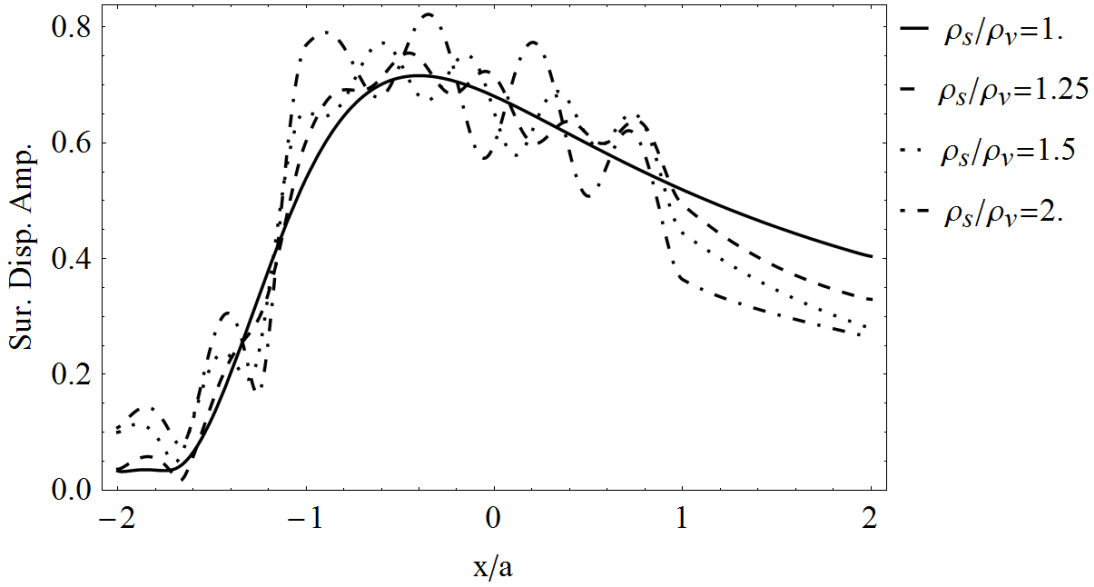

Figure A.46 : Effect of Density Differentness for $N = 100$, $\eta = 3$, $a_f/a = 2$, $\alpha_f = \pi/6$, $\alpha_{fl} = \pi/8$, $\mu_s/\mu_v = 1$.

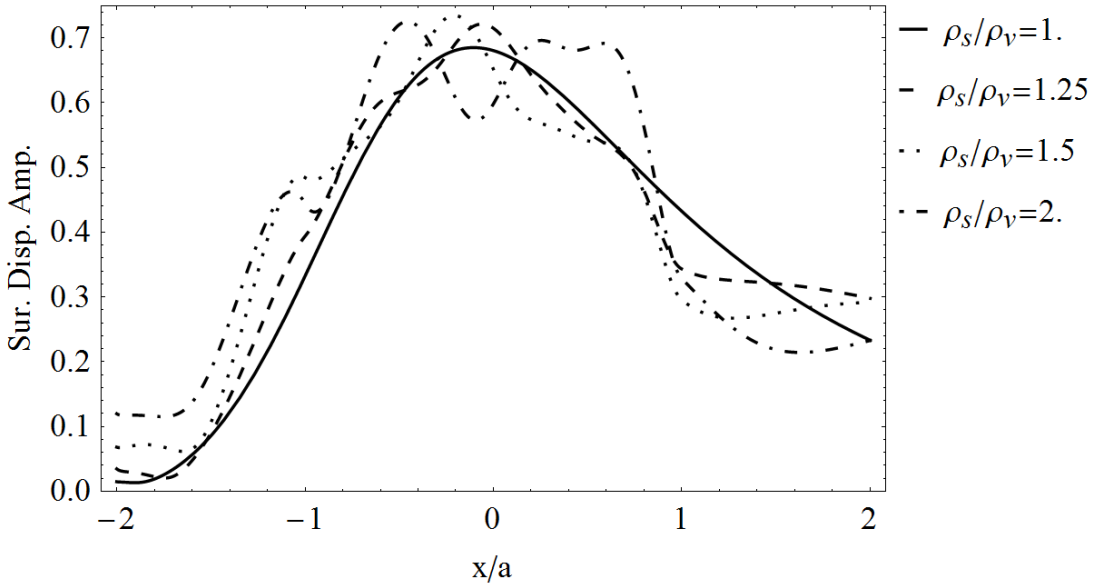

Figure A.47 : Effect of Density Differentness for $N = 100$, $\eta = 3$, $a_f/a = 2$, $\alpha_f = \pi/3$, $\alpha_{fl} = \pi/8$, $\mu_s/\mu_v = 1$.

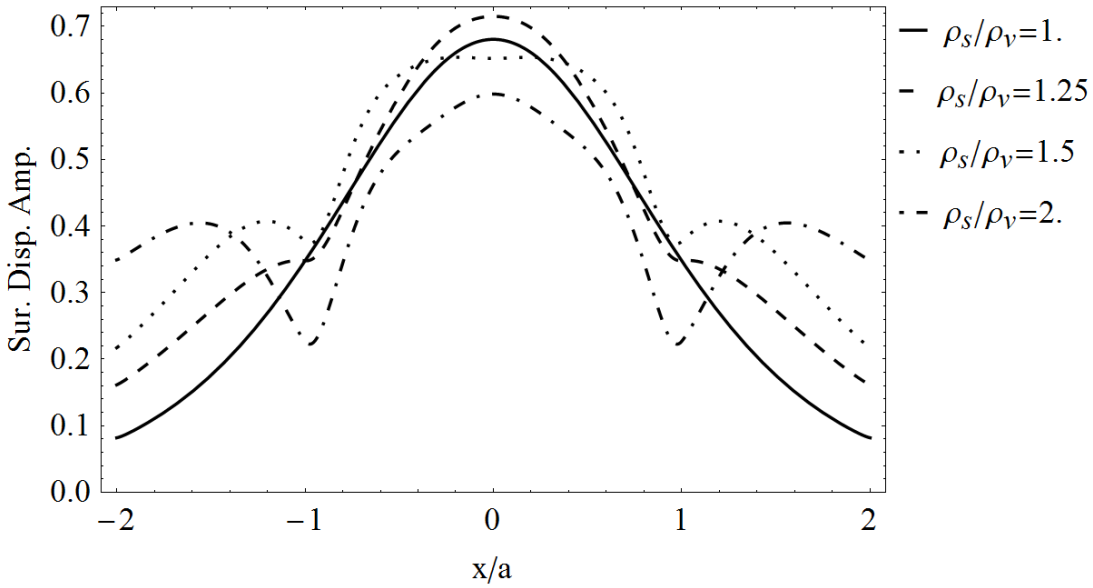

Figure A.48 : Effect of Density Differentness for $N = 100$, $\eta = 3$, $a_f/a = 2$, $\alpha_f = \pi/2$, $\alpha_{fl} = \pi/8$, $\mu_s/\mu_v = 1$.

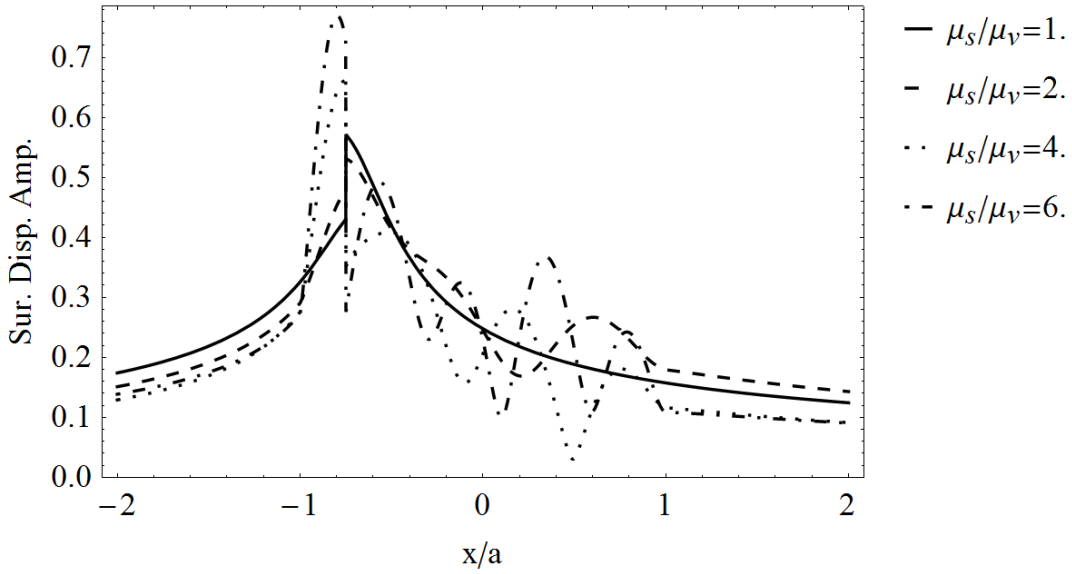

Figure A.49 : Effect of Shear Modulus Differentness for $N = 100$, $\eta = 1$, $a_f/a = 0.75$, $\alpha_f = \pi/16$, $\alpha_{fl} = \pi/8$, $\rho_s/\rho_v = 1$.

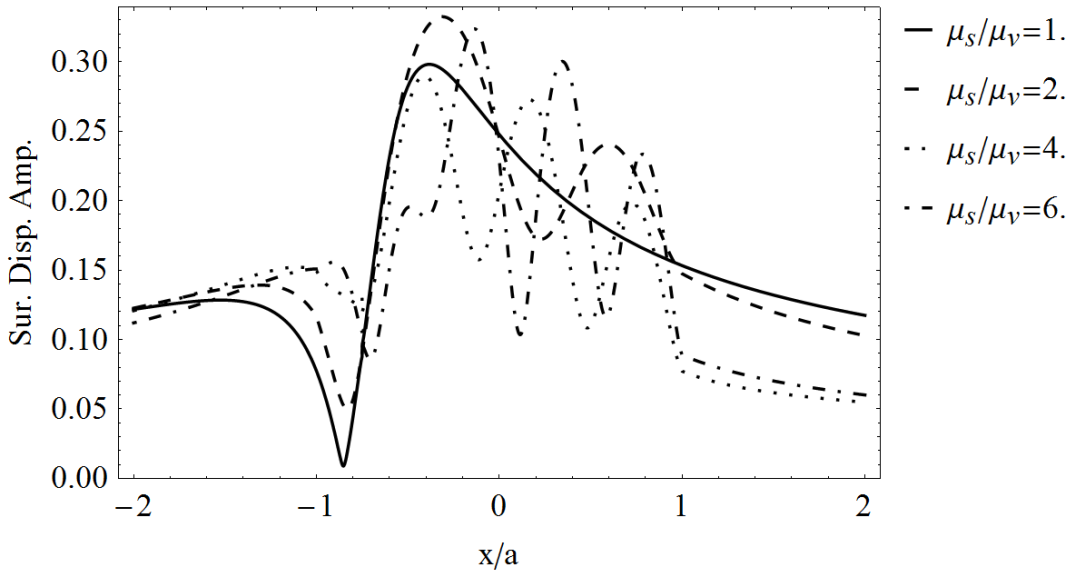

Figure A.50 : Effect of Shear Modulus Differentness for $N = 100$, $\eta = 1$, $a_f/a = 0.75$, $\alpha_f = \pi/6$, $\alpha_{fl} = \pi/8$, $\rho_s/\rho_v = 1$.

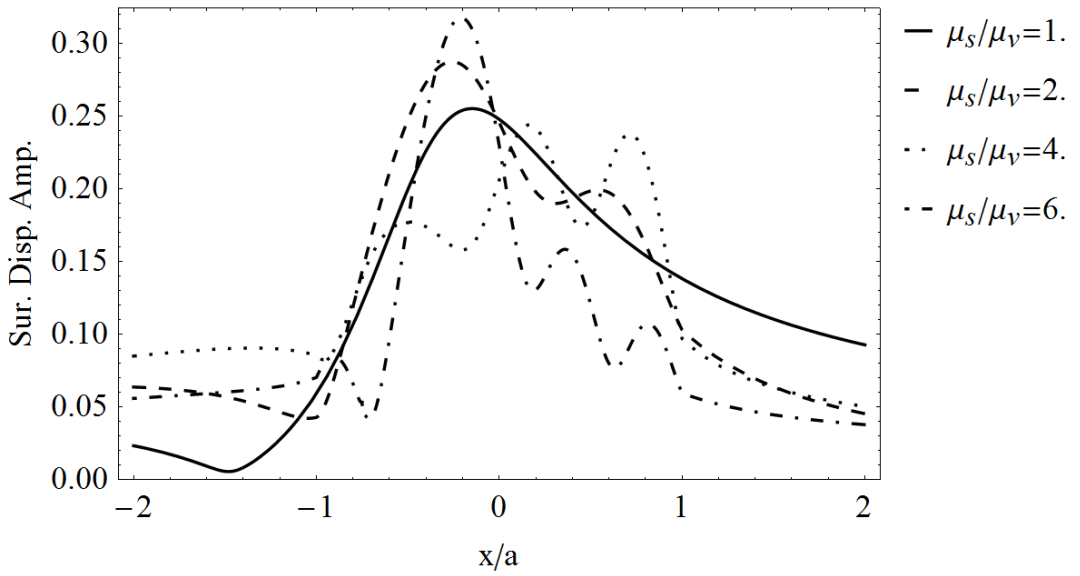

Figure A.51 : Effect of Shear Modulus Differentness for $N = 100$, $\eta = 1$, $a_f/a = 0.75$, $\alpha_f = \pi/3$, $\alpha_{fl} = \pi/8$, $\rho_s/\rho_v = 1$.

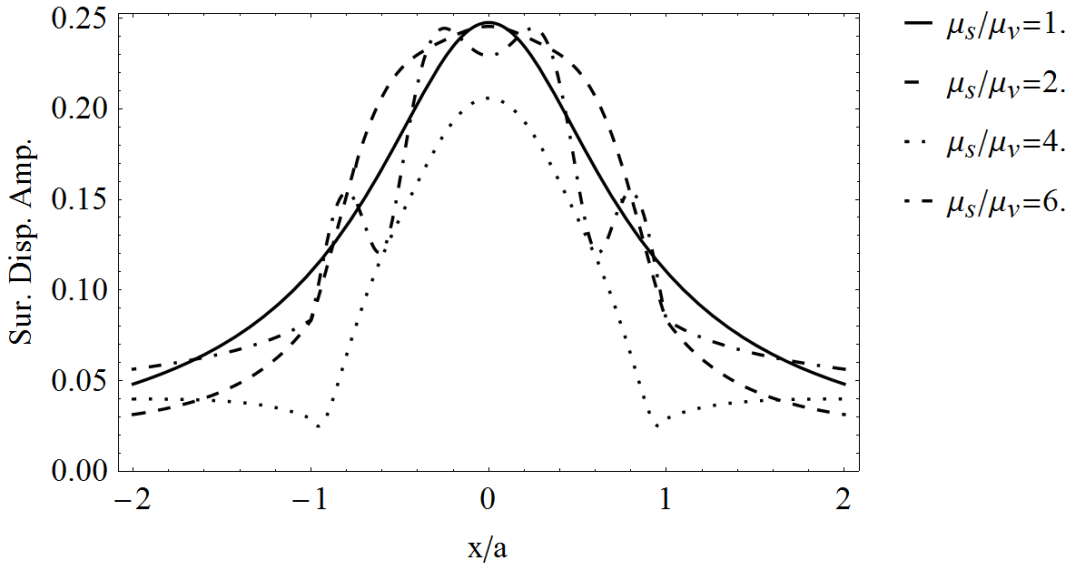

Figure A.52 : Effect of Shear Modulus Differentness for $N = 100$, $\eta = 1$, $a_f/a = 0.75$, $\alpha_f = \pi/2$, $\alpha_{fl} = \pi/8$, $\rho_s/\rho_v = 1$.

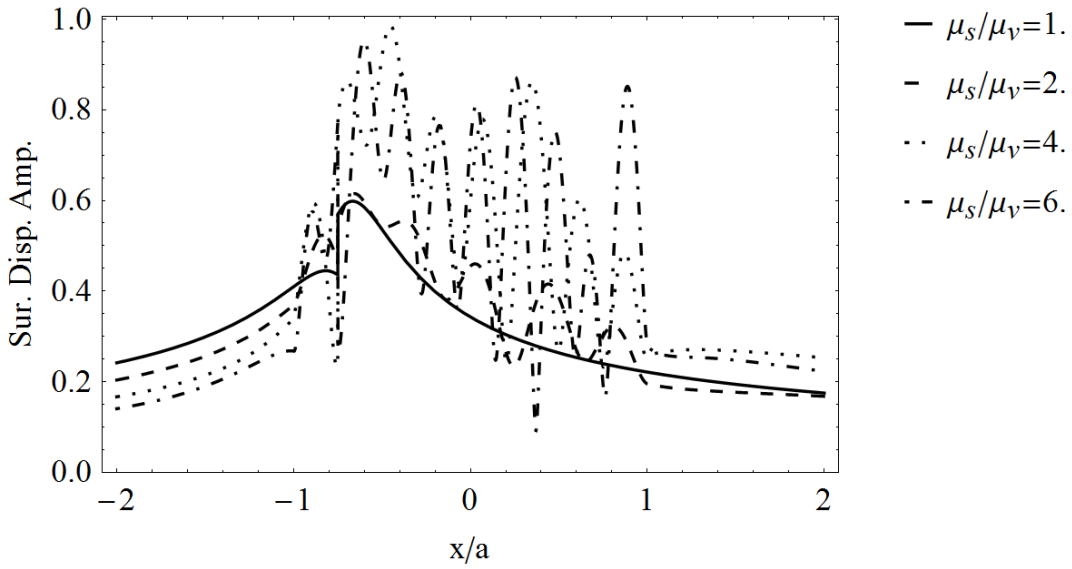

Figure A.53 : Effect of Shear Modulus Differentness for $N = 100$, $\eta = 2$, $a_f/a = 0.75$, $\alpha_f = \pi/16$, $\alpha_{fl} = \pi/8$, $\rho_s/\rho_v = 1$.

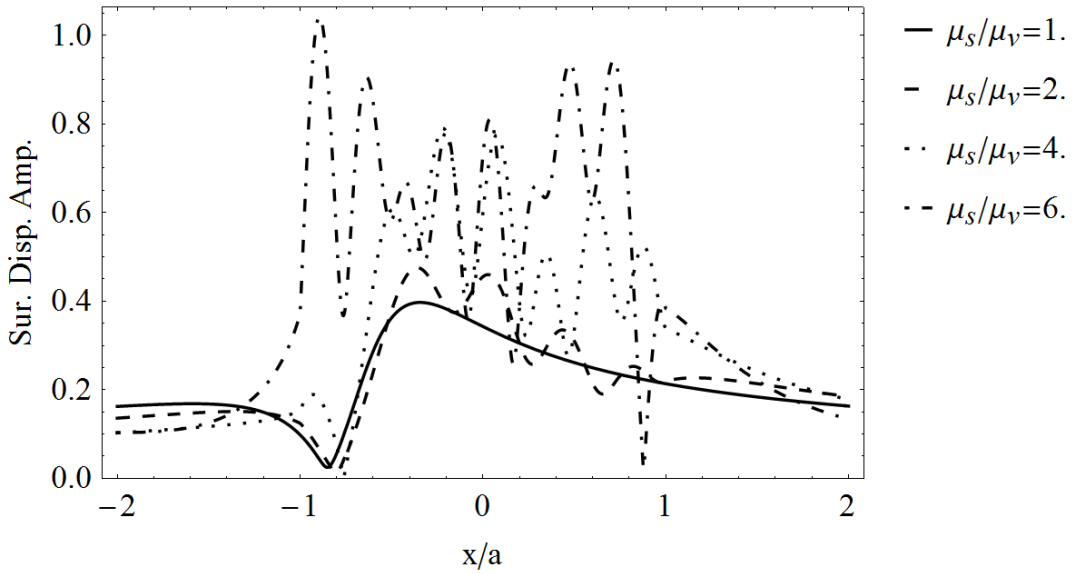

Figure A.54 : Effect of Shear Modulus Differentness for $N = 100$, $\eta = 2$, $a_f/a = 0.75$, $\alpha_f = \pi/6$, $\alpha_{fl} = \pi/8$, $\rho_s/\rho_v = 1$.

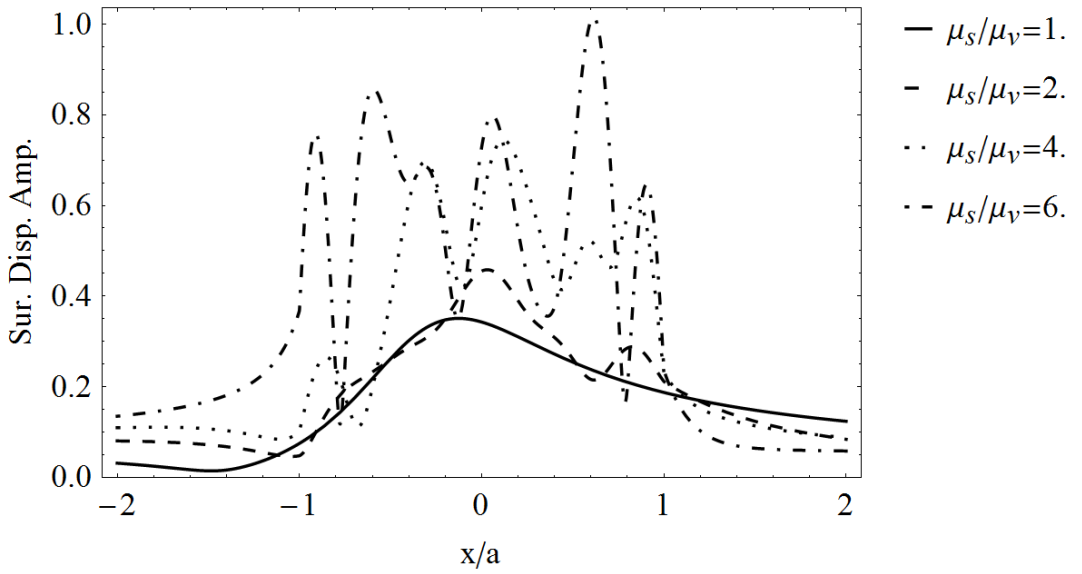

Figure A.55 : Effect of Shear Modulus Differentness for $N = 100$, $\eta = 2$, $a_f/a = 0.75$, $\alpha_f = \pi/3$, $\alpha_{fl} = \pi/8$, $\rho_s/\rho_v = 1$.

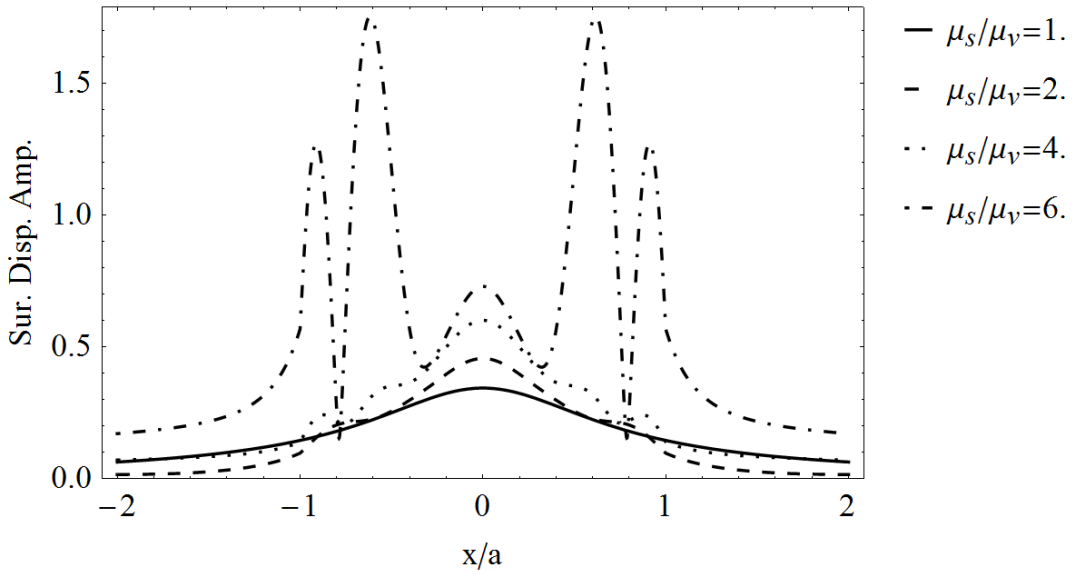

Figure A.56 : Effect of Shear Modulus Differentness for $N = 100$, $\eta = 2$, $a_f/a = 0.75$, $\alpha_f = \pi/2$, $\alpha_{fl} = \pi/8$, $\rho_s/\rho_v = 1$.

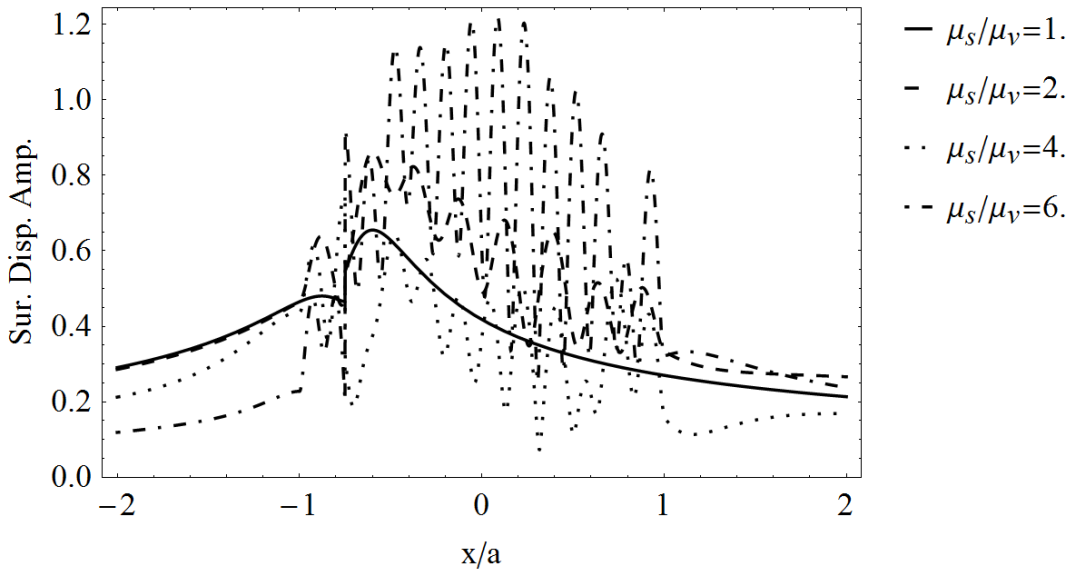

Figure A.57 : Effect of Shear Modulus Differentness for $N = 100$, $\eta = 3$, $a_f/a = 0.75$, $\alpha_f = \pi/16$, $\alpha_{fl} = \pi/8$, $\rho_s/\rho_v = 1$.

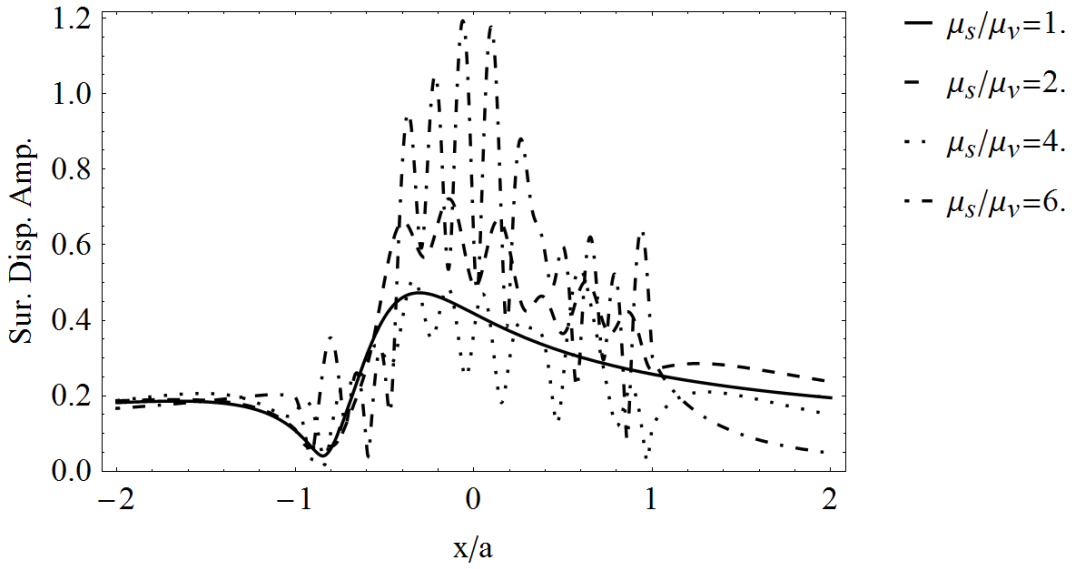

Figure A.58 : Effect of Shear Modulus Differentness for $N = 100$, $\eta = 3$, $a_f/a = 0.75$, $\alpha_f = \pi/6$, $\alpha_{fl} = \pi/8$, $\rho_s/\rho_v = 1$.

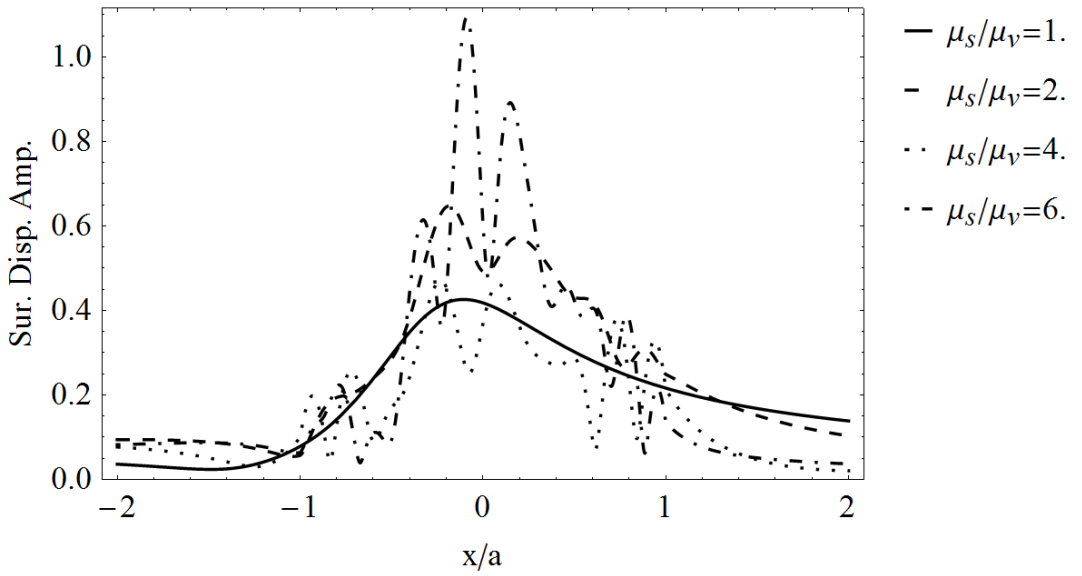

Figure A.59 : Effect of Shear Modulus Differentness for $N = 100$, $\eta = 3$, $a_f/a = 0.75$, $\alpha_f = \pi/3$, $\alpha_{fl} = \pi/8$, $\rho_s/\rho_v = 1$.

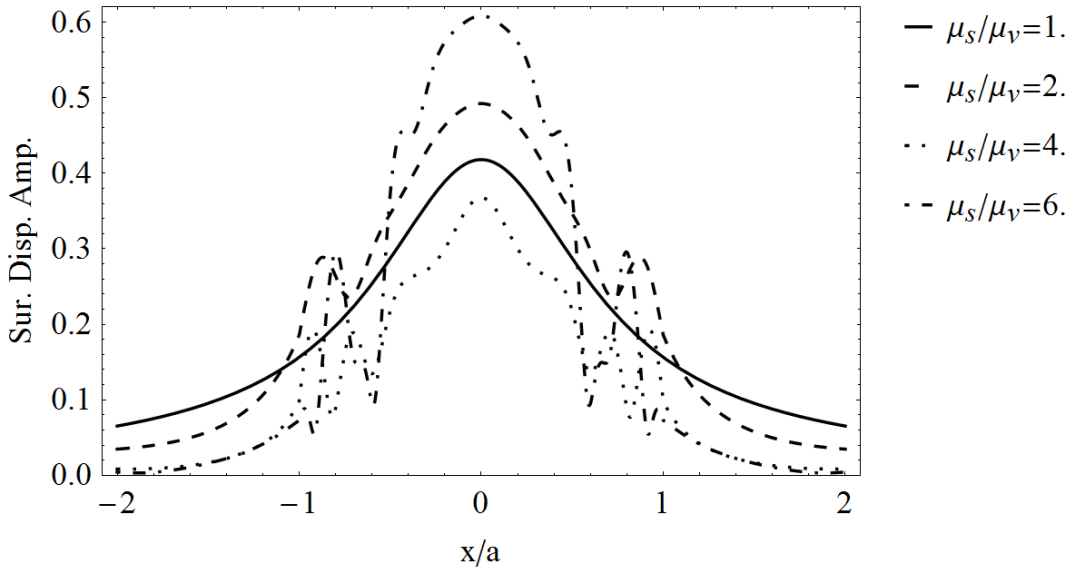

Figure A.60 : Effect of Shear Modulus Differentness for $N = 100$, $\eta = 3$, $a_f/a = 0.75$, $\alpha_f = \pi/2$, $\alpha_{fl} = \pi/8$, $\rho_s/\rho_v = 1$.

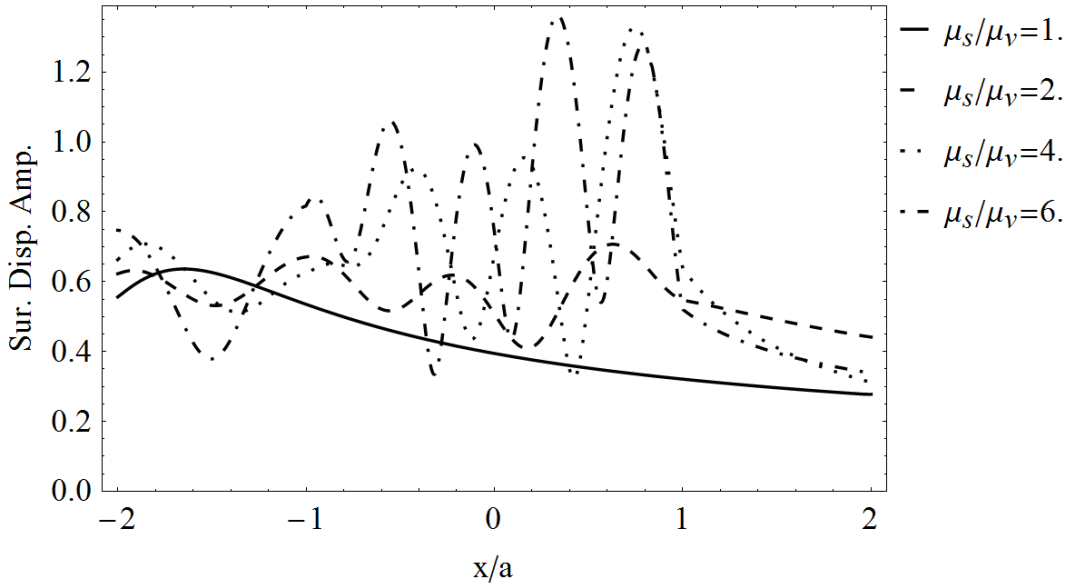

Figure A.61 : Effect of Shear Modulus Differentness for $N = 100$, $\eta = 1$, $a_f/a = 2$, $\alpha_f = \pi/16$, $\alpha_{fl} = \pi/8$, $\rho_s/\rho_v = 1$.

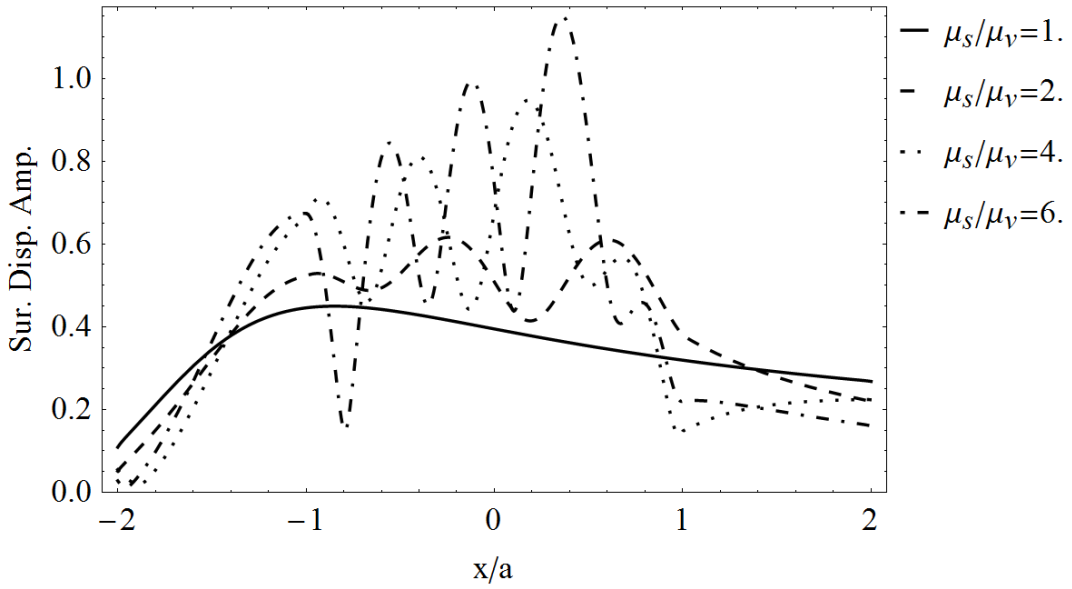

Figure A.62 : Effect of Shear Modulus Differentness for $N = 100$, $\eta = 1$, $a_f/a = 2$, $\alpha_f = \pi/6$, $\alpha_{fl} = \pi/8$, $\rho_s/\rho_v = 1$.

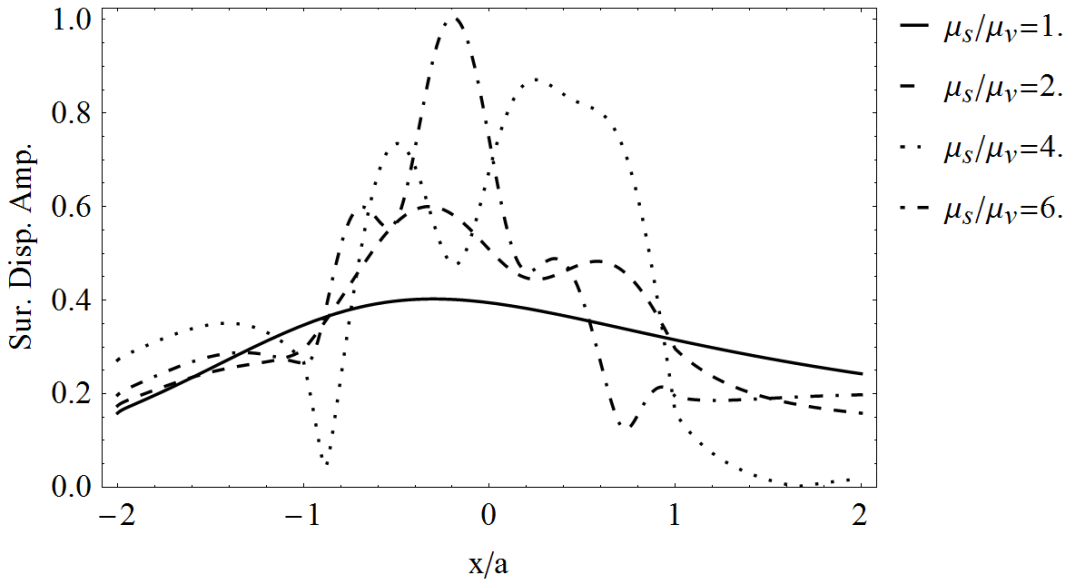

Figure A.63 : Effect of Shear Modulus Differentness for $N = 100$, $\eta = 1$, $a_f/a = 2$, $\alpha_f = \pi/3$, $\alpha_{fl} = \pi/8$, $\rho_s/\rho_v = 1$.

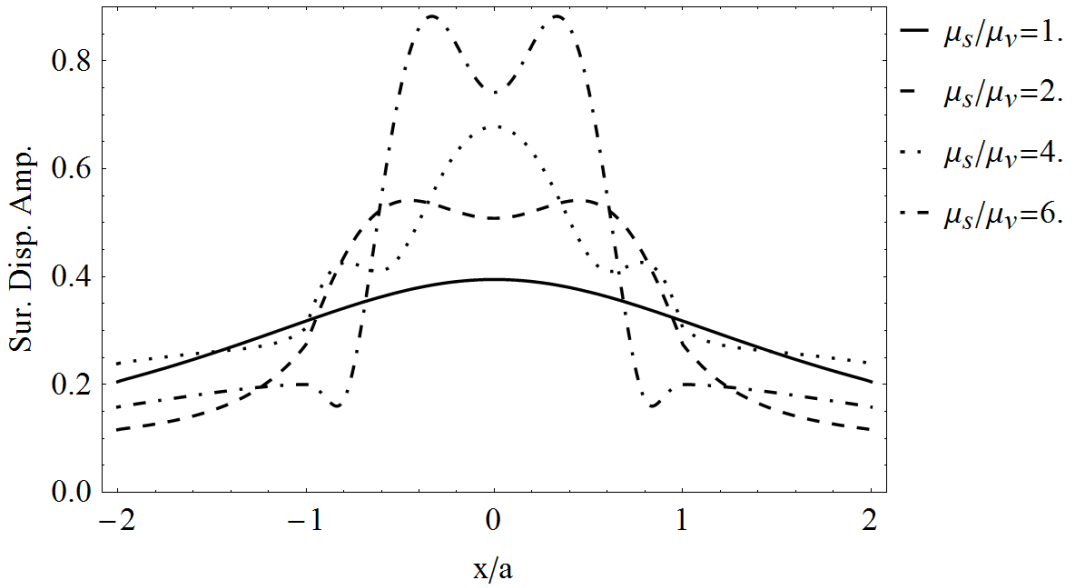

Figure A.64 : Effect of Shear Modulus Differentness for $N = 100$, $\eta = 1$, $a_f/a = 2$, $\alpha_f = \pi/2$, $\alpha_{fl} = \pi/8$, $\rho_s/\rho_v = 1$.

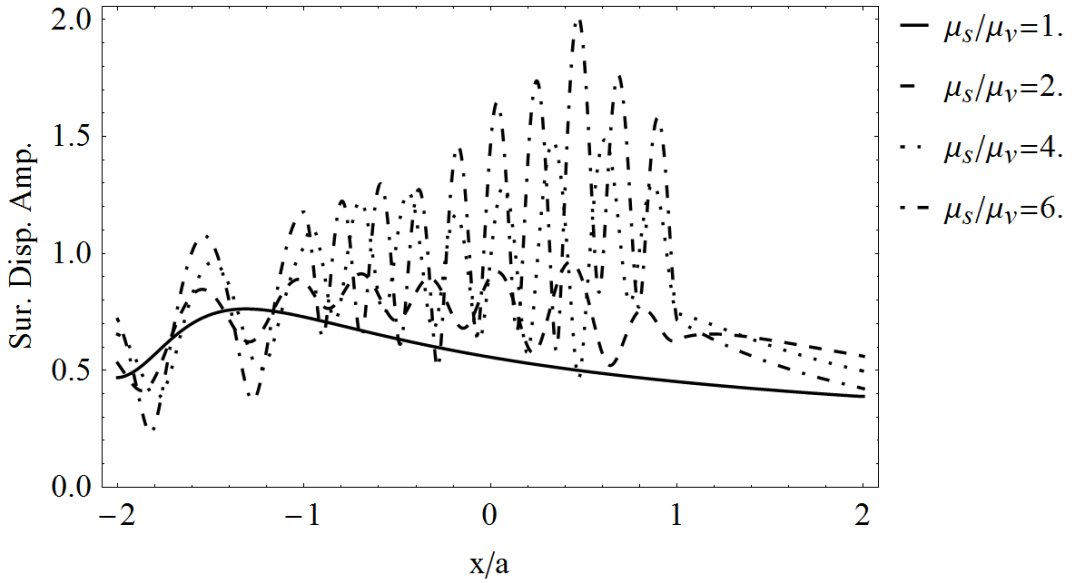

Figure A.65 : Effect of Shear Modulus Differentness for $N = 100$, $\eta = 2$, $a_f/a = 2$, $\alpha_f = \pi/16$, $\alpha_{fl} = \pi/8$, $\rho_s/\rho_v = 1$.

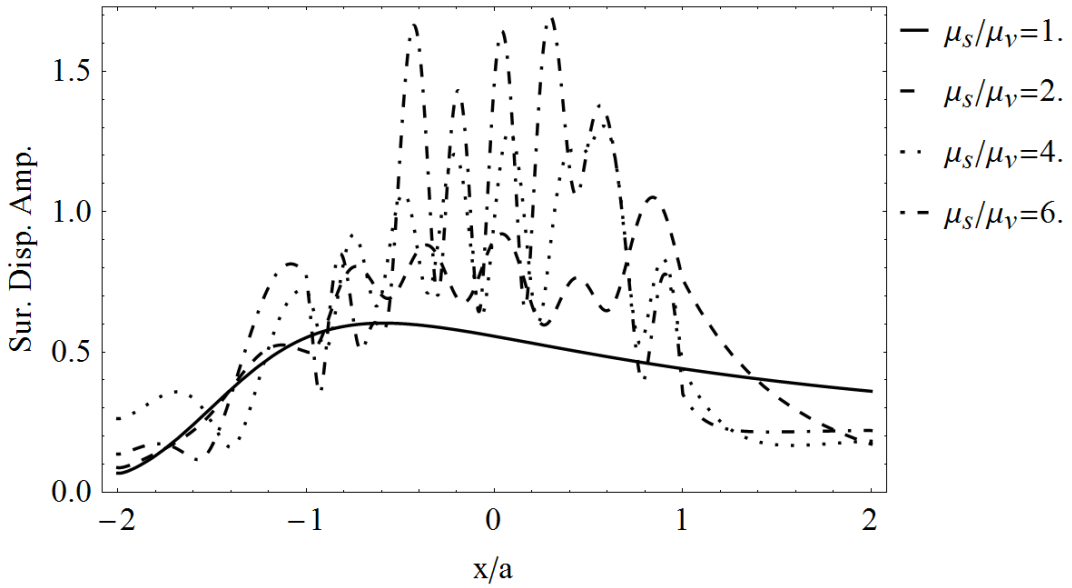

Figure A.66 : Effect of Shear Modulus Differentness for $N = 100$, $\eta = 2$, $a_f/a = 2$, $\alpha_f = \pi/6$, $\alpha_{fl} = \pi/8$, $\rho_s/\rho_v = 1$.

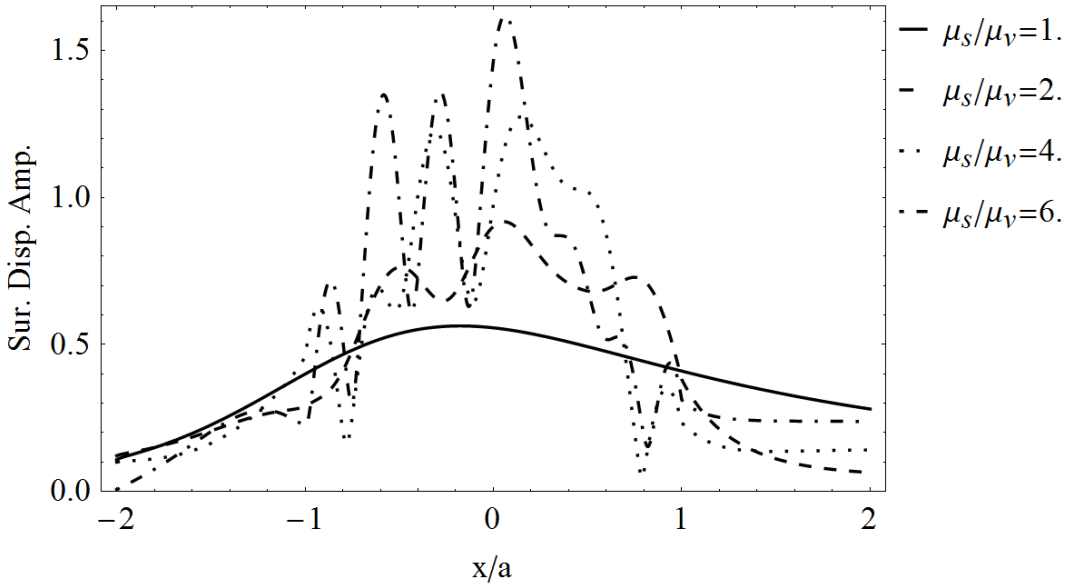

Figure A.67 : Effect of Shear Modulus Differentness for $N = 100$, $\eta = 2$, $a_f/a = 2$, $\alpha_f = \pi/3$, $\alpha_{fl} = \pi/8$, $\rho_s/\rho_v = 1$.

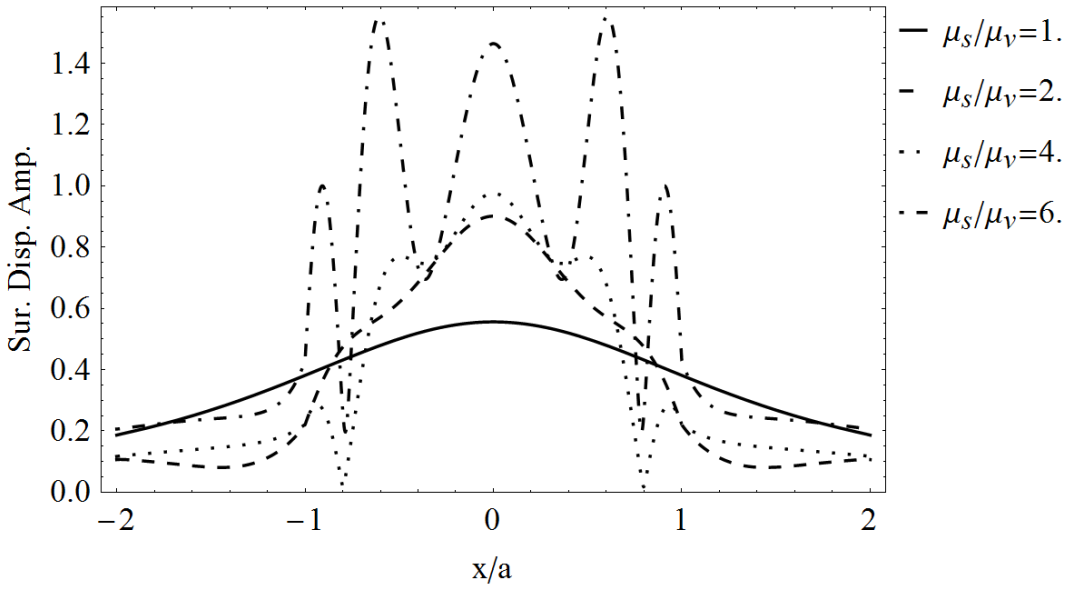

Figure A.68 : Effect of Shear Modulus Differentness for $N = 100$, $\eta = 2$, $a_f/a = 2$, $\alpha_f = \pi/2$, $\alpha_{fl} = \pi/8$, $\rho_s/\rho_v = 1$.

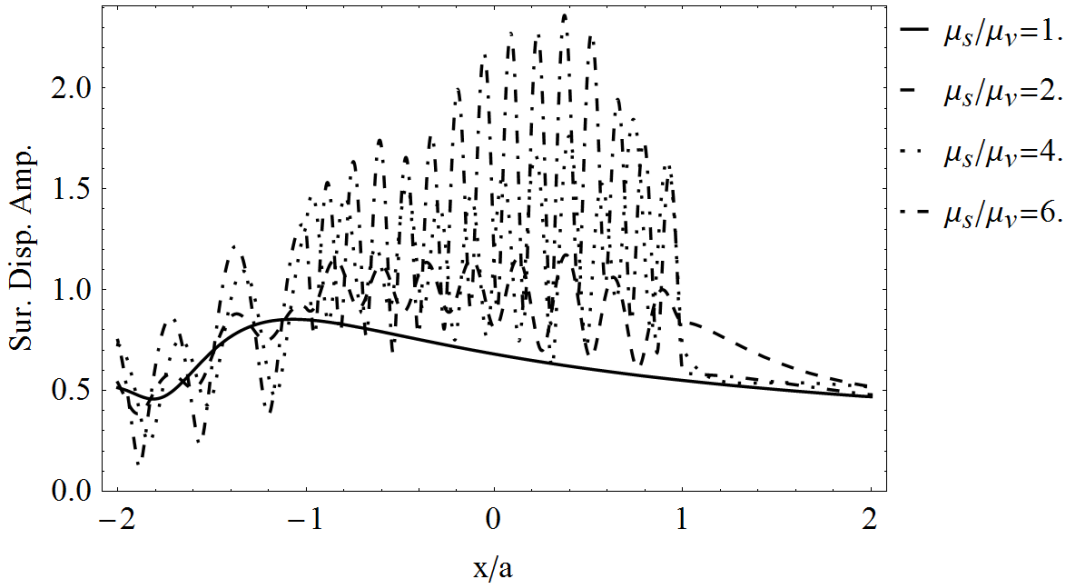

Figure A.69 : Effect of Shear Modulus Differentness for $N = 100$, $\eta = 3$, $a_f/a = 2$, $\alpha_f = \pi/16$, $\alpha_{fl} = \pi/8$, $\rho_s/\rho_v = 1$.

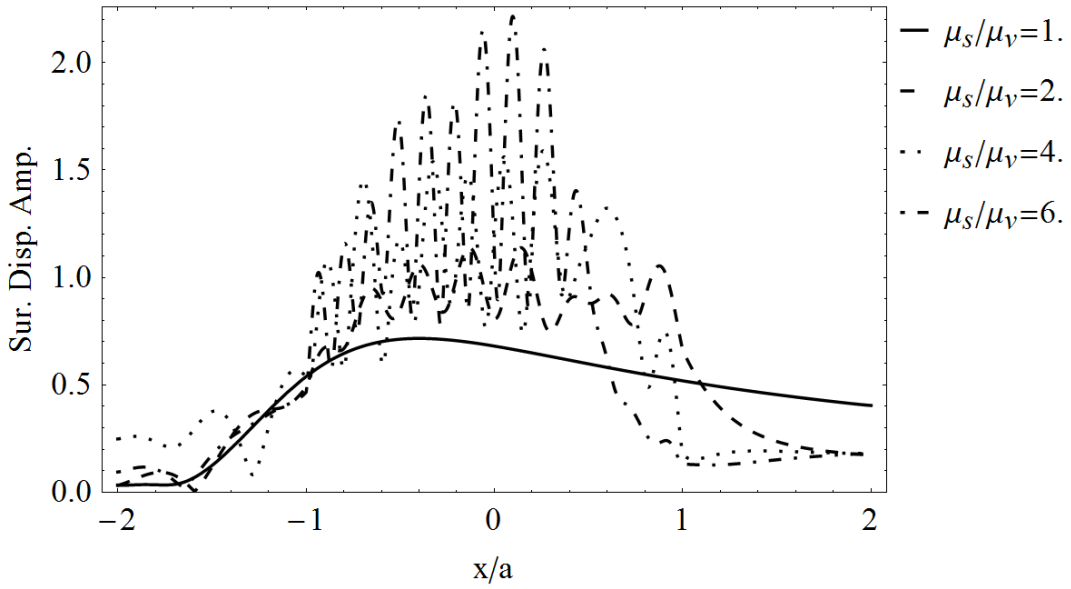

Figure A.70 : Effect of Shear Modulus Differentness for $N = 100$, $\eta = 3$, $a_f/a = 2$, $\alpha_f = \pi/6$, $\alpha_{fl} = \pi/8$, $\rho_s/\rho_v = 1$.

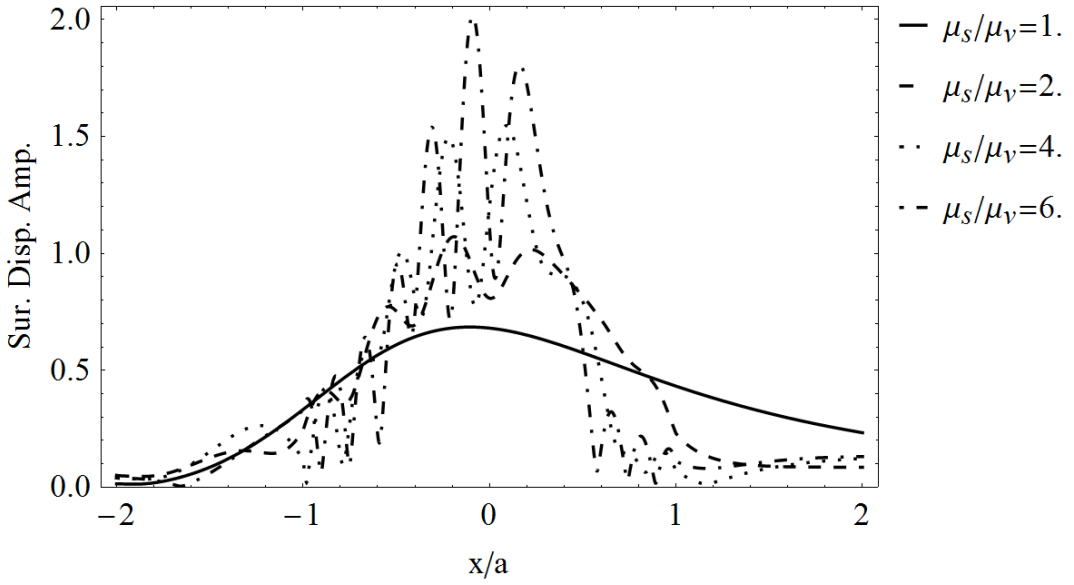

Figure A.71 : Effect of Shear Modulus Differentness for $N = 100$, $\eta = 3$, $a_f/a = 2$, $\alpha_f = \pi/3$, $\alpha_{fl} = \pi/8$, $\rho_s/\rho_v = 1$.

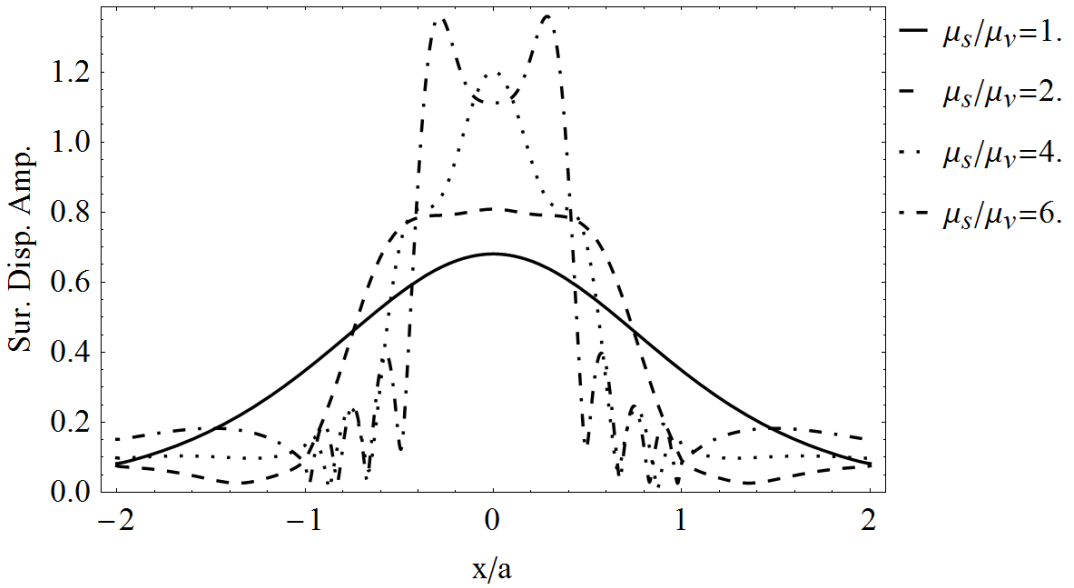

Figure A.72 : Effect of Shear Modulus Differentness for $N = 100$, $\eta = 3$, $a_f/a = 2$, $\alpha_f = \pi/2$, $\alpha_{fl} = \pi/8$, $\rho_s/\rho_v = 1$.

CURRICULUM VITAE

Name Surname: Hasan Faik KARA

Place and Date of Birth: Konya, 08/05/1982

Adress: ITU, Faculty of Civil Engineering, Room number:359 34469 Maslak, Istanbul, Turkey

E-Mail: faikkara@gmail.com

B.Sc.: Istanbul Technical University

M.Sc.: Istanbul Technical University

Professional Experience and Rewards:
TUBITAK Research Fellowship
Visiting scholar at University of Southern California, 2011-2012

PUBLICATIONS/PRESENTATIONS ON THE THESIS

- **Kara, H. F.**, Trifunac, M. D., 2013: A note on plane-wave approximation. *Soil Dynamics and Earthquake Engineering 51*: 9-13